Universität Stuttgart
Institut für Energieübertragung und Hochspannungstechnik, Band 36

Optimized Planning of Distribution Power Grids considering Conventional Grid Expansion, Battery Systems and Dynamic Power Curtailment

Optimized Planning of Distribution Power Grids considering Conventional Grid Expansion, Battery Systems and Dynamic Power Curtailment

Von der Fakultät
Informatik, Elektrotechnik und Informationstechnik
der Universität Stuttgart
zur Erlangung der Würde einer Doktor-Ingenieurin (Dr.-Ing.)
genehmigte Abhandlung

vorgelegt von
Ouafa Laribi
aus Monastir, Tunesien

Hauptberichter:	Prof. Dr.-Ing. habil. K. Rudion
Mitberichter:	Prof. Dr.-Ing. T. Leibfried
Tag der mündlichen Prüfung:	20.04.2022

Institut für Energieübertragung und Hochspannungstechnik
der Universität Stuttgart

2022

Bibliografische Information der Deutschen Nationalbibliothek:

Die Deutsche Nationalbibliothek verzeichnet diese Publikation in der Deutschen Nationalbibliografie, detaillierte bibliografische Daten sind im Internet über http://dnb.dnb.de abrufbar.

Universität Stuttgart
Institut für Energieübertragung und Hochspannungstechnik, Band 36

D 93 (Dissertation Universität Stuttgart)

Optimized Planning of Distribution Power Grids considering Conventional Grid Expansion, Battery Systems and Dynamic Power Curtailment

Herstellung und Verlag: BoD – Books on Demand, Norderstedt

ISBN: 978-3-75685-977-1

Acknowledgement

I would like to give special thanks to my supervisor Prof Dr.-Ing. habil. Krzysztof Rudion for giving me the chance to conduct my thesis at the Institute of Power Transmission and High Voltage Technology (IEH) of the University of Stuttgart. I thank him sincerely for his guidance and support, his advice, and the good and smooth communication during my time at the IEH. I also thank Prof Thomas Leibfried, director of the Institute of Electric Energy Systems and High Voltage Engineering (IEH) in the Karlsruhe Institute of Technology, for agreeing to be my co-examiner.

I also would like to express my thanks to Prof Dr. -Ing. Stefan Tenbohlen, director of the IEH at the University of Stuttgart, for his support and the constructive discussions that we conducted. In addition, I thank the administrative staff, especially Dr Schärli, Ms Schärli and Ms Gugel, who contributed to my work by their accurate and careful administrative support.

I also thank all my colleagues at the IEH for the good cooperation and the constructive technical discussions. Special thanks go to Markus Miller, my office mate, and Deepak Deepak for correcting my thesis, as well as to all the students who I supervised for their contribution to my research work.

Furthermore, I thank my parents, to whom I owe everything good I achieved in my life, for their unconditional love and always giving me trust and strength to progress and go forward. Of course, I also thank my beloved husband, my brothers and my friends for their love and support and always being there for me.

Last but not least, I thank every teacher, professor and each person who supported me and taught me even one letter during my learning journey as pupil, student, doctorand and employee.

Abstract

The increasing integration of renewable energies is driving the transformation of the power grid in Germany. Renewable energy sources, which are mostly allocated in distribution grids, are replacing fossil power plants, that are mostly applied in the transport grid. This shift to more renewable energies entails the expansion of the power transport capacities in the distribution grid. The conventional expansion of the power grid in Germany is, however, proceeding slowly, due to the delay in the authorization procedures. Therefore, new solutions that enable a higher utilization of the existing grid must be adopted besides the classical grid expansion in order to achieve the planned energy transition goals [1].

This research work presents a new grid planning method which applies innovative technologies, in addition to the conventional planning instruments with overhead lines and cables, to optimize and expand the existing grid. The innovative planning instruments considered are battery storage systems and dynamic power curtailment. The proposed approach has been implemented in a time series-based framework as an automated planning algorithm. Based on the selected planning instruments, the planning algorithm determines for a given distribution grid the tailored and most cost-efficient measures to prevent prognosticated grid congestion.

The results of the planning algorithm depend on the considered grid, the renewable expansion scenario and the grid voltage level. The application of the proposed planning method on a real high-voltage grid has revealed that the use of dynamic power curtailment in the grid planning in addition to the conventional grid expansion reduces the required overhead lines to 63 % in case of grid expansion with overhead lines. In case of grid expansion with underground cables, the required cables could be reduced to 51 % through the application of the dynamic power curtailment. The total expansion costs could be, thereby, decreased by about 30 % as compared to the grid expansion with mere overhead lines, and by about 43 % as compared to the grid expansion with mere underground cables.

Furthermore, the results of the planning algorithm have proven that the application of battery storage systems in the grid planning in combination with the dynamic power curtailment and the conventional grid expansion with cables could lead to a reduction of the required cables to about 40.5 %. At the same time, the total costs of the grid expansion can be reduced by about 46 % as compared to the grid expansion costs based on cables.

The combined application of overhead lines and dynamic power curtailment has proven to be the most economical planning variant for the considered high-voltage grid. Nonetheless, in case of slow authorization processes for the conventional grid expansion with overhead lines, a combined application of underground cables, Battery storage systems and dynamic power curtailment can be conceivable although several times more expensive than the first variant.

The proposed planning methodology provides a reliable remedy for an economical and need-based planning of the grid. In case of faltering conventional grid expansion, the planning method enables different expansion variants using flexibilities, such as battery storage systems and dynamic power curtailment to reach a higher utilization of the existing grid and reduce the application of conventional measures such as overhead lines and cables.

Kurzfassung

Die aktuell zunehmende Integration von erneuerbaren Energien in Deutschland heutzutage treibt die Transformation des Stromnetzes voran. Erneuerbare Energieanlagen, die dezentral im Verteilnetz verbreitet sind, ersetzen zunehmend fossile Kraftwerke, die überwiegend auf der Übertragungsebene eingesetzt sind. Dieser Übergang zu mehr erneuerbaren Energien erfordert den Ausbau von höheren Transportkapazitäten im Verteilnetz. In manchen Regionen in Deutschland kommt der konventionelle Netzausbau allerdings aufgrund von schleppenden Neubaugenehmigungen nur langsam voran. Deshalb ist heutzutage neben dem unerlässlichen klassischen Netzausbau eine bessere Ausnutzung des Bestandnetzes erforderlich, um die geplanten Ziele der Energiewende zu erreichen [1]. Dies erfordert einen Netzplanungsansatz, welcher unterschiedliche Lösungen und Maßnahmen berücksichtigt. Diese Arbeit präsentiert eine neue Planungsmethode für Verteilnetze, die neben dem klassischen Netzausbau mit Freileitungen und Kabeln innovative Planungsinstrumente wie Batteriespeichersysteme oder die dynamische Spitzenkappung zur Netzoptimierung und -verstärkung nutzt. Die vorgeschlagene Planungsmethode wurde als automatisierter Planungsalgorithmus in einer zeitreihenbasierten Umgebung implementiert. Ausgehend von den gewählten Planungsinstrumenten ermittelt der Planungsalgorithmus die bedarfsorientierten und kostengünstigsten Maßnahmen zur Optimierung und Verstärkung des betrachteten Netzes, um prognostizierte Engpässe zu verhindern.

Die resultierenden Maßnahmen aus dem Planungsalgorithmus hängen von dem betrachteten Netz, dem Ausbauszenario für erneuerbare Energien und von der Netzspannungsebene ab. Der Einsatz der vorgeschlagenen Planungsmethode an einem realen Hochspannungsnetz in Deutschland hat ergeben, dass die Nutzung der zeitreihenbasierten dynamischen Spitzenkappung neben dem konventionellen Netzausbau zu einer Verringerung der benötigten Freileitungsmaßnahmen auf ca. 63 % im Falle des Netzausbaus mit Freileitungen, und auf 51 % im Falle des Netzausbaus mit Kabeln führen kann.

Dabei können die Gesamtkosten der Netzausbaumaßnahmen durch den Einsatz der dynamischen Spitzenkappung um ca. 30 % im Vergleich zum Netzausbau mit Freileitungen und ca. 43 % im Vergleich zum Netzausbau mit Kabeln reduziert werden.

Darüber hinaus haben die Ergebnisse des Planungsalgorithmus erwiesen, dass der Einsatz von Batteriespeichern in Kombination mit der dynamischen Spitzenkappung und dem konventionellen Netzausbau mit Kabeln zu einer Reduktion der benötigten Kabelmaßnahmen auf ca. 40.5 % führen kann.

Gleichzeitig können die Gesamtnetzausbaukosten um ca. 46 % im Vergleich zum Netzausbau mit Kabeln reduziert werden.

Der kombinierte Einsatz von Freileitungen und dynamischer Spitzenkappung hat sich für das betrachtete Hochspannungsnetz als kostengünstigste Planungsvariante erwiesen. Im Falle von stockenden Neubaugenehmigungen könnte ein kombinierter Einsatz von Kabeln, Batteriespeichern und dynamischer Spitzenkappung eine mögliche Alternative sein, auch wenn dies mit mehrfachen Kosten im Vergleich zum Netzausbau mit Freileitungen verbunden ist.

Die vorgeschlagene Planungsmethode stellt eine zuverlässige Abhilfe für eine wirtschaftliche und bedarfsorientierte Netzplanung dar. Sie ermöglicht auch unterschiedliche Netzausbauvarianten durch den Einsatz von Flexibilitäten wie Batteriespeichern und dynamischer Spitzenkappung, um eine höhere Nutzung des Bestandnetzes zu erreichen und den konventionellen Netzausbau zu reduzieren.

List of Content

List of Abbreviations

Abbreviation	Definition
BSS	Battery storage system
CGE	Conventional grid expansion
DoD	Depth of discharge
DPC	Dynamic power curtailment
DSO	Distribution system operator
EHV	Extra-high voltage
EnWG	The German energy industry act
EPEX	European power exchange
GA	Genetic algorithm
GE	Grid expansion
HV	High voltage
LFC	Load flow calculation
LS	Line segment
LV	Low voltage
MILP	Mixed-integer linear programming
MV	Medium voltage
OHL	Overhead line
PC	Power curtailment
PV	Photovoltaic
PVF	Present-value factor
RES	Renewable energy systems
SS	Substation
UGC	Underground cable

List of Symbols

Symbol	Definition	Unit
A	Set of the considered line states of the grid $\{1,2,\dots,N_{outages}\}$ comprising (n-0) and (n-1) line states	
AE_{max}	Maximum absolute error	
AE_{mean}	Mean absolute error	
α_{ij}	Admittance angle of the line between node i and j	rad
b_{ij}	Susceptance of the line connected between node i and j	pu
$b_{l,v}$	Binary variable associated to the line l and the CGE variant v (optimization variable)	
$b_{m,v}$	Binary variable associated to the line segment m and the CGE variant v (optimization variable)	
C'	Insulator capacitance of the underground cable	F/km
$Cost_{BSS}$	Costs of the BSS application (optimization variable)	$EUR\ million$
$Cost_{DPC}$	Total costs of the DPC application over the economic life (optimization variable)	$EUR\ million$
$Cost_{CGE}$	Costs of the CGE measures (optimization variable)	$EUR\ million$
$Cost_{Loss}$	Total costs of incurred losses in the lines and in the BSS	$EUR\ million$
$C'_{l,v}$	Resulting insulator capacitance of the cable of line l in case of the CGE variant v	F/km
ε	Accuracy level in the iterative process of the Newton-Raphson LFC	

$\Delta P_{PV,i,t}$	Curtailed PV active power on node i at time step t (optimization variable)	MW
$\Delta P_{Wind,i,t}$	Curtailed wind active power on node i at time step t (optimization variable)	MW
$(\Delta P_{PV,t})$	Column vector of the curtailed PV power amount on the grid nodes at time step t (optimization variables)	MW
$(\Delta P_{RES,t})$	Column vector of the curtailed PV and wind power amount on the grid nodes at time step t	MW
$(\Delta P_{Wind,t})$	Column vector of the curtailed wind power amount on the grid nodes at time step t (optimization variables)	MW
$\Delta Q_{PV,i,t}$	Curtailed PV reactive power on node i at time step t (optimization variable)	$MVar$
$\Delta Q_{Wind,i,t}$	Curtailed wind reactive power on node i at time step t (optimization variable)	$MVar$
$(\Delta Q_{PV,t})$	Column vector of the curtailed PV reactive power on the grid nodes at time step t (optimization variables)	$MVar$
$(\Delta Q_{Wind,t})$	Column vector of the curtailed wind reactive power on the grid nodes at time step t (optimization variables)	$MVar$
Δt_{market}	Time step of the transactions which equals 1 hour on the Day-Ahead market	h
Δt_{step}	Duration of a time step t	h
$E_{curt,PV,i}$	Curtailed PV energy on node i in a year (optimization variable)	MWh
$E_{curt,Wind,i}$	Curtailed wind energy on node i in a year (optimization variable)	MWh
E_{DPC}	Total curtailed energy during the simulated year (optimization variable)	MWh/a
$E_{Loss,BSS}$	Energy losses incurred in the BSS over the simulated year	MWh

$E_{Loss,I}$	Current dependent energy losses over the simulated year	MWh
$E_{Loss,U}$	Voltage dependent energy losses over the simulated year	MWh
$E_{Loss,Comp}$	Compensation energy losses over the simulated year	MWh
$E_{market,s,t}$	Resulting energy amount from the electricity trade in the BSS s at time step t	MWh
$E_{max,s}$	Capacity of the BSS s (optimization variable)	MWh
$E_{s,t}$	Storage energy of a BSS s at time step t (optimization variable)	MWh
η_{BSS}	Charge and discharge efficiency factor of the BSS	
F_{BSS}	Multiplication factor to vary the specific investment costs for BSS applications within the sensitivity analysis	
F_D	Detour factor	
F_{DPC}	Multiplication factor to vary the specific costs for DPC applications within the sensitivity analysis	
$Fee_{Transaction}$	Specific levied fees for the use of the market platform	EUR/MWh
F_{CGE}	Multiplication factor to vary the specific investment costs for CGE within the sensitivity analysis	
F_{length}	Multiplication factor to vary the length of the grid lines within the sensitivity analysis	
F_{PV}	Multiplication factor to vary the installed PV power in the grid within the sensitivity analysis	
F_{Wind}	Multiplication factor to vary the installed wind power in the grid within the sensitivity analysis	

g	Quality factor of the compensation reactor	
$Gain_{Spot,a}$	Yearly profits from the participation of the BSS in the Day-Ahead Market (optimization variable)	EUR/yr
$Gain_{tot}$	Total profits from the participation of the BSS in the Day-Ahead Market over the economic life	$EUR\ million$
g_{ij}	Conductance of the line connected between node i and j	pu
$G'_{l,v}$	Resulting shunt conductance per unit length of line l in case of CGE variant v	S/km
$I_{BSS,ini}$	Initial investment costs in the BSS project (optimization variable)	$EUR\ million$
$I_{BSS,rep}$	Replacement investment in battery cells and converters (optimization variable)	$EUR\ million$
I_{CF}	Capacitive fault current in case of a single line to ground fault (optimization variable)	A
$I_{CGE,comp}$	Investment costs in new compensation reactors (optimization variable)	$EUR\ million$
$I_{CGE,grounding}$	Investment costs in new Peterson coils (optimization variable)	$EUR\ million$
$I_{CGE,line}$	Investment costs in new lines (optimization variable)	$EUR\ million$
$I_{CGE,panel}$	Investment costs in new feeder panels (optimization variable)	$EUR\ million$
$\underline{i}_{ij}$	Complex current through a line connected between node i and j	pu
$i_{ij,p}$	Active current flow through a line connected between node i and j	pu
$i_{ij,q}$	Reactive current flow through a line connected between node i and j	pu
$I_{max,l,v}$	Current capacity of line l in case of CGE variant v	A

$I_{rep,batt}$	Replacement investment in battery cells (optimization variable)	EUR
$I_{rep,conv}$	Replacement investment in converters (optimization variable)	EUR
(J)	Jacobian matrix	
$K_{batt,i}$	Specific costs of battery cells at the time of the investment i	EUR/MWh
$K_{BSS,op}$	Total ongoing operating costs of the BSS (optimization variable)	$EUR\ million$
$K_{BSS,spec}$	Specific investment costs in BSS projects	EUR/MWh
K_{CE}	Average value of the purchase price of the compensation energy	EUR/MWh
$K_{CGE,op}$	Total ongoing operating costs of the new lines (optimization variable)	$EUR\ million$
$K_{conv,i}$	Specific costs of converters at the time of the investment i	EUR/MW
$K_{DPC,spec}$	Specific costs of the power curtailment	EUR/MWh
$K_{fees,s,t}$	Stock market fees occurring at time step t due to the participation of the BSS s in the Day-Ahead market (optimization variable)	EUR
$K_{Loss,BSS}$	Costs of the losses incurred in the BSS	$EUR\ million$
$K_{Loss,Comp}$	Costs of the compensation losses	$EUR\ million$
$K_{Loss,I}$	Costs of the current dependent losses incurred in the power lines	$EUR\ million$
$K_{Loss,U}$	Costs of the voltage dependent losses incurred in the power lines	$EUR\ million$
K_{panel}	Specific investment costs of a new outgoing feeder panel in transformer stations	$EUR/unit$
$K_{Peterson}$	Costs of the Peterson coil	EUR/A
$K_{Reactor}$	Costs of the compensation reactors	$EUR/Mvar$

$K_{tax,s,t}$	Tax expenses occurring by charging the electricity from the grid into the BSS s at time step t (optimization variable)	EUR
$K_{trade,s,t}$	Expenses or revenues of the BSS s occurring from the electricity trade at time step t (optimization variable)	EUR
K_v	Specific costs of the variant v	EUR/km
L	Set of the grid lines $\{1,2,\ldots,N_{lines}\}$	
l_l	Length of the line l	km
l_m	Length of the line segment m	km
M	Set of line segments in the grid $\{1,2,\ldots,N_{seg}\}$	
N	Set of the grid nodes $\{1,2,\ldots,N_{nodes}\}$	
$(NACLODF)^{(a)}$	Matrix containing the distribution factors of the nodal injection power for the line state a	
$(NACLODF)^{(a)}[l;N]$	The l^{th} row of the matrix $(NACLODF)$ for the line state a	
N_{BSS}	Number of BSS	
N_{cycle}	Number of reachable full cycles of the BSS	
$N_{life,batt}$	Service life of battery cells	yr
$N_{life,conv}$	Service life of converters	yr
N_{lines}	Number of the grid lines	
$N_{m,lines}$	Number of overhead lines included in the line segment m	
N_{nodes}	Number of the grid nodes	
$N_{outages}$	Number of the line states including the (n-0) state and the (n-1) outages of the lines	
$N_{rep,batt}$	Count of required replacements of battery cells	
$N_{rep,conv}$	Count of required replacements of converters	

N_{Seg}	Number of line segments in the grid	
$N_{steps,h}$	Number of time steps over one year with a time resolution of an hour	
$N_{steps,q}$	Number of time steps over one year with a time resolution of a quarter-hour	
$n_{panel,l}$	Number of feeder panels connected to the line l	
$n_{panel,m}$	Number of feeder panels connected to the line segment m	
N_{var}	Number of considered CGE variants	
N_{years}	Economic life considered	yr
ν	Iteration count	
ω	Angular frequency	rad/s
$P_{L,i,2017}$	Installed load on a node i of the grid for the scenario 2017	MW
$P_{L,i,2017,t}$	Load power on a node i at time step t	MW
$(P_{L,t})$	Column vector of the power flow through the grid lines	MW
$P_{l,t}^{(a)}$	Active power flow through a line l for a grid state a at time step t	MW
$P_{L,T,2017}$	Load power installed in the grid that is connected to the transformer T for the scenario 2017	MW
$P_{L,T,2017,t}$	Cumulated load power on the transformer T at time step t for the scenario 2017	MW
$P_{market,c,s,t}$	Charging power of the BSS s for the electricity trade at time step t	MW
$P_{market,d,s,t}$	Discharging power of the BSS s for the electricity trade at time step t	MW
$(P_{Market,S,t})$	Column vector of the charging and discharging power of the BSS for the	

	electricity trade at time step t (optimization variables)	
$P_{market,s,t}$	Charging or discharging power of the BSS s for the electricity trade at time step t (optimization variable)	MW
$P_{max,s}$	Rated power of the BSS s (optimization variable)	MW
$(P_{N,t})$	Column vector of the original residual power injection in the grid nodes at time step t	MW
$P_{PV,i,t}$	PV power on node i at time step t	MW
$P_{RES,add,T,2030}$	Additional RES power installed in the grid connected to the transformer T for the scenario 2030	MW
$P_{RES,i,2017}$	RES power installed on a node i for the scenario 2017	MW
$P_{RES,i,2030,t}$	Injection power of RES on a node i at time step t for the scenario 2030	MW
$P_{RES,Ref,t}$	Normalized active power value to 1 kW of a reference RES plant at time step t	
$P_{RES,T,2017}$	RES power installed in the grid that is connected to the transformer T for the scenario 2017 in MW	MW
$P_{RES,T,2017,t}$	Cumulated feed-in power of RES on transformer T at time step t for the scenario 2017 at time step t	MW
$Price_{market,t}$	The electricity price on the EPEX Spot market at time step t	EUR/MWh
$P_{s,c,t}$	Charging power of the BSS s at time step t on the grid side (optimization variable)	MW
$P_{s,d,t}$	Discharging power of the BSS s at time step t on the grid side (optimization variable)	MW
$p_{set,i}$	Set active injection power at a node i in pu	

$P_{s,t}$	Storage power of the BSS s at time step t (optimization variable)	MW
$(P_{S,t})$	Column vector of the storage power on the grid nodes at time step t (optimization variables)	MW
$P_{T,2017,t}$	Residual active power on the transformer T at time step t	MW
$P_{Wind,i,t}$	Wind power on node i at time step t	MW
φ_i	Phase change angle of the power plant connected to node i	°
Q_{comp}	Capacitive-reactive power induced by the underground cables (optimization variable)	$Mvar$
$(Q_{N,t})$	Column vector of the original reactive power injection in the grid nodes at time step t	$MVar$
$q_{set,i}$	Set reactive injection power at a node i in pu	
r	Adopted rate of interest in the cost calculation	
$R'_{l,v}$	Resulting resistance per unit length of line l in case of CGE variant v	Ω/km
S	Set of BSS $\{1,2,\dots,N_{BSS}\}$	
$S_{l,t}^{(a)}$	Apparent power flow through a line l for a grid state a at time step t	MVA
$S_{l,t,max}$	Maximum resulting power flow value through line l at time step t with respect to the possible line outages	MVA
$S_{max,l,v}$	Power-carrying capacity of line l in case of CGE variant v	MVA
Tax_{Batt}	Specific tax costs by charging the BSS from the grid	EUR/MWh
$T_{year,q}$	Set of time steps over one year with a time resolution of a quarter-hour $\{1,2,\dots,N_{steps,q}\}$	

$T_{year,h}$	Set of the time steps over the simulated year with a time resolution of one hour $\{1,2,\ldots,N_{steps,h}\}$	
ϑ_i	Voltage angle on a node i	rad
u_i	Voltage magnitude on a node i	pu
$U_{lin,i,t}$	Resulting voltage magnitude value from the linearized LFC for node i at time step t	kV
U_N	Nominal voltage of the grid	V
$U_{NR,i,t}$	Resulting voltage magnitude value from the Newton-Raphson LFC for node i at time step t	kV
V	Set of conventional line expansion variants	
$\underline{y}_{ij}$	Admittance of the line connected between node i and j	pu

1 Introduction

1.1 Motivation and Background

In the context of the energy transition, several energy goals have been set by the German government. The target goals include the phaseout of nuclear energy by 2022, the increase of the renewable energy share in gross electricity consumption to 65 % by 2030 and the phaseout of coal by 2038. By 2050, the share of renewable energy in gross electricity consumption is targeted at 80 % [2]. Consequently, power generation is no longer realized centrally in big power plants at the extra-high voltage (EHV) level and then transported through the transmission and distribution grids to the end consumer. Instead, electrical power is increasingly being generated decentrally at the low- and medium-voltage levels and then transported to the end consumer. However, the distribution grid is not designed to transport high power flow values caused by the increasing feed-in power from renewable energy systems (RES). Consequently, grid congestion in distribution grids is more likely to occur. In order to enable the increasing integration of RES and simultaneously ensure a safe grid operation, the German legislator imposes a need-oriented optimization, reinforcement and expansion of the power grid [3]. Accordingly, system operators in Germany are obliged to enhance the power grid according to the NOVA (Netz-Optimierung vor Verstärkung vor Ausbau) principle, which implies that the power grid must, firstly, be optimized, then, if necessary, reinforced, and finally, if necessary, expanded [4]. The aim hereby is to reduce the conventional grid expansion (CGE) by a higher utilization of the existing grid infrastructure and further flexibility potentials [5, 6].

Therefore, the contribution of innovative technologies and means, such as battery storage systems (BSS) and dynamic power curtailment (DPC) of RES to enhance the utilization of the existing grid, is today gaining importance and being increasingly investigated.

However, these innovative technologies are generally considered separately to remedy selective grid congestion during the grid operation, and not directly integrated into the grid planning process, as are overhead lines or cables. Furthermore, automated methods which combine different types of planning instruments in the grid planning process are missing. Additionally, methods which determine automatically the most appropriate expansion measure or combination of measures for each grid impartially and need-oriented based on predefined criteria, such as the total investment and operating costs, are lacking today.

Against this background, this thesis proposes a new planning methodology that combines conventional planning instruments, such as overhead lines (OHLs) and underground cables (UGCs), with innovative planning instruments, such as BSS and DPC, in the grid planning process. The proposed planning approach considers these planning instruments impartially for the expansion of the existing grid, and determines the appropriate combination of expansion measures, as well as their location and sizing in order to fulfill the planning principles at minimal costs.

The proposed planning methodology was implemented in the form of a planning algorithm and verified on real high- (HV) and medium-voltage (MV) grids. The contribution of BSS and DPC in increasing the utilization of the existing grids, reducing the use of CGE measures and saving expansion costs were technically and economically analyzed in this work.

Furthermore, a multiuse concept for the BSS was developed which allows the participation of the BSS into the European EPEX Day-Ahead market in addition to their grid-supporting application. The contribution of the profits generated from the electricity trade to reducing the total costs of the BSS was further investigated.

1.2 Objective of the Research Work

The aim of this work is to provide an innovative planning methodology for HV and MV grids which automatically delivers the cost minimal planning solution for the grid in consideration of the grid planning principles. Accordingly, a planning algorithm based on a mixed-integer linear programming (MILP) optimization was implemented. The main objective of the optimization is to minimize the total costs of the planning measures over a specified economic life. With the help of a linearized load flow calculation, linear constraints were implemented to model the grid planning principles and restrictions. The delivered planning solution includes:

- The required conventional expansion measures for the power lines, including the type of each measure and lines concerned
- The required dimensioning, placement and scheduling of the BSS over the simulated time period
- The required scheduling of the power curtailment (PC) of RES over the simulated time period
- The total costs of the resulting planning measures over the considered economic life

A further goal of this work is to integrate innovative planning instruments, such as BSS and DPC, into the planning process. Compared with the classic planning method which typically applies only traditional planning instruments, such as OHLs and UGCs, the approach proposed in this work combines both classic and innovative planning instruments. The combination of instruments of different types could enable a higher utilization of the existing grid and a reduction of any further required CGE measures. Especially in the case of obstructed grid expansion due to faltering building permits in some regions in Germany, these new planning instruments could offer an alternative solution to integrate more RES into the grid.

In addition, this work aims to evaluate and compare the different considered planning instruments with each other based on the resulting costs when applied for the planning and expansion of the same grid and according to the same planning principles.

A further target of this work is to evaluate the cost-efficiency of each planning instrument depending on the voltage level of the grid and trace from that the tendentially most appropriate planning instruments for each voltage level. Based on that, a general application framework of each planning instrument could be deduced.

1.3 Scientific Thesis

The increasing integration of RES is leading to a higher loading of the distribution grid. In order to prevent network congestion, system operators typically resort to the CGE with OHLs or UGCs to increase the power transmission capacity of the grid. Yet, the CGE of the distribution grid is not always accepted by the local population, which begs the question as to whether other expansion solutions could be applied to reduce the required CGE due to the RES integration without increasing the total costs. Out of this question, the following scientific thesis of this dissertation is derived:

It is possible to reduce the required CGE due to the increasing integration of RES through the inclusion of the innovative planning instruments BSS and DPC in the grid planning, and still decrease the total expansion costs.

1.4 Structure of the Work

This dissertation is divided into eight chapters. The first chapter introduces this research work and describes its background and objectives. The second chapter gives an overview of the state of the art regarding the classic planning of distribution grids in Germany and the use of innovative methods and technologies, such as grid-supporting battery systems and dynamic curtailment, in the grid planning. The third chapter outlines the methodology adopted for the generation of the input data and the modelling of the distribution grids that are examined in this work. In the fourth chapter, the developed planning algorithm is presented, giving a detailed description of the implemented optimization. The results of the planning algorithm are illustrated in the fifth chapter through an application on real HV and MV grids. In the sixth chapter, a multiuse application of BSS to generate profits is examined and evaluated. The seventh chapter describes the approach adopted to analyze the sensitivity of the planning algorithm's output to relevant input parameters. The eighth chapter summarizes all results of the examined issues and gives an overview of the findings of this research work and further suggestions for its improvement.

2 State of the Art in the Planning of Power Distribution Grids

An outline of the state of the art in the planning of distribution grids is presented in this chapter. In this regard, the planning and expansion principles currently adopted by grid operators for MV and HV grids are described in detail. Furthermore, an overview of the state of the art concerning the use of grid-supporting BSS and DPC in the grid planning is given.

2.1 Classical Planning of Distribution Grids

The elaboration of a grid expansion plan requires the consideration of the framework conditions and grid planning principles. The framework conditions consist of the prognosis of additional load and RES in the grid during a specific time frame. With the help of the grid analysis, the maintaining of the current-carrying capacity of the grid components and the voltage limits are examined according to the planning principles for the considered power grid. Hereby, two relevant planning cases are considered: the high-load case and the high-generation case of RES. Due to the increasing integration of RES, the high generation case is becoming increasingly the relevant operation case in grid planning [7]. Based on the results of the grid analysis, the appropriate CGE measures are adopted to prevent prognosticated grid congestion. A detailed description of the classic grid planning steps in Germany is given in the following chapters.

2.1.1 Framework Conditions

At first, the expansion scenarios of the load and of RES for every federal state in Germany are estimated based on the political goals of the federal government and the state governments until a target year, for example, 2030. The RES power installed in a state until 2030 is then distributed over the regions and municipalities of each state.

The prognosticated wind power installed in each state is distributed over the municipalities in proportion to the total arable surface of the municipality compared to that of the considered state [8]. The wind resources and a 1000 m distance to residential areas are also considered [9]. Additional solar parks are, however, distributed along highways, whereas on-roof photovoltaic (PV) systems are distributed inside residential areas, depending on the number of inhabitants per building [9].

In a next step, the additional RES power installed in every region is divided over the voltage levels of the grid, depending on the technology and the expected plant sizes. The additional wind plants and solar parks are mostly connected to the MV grid, whereas on-roof PV systems are connected to the low-voltage (LV) grid [9].

2.1.2 Relevant Load and Generation Cases for the Grid Planning

Power grids within the classic deterministic grid planning are dimensioned for two extreme load situations in order to ensure the reliability of the power supply. For this purpose, scaling factors are used to model the high load consumption case by minimal feed-in power from RES and the high RES generation case by minimal load consumption. The applied scaling factors depend on the weather conditions of the considered region. Table 2-1 and 2-2 show some of the scaling factors adopted within the deterministic planning of HV and MV grids in Germany. For the high load case, 100 % of the installed load and 0 % of the installed PV and wind power are generally considered for both HV and MV grids. For the high generation case in HV grids, 30 – 45 % of the installed load is adopted for the power demand, whereas 85 – 90 % of the installed PV power and 90 – 100 % of the installed wind power are applied for the simultaneous feed-in power of PV and wind plants, respectively.

For the high generation case in MV grids, 15 – 30 % of the installed load is adopted for the power consumption, whereas 85 % of the installed PV power and 100 % of the installed wind power are applied for the simultaneous feed-in power of PV and wind plants, respectively.

The values adopted for the load consumption and feed-in power from RES could deviate from the values presented in the tables, depending on the grid operator and the considered region.

Table 2-1 Load and generation cases considered for the planning of HV grids

	Load	**PV**	**Wind**
High load case	100 % [7, 8, 9]	0 % [7, 8, 9]	0 % [7, 8, 9]
High generation case	30 % [7], 35 % [8], 45 % [9]	85 % [7, 8] 90 % [9]	90 % [9] 100 % [7, 8]

Table 2-2 Load and generation cases considered for the planning of MV grids

	Load	PV	Wind
High load case	100 % [7, 8]	0 % [7, 8, 9]	0 % [7, 8, 9]
High generation case	15 % [8, 9] 30 % [7]	85 % [7, 8, 9]	100 % [7, 8, 9]

2.1.3 Relevant Grid Restrictions

Based on the considered load and generation cases, LFCs are realized in order to identify any possible violations of grid restrictions. The relevant grid restrictions for the planning of distribution grids are:

- Compliance with the current-carrying capacity of grid components
- Compliance with the permitted node voltage range

According to the planning principles, the grid restrictions are considered differently depending on the voltage level of the grid.

2.1.3.1 Grid Restrictions Adopted for HV Grids

Compliance with the current-carrying capacity of grid components in consideration of the (n-1) security criterion is required in HV grids. The (n-1) criterion is a fundamental planning principle for HV grids in Germany for both high load and high generation cases [7, 8, 10]. Accordingly, the grid components must be steadily operated in consideration of a sufficient capacity reserve, so that the (n-1) security criterion can be preventively fulfilled. To identify eventual overloads and violations of the (n-1) security criterion, a contingency analysis is realized within the grid planning comprising (n-1) outages of all HV power lines and EHV/HV transformers. The maximal loading of grid components in HV grids must not generally exceed 100 % of their thermal capacity for both normal and (n-1) states [7, 8, 9]. It should be noted that the (n-1) criterion is not compulsory for the lines which connect decentralized RES to the grid [9, 10].

2.1.3.2 Grid Restrictions Adopted for MV Grids

The (n-1) security criterion in the MV grid must be fulfilled only for the consumption case [7, 8, 10]. The MV grids are mostly designed in the form of open rings comprising two parallel line systems. In the high load case, the parallel power lines and the HV/MV transformers are operated with a maximum of 50 [7] – 60 % [8, 10] of their current-carrying capacity in the normal state, so that they can be operated with 100 [7] – 120 % [8, 10] of their capacity in the (n-1) state. The fulfilment of the (n-1) criterion in the high generation case is still not required in the planning of MV grids nowadays. In the case of high feed-in power from RES, the power lines can, therefore, be operated with their 100 % thermal capacity in the normal state [7–10]. In the (n-1) state, system operators can curtail the exceeding RES power or disconnect the power plant manually or through distant control in order to prevent overloads.

In addition to the current-carrying capacity of the grid components, the compliance of the node voltage with the voltage limits allowed in the MV grid must be fulfilled. According to the European norm EN 50160 [11], the node voltage at the end consumer in the LV grid must be maintained within the voltage range of ±10 % of the nominal voltage. Therefore, grid operators divide the permitted ±10 % voltage range between the LV grid, LV/MV substation and MV grid.

Figure 2-1 shows the voltage range division according to [7] for the normal state of the grid. The node voltage limits for MV grids are set in this case at +5 % and −1.5 % of the nominal voltage [7].

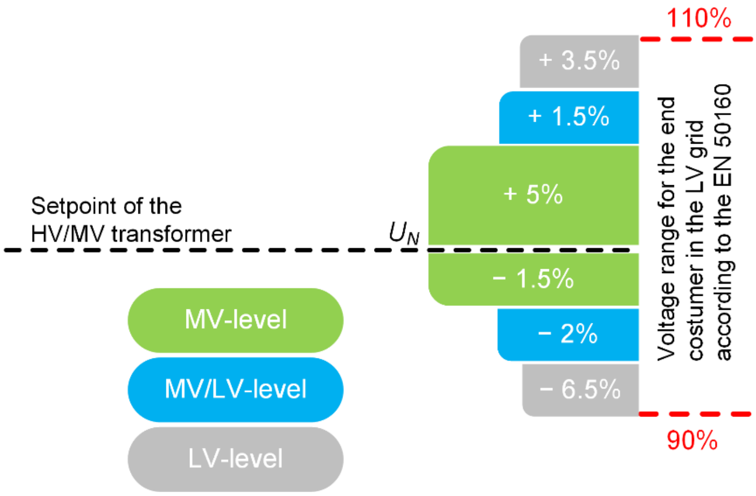

Figure 2-1 Division of the voltage range in the normal state [7]

The voltage in MV grids has been restricted to ±4 % of the nominal voltage in [8], whereas it amounts to +7 % and −3 % of the nominal voltage according to [9].

2.1.4 Standard Equipment for the Conventional Grid Expansion

The grid state is analyzed based on LFCs. In the case where the loading of the grid components or the node voltages do not comply with the grid restrictions described in 2.1.3, CGE measures are applied to remedy the limit violations. The adopted measures depend on the type and extent of the identified congestion and the grid voltage level.

2.1.4.1 Standard Equipment for the CGE of HV Grids

The common congestion determined in HV grids is due to the overload of power lines in the normal or (n-1) state. In this case, the overloaded power lines are expanded based on standard equipment, such as OHLs or UGCs. Table 2-3 shows the standard grid equipment that is typically used for the CGE of HV grids in Germany [7, 8, 12]. It should be noted that the standard equipment used by grid operators for the expansion of the HV grid includes, but is not necessarily limited to, the equipment mentioned in this work.

In addition to single and double conductor OHLs, 800 mm^2 UGCs with 890 A current-carrying capacity are applied in HV grids. Due to the reduced thermal conductivity in the ground and depending on how the cables are laid in the ground, a 71 % to 80 % reduction of the current-carrying capacity of the cables compared to the nominal value is adopted for the steady state operation.

Table 2-3 Standard equipment for the CGE of HV grids

	Nominal Current-Carrying Capacity / A	**Permitted Current-Carrying Capacity / A**
Single conductor OHL 265/35 Al/St	680	680 [7, 8, 12]
Two bundle conductor OHL 265/35 Al/St	1360	1360 [7, 8, 12]
Cable N2XS(FL)2Y 3x1x800RM/50	890	632 [12] - 712 [7, 8]

2.1.4.2 Standard Equipment for the CGE of MV Grids

In the MV grid, CGE measures are applied to prevent the overload of grid components or the violation of the node voltage limits. In the case of an overload problem, the MV grid can be expanded using standard equipment to overcome the congestion. Table 2-4 shows the standard equipment that can be used for the CGE of MV grids [7, 8, 13].

Table 2-4 Standard equipment for the CGE of MV grids

	Type	**Current / Power Rating**
Underground cable	NA2XS2Y 3x1x185	361 A
HV/MV transformer		40 MVA

It should be noted that the standard equipment and measures applied by grid operators for the CGE of MV grids could include, but is not necessarily limited to, the equipment and measures mentioned in this work.

2.1.5 Determination of the CGE Measures Required

The determination of the CGE measures required for a given grid is realized depending on the grid voltage level. The methods adopted for the determination of the CGE measures required in HV and MV grids within classic grid planning will be explained in detail in the following sections.

2.1.5.1 Determination of the CGE Measures Required in HV Grids

At first, the prognosticated installed power of additional loads and RES is allocated to the appropriate power grids and distributed over the grid nodes. In a second step, a contingency analysis is realized for all OHLs, cables and transformers in the grid according to the defined extreme load and generation scenarios. The aim of this analysis is to determine the grid components on which overloads are prognosticated.

Once the prognosticated overloads have been identified, the CGE measures required to prevent these overloads are determined stepwise. A single uniform guideline for the determination of the required CGE measures does not exist. Nevertheless, grid operators have recourse to standard equipment and common methods to prevent prognosticated overloads. Figure 2-2 shows the expansion stages adopted in [7, 8, 12].

In the case where an overloaded OHL system is identified, the addition of an identic parallel line system with the same current-carrying capacity is suggested in the first stage [7, 8, 12]. It is assumed hereby that the existing electricity pylons can bear both line systems without further reinforcement of the pylons.

If the additional line system is not sufficient to overcome the identified congestion, both old and new line systems are replaced by single conductor lines with a current-carrying capacity of 680 A [7, 8, 12]. This expansion variant could imply the reinforcement of the electricity pylons if the existing ones do not comply with the weight of the double line systems, which would lead to further investment costs.

If the second expansion measure, after renewing the grid analysis, does not prove to be enough to remedy the identified congestion, the single conductor lines are then replaced by two bundle conductors with a combined current-carrying capacity of 1360 A [7, 8, 12]. If this is still insufficient, the OHL systems are preferably replaced with UGCs. As many cables as necessary are then applied in parallel to overcome the identified congestion.

In order to ensure a uniform static load on electricity pylons, parallel systems of the same line segment (LS) are expanded identically, even if only one system is overloaded [7, 12].

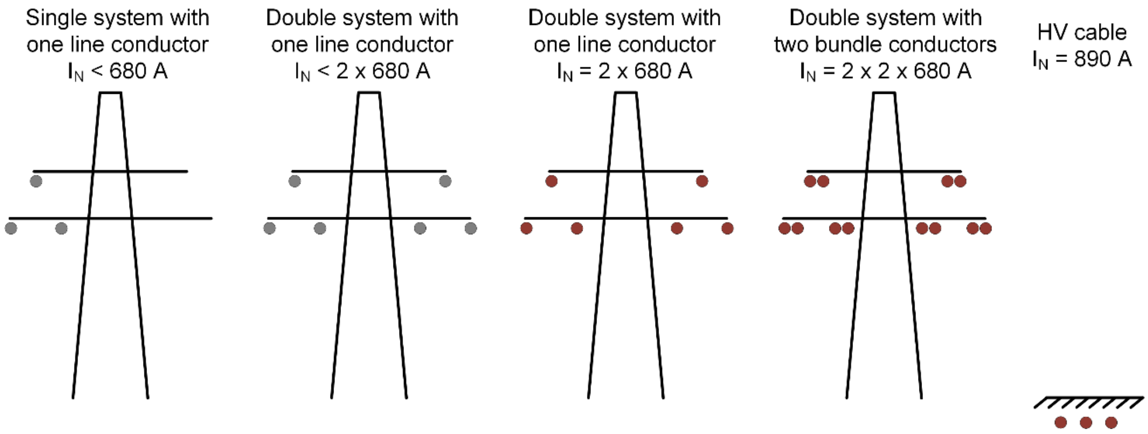

Figure 2-2 Expansion stages of power lines in the HV grid within the classical grid planning [7]

In addition to the grid expansion with OHLs and cables, the modification of the switching state of the grid or the addition of a new 380 kV substation could be adopted as a further measure to reduce overloads [8]. However, switching measures have only a limited impact on reducing grid overloads, and the integration of a new 380 kV connection point is only possible when a 380 kV grid is near the overloaded line. Moreover, the integration of a new 380 kV connection point could lead to further CGE measures being required in the 110 kV grid [8].

Once all the required CGE measures have been identified, a calculation of the expansion costs is performed based on the investment costs of the equipment.

2.1.5.2 Determination of the CGE Measures Required in MV Grids

In a first step, the prognosticated installed power of additional loads and RES is allocated to the appropriate power grids and distributed over the grid nodes. In the next step, an analysis of the grid state is realized for both high load and high generation cases in order to identify eventual grid congestion.

After identifying the prognosticated grid congestion, the measures required to prevent these congestions are determined stepwise. There is no single uniform guideline for the determination of the required measures in the MV grid. Grid operators also have recourse here to standard equipment and common methods to prevent prognosticated overloads.

These methods include, for instance, the adjustment of the operation point of HV/MV transformers mainly to remedy voltage range violations. This corrective measure can also be realized during the operation of the HV/MV transformer with the help of on-load tap-changers [7].

Another method to overcome voltage violations consists of splitting the feeder, on which the voltage violation has been determined, between the transformer busbar and the furthest critical node. The disconnected feeder is then directly connected to the transformer busbar, which reduces the load flow through the original feeder and the feeder impedance, and leads, thus, to the reduction of the node voltages [7, 8].

In the case of overloaded transformers or lines, switching measures can be applied to improve the load flow through the grid components and reduce limit violations. Alternatively, the overloaded components are reinforced or replaced by equipment with a higher current-carrying capacity [8, 14, 15].

After each measure has been applied, the load flow is calculated and the grid is analyzed to determine the impact of the applied measure on the grid state. Once all required CGE measures have been identified, the grid expansion costs can finally be calculated based on the investment costs of the measures.

2.1.6 Limits of the Classical Grid Planning Method

As described in the previous sections, the classic grid planning is realized based on a deterministic approach, where only the high load and the high generation cases are considered [7, 8, 16]. Yet, this deterministic approach considers neither the variability and fluctuation of the connected loads and RES nor the frequency of occurrence of these extreme load and generation scenarios, which can lead to an undersizing or an oversizing of the power grid [17, 18].

An evaluation of the traditional grid planning methods is given in [19]. The underlined limits and deficits here consist, among other things, of the poor degree of automation of these methods and the noninclusion of innovative technologies, such as PC and the application of BSS.

Furthermore, although the German regulatory framework dictates a cost-efficient grid expansion for both utility and customer, the costs of the expansion measures are not considered directly in the planning process. The costs are generally calculated after determining the required measures [7, 8]. Moreover, standardized financial analysis models have not yet been adopted [19].

2.2 Innovative Technologies and Grid Planning Methods

2.2.1 Use of Grid-Supporting Battery Systems in the Grid Planning

Several works have treated the application of storage systems to prevent grid congestion or contribute to grid-supporting ancillary services. Many research papers propose the use of BSS for grid-supporting peak shaving [20, 21, 22], or to reduce the power losses in distribution grids [23, 24, 25]. In other works, the contribution of BSS to voltage stability in the grid is examined [26, 27, 28]. The use of BSS to prevent overloads of power lines in consideration of an optimal dimensioning and placement of the storages is investigated in [29, 30]. An application of the BSS for the fulfillment of the (n-1) criterion in HV distribution grids is proposed in [31, 32]. A combined use of BSS and PC of RES to prevent grid congestion is considered to fulfill the (n-1) criterion and improve the grid planning in [33, 34, 35].

Apart from research work, the first real application of large-scale battery systems in the grid planning in Germany was proposed by German EHV grid operators in the power grid development plan 2030 [36]. This concept consists of integrating large-scale batteries, “grid boosters” of the order of several hundreds of megawatt hours, in the EHV grid combined with redispatch application to reach a higher utilization of the existing power lines in the grid in consideration of the (n-1) criterion. The classic definition of the (n-1) security criterion implies the operation of the lines with less than their real current-carrying capacity during the normal (n-0) state, hence, maintaining a reserve for the power transmission in case of a (n-1) outage. This new grid booster concept, however, suggests the operation of the power lines with 100 % of their current-carrying capacity during the (n-0) state. In the case where a (n-1) line outage occurs in the grid, a short-term overload of the power lines with values in a range of 4000 A are permitted by the time further curative measures take effect. A grid booster placed after the line congestion and a controlled load placed before the line congestion are intended as curative measures and will be activated in order to maintain the loading of the line beneath its current-carrying capacity. The activation of the grid booster must be fast, but takes effect after the activation of the power system protection that is in the range of 100 ms. This reduces the requirements concerning the activation time of the boosters [36].

The grid operators intend to apply this concept as a preventive measure only for the (n-0) state. For the (n-1) state, the grid boosters combined with redispatch measures will be applied curatively as a corrective measure that encroaches after the occurrence of an outage. This concept deviates from the classic (n-1) criterion definition and hence does not comply with the state-of-the-art planning and operation principles of the power grid. It also allows the shutdown of RES, for example, offshore wind farms, as a redispatch measure, thus, renouncing the feed-in priority of RES into the grid [36].

2.2.2 Use of Power Curtailment in the Grid Planning

The very high feed-in power of RES into the grid could lead to grid congestion or a noncompliance with the (n-1) criterion because of the limited transmission capacity of the lines. The PC of RES is principally a last resort to prevent prognosticated grid congestion by decreasing the high feed-in power values of RES. Due to the slow progress in getting building permits for new power lines and the low social acceptance toward CGE, the German Energy Industry Act (EnWG) introduced the PC as a further degree of freedom in the grid planning. According to paragraph §11 of the EnWG, grid operators are allowed to plan the power grid considering a 3 % reduction of the annual prognosticated energy of every PV or wind plant that is connected to the grid [3].

The Forum Network Technology/Network Operation in the VDE released a guideline discussing the application variants of PC in the grid planning in consideration of the allowed 3 % limit [37]. These variants can be separated into two categories: the static PC and the DPC.

The static PC variant implies a permanent reduction of the maximal possible feed-in power of a power plant. The maximal feed-in power is, thus, limited to a predefined constant value that is lower than the possible one. In order to define its reduced maximal power, the original maximal power of the plant is multiplied by a specific reduction factor, depending on the plant type. The static PC can be realized using constant standardized reduction factors for PV and wind plants or individual reduction factors that depend on the load duration curve of each plant [37]. The advantage of this variant is that no extra communication infrastructure is needed to control or monitor the plants.

Unlike the static PC, where the original maximal power of all plants is permanently reduced to a specific lower value, the DPC reduces the feed-in power of every plant individually and situationally depending on the prognosticated grid congestion [37]. The curtailed feed-in power over a period of time depends on the extent of the congestion and the relevance of the plant to prevent the congestion. Consequently, the time series-based DPC does not reduce the maximal possible feed-in power of the plants sweepingly but, instead, reduces the feed-in power of every plant over limited periods of time individually. In this way, unnecessary PC can be avoided. This variant, thus, enables a targeted and more effective use of the 3 % permitted curtailment limit.

The consideration of the PC in the planning process of power grids enables a reduction of the required CGE measures and, thus, cost savings. Consequently, the power grid does not have to be designed according to very high generation cases that occur only rarely. In addition, the PC variant adopted in the planning process has a great influence on the planning results. In the following, an overview of research works applying PC in the grid planning is given.

Two approaches for the application of the dynamic PC in the planning process of HV grids are suggested in [18]. The first is an iterative process which treats line overloads in consideration of the (n-1) criterion in sequential steps. The line with the highest prognosticated overload is considered first. The node with the highest impact on the line overload is then determined and used for the application of the PC. The state of the grid is then analyzed again. In case of remaining overloads, the process is renewed, beginning again with the highest determined overloaded line. This approach enables the overload problems to be remedied, yet does not consider the 3 % curtailment limit for every plant in the sequential process. Furthermore, this approach can lead to a bigger reduction of the line loading than is actually needed and, hence, to an unnecessary curtailment of RES since it considers only one overloaded line at a time [18].

The second approach suggested in [18] is based on a linear optimization which minimizes the curtailed energy over the simulated time. The implemented constraints limit the load flow to the power-carrying capacities of the lines. The second approach is more efficient than the first suggested one, but, depending on the grid and the prognosticated overloads, it cannot always remedy all the overloads prognosticated in the grid due to the 3 % curtailment limit. Therefore, a simplified stepwise determination of the required CGE is realized after the application of the PC. The combination of the DPC and the CGE measures in the same optimization to determine the best planning solution and reduce unnecessary curtailment and CGE measures has not been considered in [18]. The contribution of the DPC in reducing the total costs of the grid expansion has not been treated either.

In the grid study [7], a static PC with individual factors has been considered in the grid planning. The contribution of the PC to reducing CGE measures and saving expansion costs are illustrated here. Nonetheless, the static PC variant applied in [7] based on individual factors is not as efficient as the dynamic PC and leads to the unnecessary curtailment of RES even when no grid congestion is prognosticated. This reduces the amount of curtailable energy left to prevent congestion.

2.2.3 Innovative Planning Methods

The increasing call for the application of innovative planning instruments in the grid planning also implies the adaptation of the classic planning method to these innovative instruments. Accordingly, the classic planning method must be adjusted toward more automation of the planning process. In addition, an overall consideration of the planning instruments must be made in order to take advantage of the synergy between these instruments. Furthermore, the inclusion of the costs in the grid planning process is also necessary to ensure a cost-efficient application of these innovative instruments in the grid planning.

New grid expansion methods for distribution grids are proposed in [38, 39] to automate the grid planning process using expansion factors to determine the lines that must be expanded. In these methods, the required CGE measures are determined iteratively by treating one grid congestion at each iteration. A PC of RES is also realized in [38] before application of the CGE measures in order to reduce the power feed-in into the grid. This leads to the reduction of the required CGE measures, but does not necessarily ensure the cost optimal planning solution of the grid, because the PC and costs occurring are not considered within the grid expansion process.

A genetic algorithm (GA) is proposed in [40] to model a multistage distribution grid expansion planning and storage deployment. The fitness of the GA considers here the investment and the operating costs for each investment stage. However, the investment costs of the storages are not considered in the fitness and, thus, in the decision-making process. The authors consider that the storage units already exist in the grid and are not owned by the distribution system operator (DSO) but only used based on contracts for grid services for an annual fee. On the other hand, the profits made from the energy trade in the market are included in the operating costs and, thus, in the fitness, which is contradictory. Such an application of storages in the grid planning is not efficient since the DSO would be dependent on the location of existing storages and, consequently, cannot place the storages depending on the grid requirements. Furthermore, the GA may fail to find the global optimum for complex problems. In fact, the GA tends to converge toward local optima, because the final solution generally represents only the better solution in comparison to the other solutions found.

A multistage expansion method for active distribution networks using centralized and distributed energy storage systems is proposed in [41]. The co-optimization model used aims at the minimization of the total cost of the network investment and operation. The method has been validated on a 20 kV grid for an extreme daily load scenario. The application of the method on high generation cases has not been considered here. The reactive power has also been neglected in this case, which leads to nodal voltage and power flow errors that can have an influence on the planning results.

2.3 Differentiation from Other Works

The novelties of the planning method proposed in this thesis consist, firstly, of the extension of the classic grid planning approach based on OHLs or UGCs to include the application of BSS and DPC as innovative planning instruments. The use of BSS and DPC aims here to fulfil the required planning principles including compliance with the voltage limits for MV grids and the classic definition of the (n-1) criterion for HV grids, thus, enabling a higher utilization of the existing grid and a reduction of the required CGE measures. The proposed approach offers a preventive and corrective concept for planning and operating the power grid because it intervenes in the operation of the power lines already during the normal (n-0) state, enabling a higher utilization of the power line capacity during this state and ensuring the safe operation of the power lines without any overload in case an (n-1) outage occurs.

Secondly, unlike classic planning methods, a time series-based environment is implemented here in order to simulate the variability of loads and RES feed-in power and reproduce realistic scenarios of the grid state. The time series-based environment in this work represents a prerequisite for the application of the BSS and DPC. Furthermore, the total costs of the grid expansion measures are considered in this work within the planning process and not after determination of the required expansion measures as is the case in the classic planning methods. The proposed optimized planning approach, therefore, delivers the most cost-efficient solution of the grid planning, subject to the correspondent planning principles. The delivered results include the most cost-efficient measures to expand the grid, including the type of CGE measures, the dimensioning and placement of the BSS, and the scheduling of the BSS and DPC.

In addition, unlike the multistage planning methods stated in 2.2.3, the new planning approach proposed in this work is a single-stage method which considers all planning instruments simultaneously in the decision-making process. The aim of this combined consideration is to ensure the most cost-efficient application of the instruments and, hence, the most economical grid planning solution. Accordingly, an automated planning algorithm based on an MILP is implemented to minimize the total investment, and the replacement and operating costs of all considered planning instruments at the same time. Grid operators have so far applied stepwise and iterative methods for the grid planning, where each congestion is treated separately by applying conventional planning instruments. However, the application of each planning instrument separately and out of a global optimization cannot guarantee the cost optimal solution. Therefore, the proposed planning algorithm could offer a cost optimizing planning alternative.

Furthermore, a multiuse application of BSS is considered in this work, combining the previously described grid-supporting use of the BSS with a market-based application to generate profits from the electricity trade and, hence, reduce the total costs of the BSS.

3 Generation of the Input Data

The generation of the time series for loads and RES, the modelling of the power grid and the LFC realized in this work depend on the grid voltage level. In this chapter, the methods adopted for the generation of the input data depending on the voltage grid level are described in detail.

3.1 Modelling of a High-Voltage Grid

In what follows, the time series generation, the topology of the HV grid modelled and the linearization method of the load flow calculation LFC are described.

3.1.1 Generation of the Time Series for Load and RES Power

A real 110 kV grid in Germany was modelled as a test grid in order to verify the planning algorithm proposed in this work. The modelling of the HV grid and the simulation of the time series for the power of the loads and RES connected in the grid were realized based on the research work [18], in which the adopted approach is described in detail. The time series of the RES power was generated based on measurements in reference power plants. Only measurements of the residual power in HV/MV substations are available, therefore, the power time series of the connected loads in the underlying voltage grids was calculated by subtracting the simulated RES power from the residual power measured in the HV/MV substations (passive sign convention). In a further step, the time series of the RES power was normalized and upscaled, depending on the prognosticated installed RES power for the target year 2030. Following that, the time series of the residual load regarding the expansion scenario 2030 was calculated by the addition of the upscaled time series for the RES power to the time series of the load. It was assumed in this process that the connected load in the grid remains unchanged until 2030 [18]. Table 3-1 shows the adopted PV, wind and load installed by 2030 in the grid analysis.

Table 3-1 PV, wind and load installed in the modelled HV grid

Installed PV power by 2030 / MW	895.27
Installed Wind power by 2030 / MW	596.60
Installed load by 2030 / MW	1325.55

3.1.2 Topology of the Modelled Real Grid

Table 3-2 summarizes the characteristics of the considered HV grid, including the number of nodes and lines and the total length of the power lines.

Table 3-2 Characteristics of the modelled HV grid

Voltage level	110 kV
Nodes' number	41 nodes
Power lines' number	79 lines
Total length of the power lines	708 km

Figure 3-1 shows a simplified representation of the part of the modelled HV grid which showed grid congestion in the grid analysis, and is, therefore, relevant for the grid planning. The grid part shown comprises nine nodes representing HV/MV substations and two representing EHV/HV substations. For reasons of simplification, the subordinate connected loads, PV and wind plants under every HV/MV substation were aggregated according to the plant type and represented respectively through one element of each type. Most of the HV lines are designed and operated in the form of two parallel OHL systems that are carried by the same electricity pylon, as shown in the figure. The parallel OHL systems constitute together an LS. Figure 3-1 illustrates the relevant LSs that were considered in this work for the fulfilment of the grid restrictions. Each LS represents, depending on the grid design, one or two parallel line systems including the electricity pylons. The black dots here represent the junctions between two or three power lines.

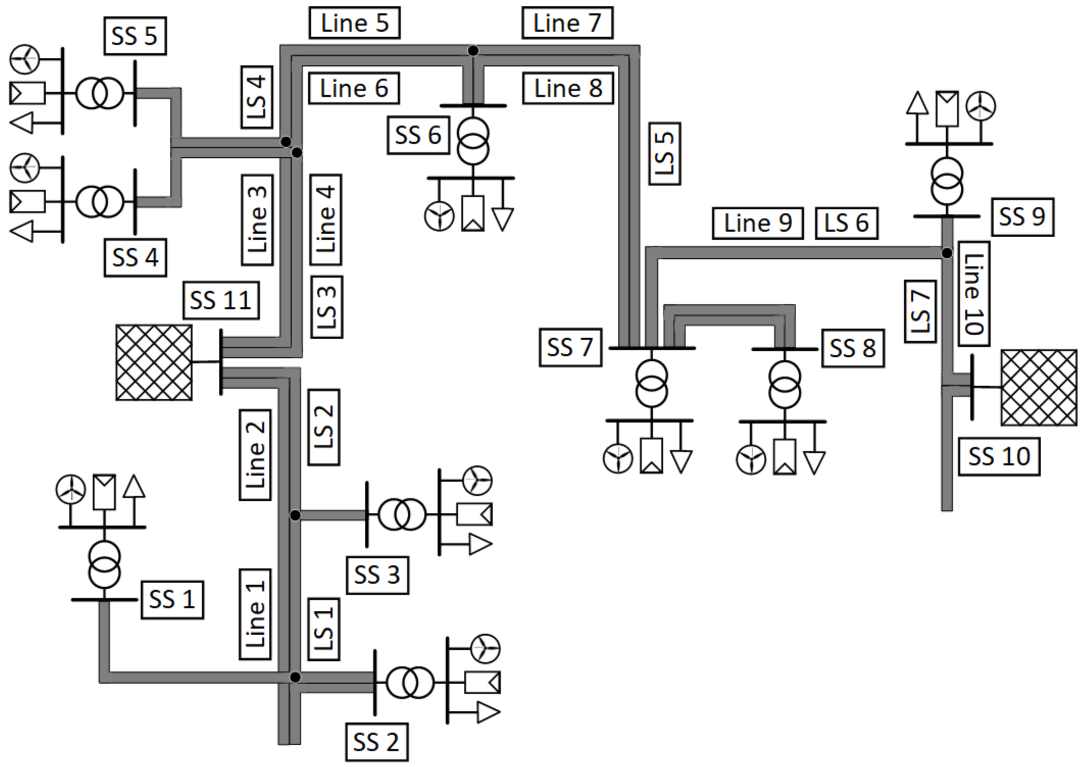

Figure 3-1 Simplified representation of a part of the modelled HV grid

3.1.3 Linearization of the Load Flow Calculation

In a further step, the LFC in HV grids were linearized in consideration of all possible (n-1) line outages in the grid according to the method proposed in [18, 42, 43]. The linear contingency analysis adopted uses distribution factors in order to distribute the nodal power over the lines depending on the (n-1) state of the grid. The $(NACLODF)$ matrix is three-dimensional and contains the distribution factors of the nodal active power for all possible (n-1) line outages, depending on the grid topology and line impedances [18]. In this work, the (n-0) state was also included in this matrix in order to consider the (n-0) state and all possible (n-1) states of the lines in the grid. The column vector of the power flow through the grid lines $(P_{L,t})^{(a)}$ for a considered grid state a is the product of the matrix $(NACLODF)^{(a)}$ and the column vector of the power injection in the nodes $(P_{N,t})$ at a time step t:

$$(P_{L,t})^{(a)} = (NACLODF)^{(\mathrm{a})} \cdot (P_{N,t}) \tag{1}$$

$$\forall\, a \in A, \forall\, t\ \in T_{year,q}$$

$(P_{L,t})^{(a)}$	Column vector of the power flow through the grid lines at time step t for the line state a in MW
$(P_{N,t})$	Column vector of the original residual power injection in the grid nodes at time step t in MW
$(NACLODF)^{(\mathrm{a})}$	Matrix containing the distribution factors of the nodal injection power for the line state a

A is here the set of the line outages considered, consisting of all (n-1) line states and the (n-0) state. The load flow linearization according to [18] implies a decoupling between the active and reactive load flow. The evaluation of the accuracy of the linearized LFC in that work revealed that the linearization of the reactive load flow is associated with a higher error than that of the active load flow [18]. In addition, the planification of the HV grid in this work aims to prevent grid congestion, basically due to the high active power feed-in from RES into the grid. On these grounds and for reasons of simplification, the reactive power flow was not considered here in the examination of the line load and the planification of HV grids, unlike [18]. The apparent load flow $S_{l,t}^{(a)}$ on a line l for a considered state a at a time step t was, thus, approximated to the active power flow through the line:

$$S_{l,t}^{(a)} \approx P_{l,t}^{(a)} \tag{2}$$

$$\forall\, l \in L, \forall\, a \in A, \forall\, t\ \in T_{year,q}$$

$S_{l,t}^{(a)}$ Apparent power flow through a line l for a grid state a at time step t in MVA

$P_{l,t}^{(a)}$ Active power flow through a line l for a grid state a at time step t in MW

The planning principles in the HV grid imply the fulfilment of the (n-1) criterion for all lines of the grid. In order to save computational time and memory space, only critical line outages were considered within the grid planning process in this work. Accordingly, a contingency analysis of the grid was initially realized, based on the linearized LFC according to the 2030 scenario. The overloaded lines in the grid and the critical line outage which leads to the maximum overload of each line over the considered year were then determined. These critical outages are considered for the grid planning in this work.

3.2 Modelling of a Medium-Voltage Grid

The following sections outline the methodology adopted to model a real MV grid, including the generation of power time series for loads and RES, implementation of the grid components and linearization of the LFC.

3.2.1 Topology of the Modelled Grid

In order to test and verify the proposed planning algorithm for MV grids, a real 20 kV grid in Germany was implemented. The modelled MV grid is one of three MV subordinate grids connected in the municipality. Table 3-3 summarizes the characteristics of the modelled MV grid including the number of nodes and power lines.

Table 3-3 Characteristics of the modelled MV grid

Voltage level	20 kV
Nodes' number	132 nodes
Power lines' number	131 lines
Total length of the power lines	71.4 km

Figure 3-2 shows a simplified representation of the MV grid (MV Grid 1) considered in this work. The grid is designed mostly based on an open ring structure. Due to the high number of nodes and lines in the MV Grid 1, only the nodes and lines which show congestion are illustrated and numbered in the figure. The MV grid includes PV plants distributed over 76 nodes and wind plants which are connected directly to the main 20 kV busbar (node 1) through line 1.

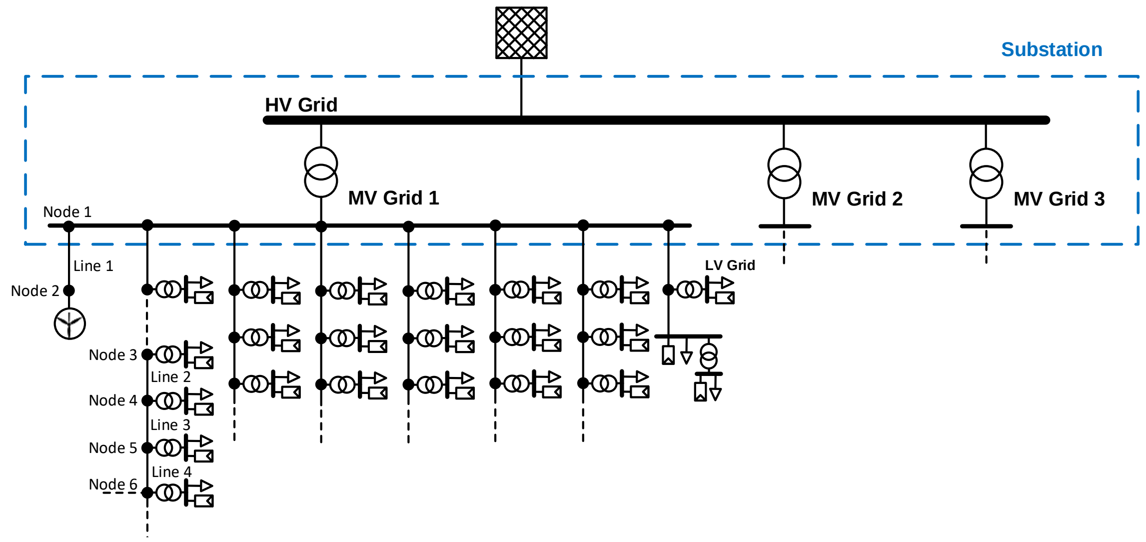

Figure 3-2 Simplified representation of the modelled MV grid (MV Grid 1)

3.2.2 Generation of the Time Series for Load and RES Power

Contrary to the HV grids, it is not common to carry out measurements at the MV level. Therefore, no time series were initially available for the injection power on the grid nodes in this work. In order to analyze the state of the grid and determine the expansion measures required, it was, thus, necessary to generate power time series for the connected loads and generators and adapt them to the expansion scenario 2030. Accordingly, the following input data was provided from the system operator [44]:

- The measured time series of the residual load on HV/MV transformers for the year 2017 with 15 minutes time resolution
- The power of RES and loads installed on every MV node in 2017
- The normalized time series for reference PV, wind and biogas plants in the considered region
- The total power of PV, wind and biogas plants installed in the considered region comprising eight MV grids in 2017
- The estimated scaling factors for the total power of PV, wind and biogas plants installed in the considered region according to the scenario 2030

In a first step, the time series of the cumulated RES at the HV/MV transformer was calculated for every RES type using the corresponding installed power in 2017 and the normalized reference time series.

$$P_{RES,T,2017,t} = P_{RES,T,2017} \cdot P_{RES,Ref,t} \qquad (3)$$

$$\forall\, t \in T_{year,q}$$

$P_{RES,T,2017,t}$ Cumulated feed-in power of RES on transformer T at time step t for the scenario 2017 in MW

$P_{RES,T,2017}$ RES power installed in the grid that is connected to the transformer T for the scenario 2017 in MW

$P_{RES,Ref,t}$ Normalized active power value to 1 MW of a reference RES plant at time step t

The time series of the cumulated load $P_{L,T,2017,t}$ at the HV/MV transformer were then calculated as the difference between the measured residual load $P_{T,2017,t}$ and the feed-in power of the RES (passive sign convention).

$$P_{L,T,2017,t} = P_{T,2017,t} - P_{PV,T,2017,t} - P_{Wind,T,2017,t} - P_{Bio,T,2017,t} \tag{4}$$

$$\forall\, t \in\, T_{year,q}$$

$P_{L,T,2017,t}$ Cumulated load power on the transformer T at time step t for the scenario 2017 in MW

$P_{T,2017,t}$ Residual active power on the transformer T at time step t in MW

$P_{PV,T,2017,t}$ Cumulated feed-in power of PV on transformer T at time step t for the scenario 2017 at time step t in MW

In a further step, the time series of the load on every node was calculated by dividing the time series of the cumulated load at the HV/MV transformer on the MV nodes, depending on the share of the node in the total installed load.

$$P_{L,i,2017,t} = P_{L,T,2017,t} \cdot \frac{P_{L,i,2017}}{P_{L,T,2017}} \tag{5}$$

$$\forall\, i \in N, \forall\, t \in\, T_{year,q}$$

$P_{L,i,2017,t}$ Load power on a node i at time step t in MW

$P_{L,i,2017}$ Load installed on a node i of the grid for the scenario 2017 in MW

$P_{L,T,2017}$ Load power installed in the grid that is connected to the transformer T for the scenario 2017 in MW

The scaling factors, shown in Table 3-4, were provided by the grid operator of the region for the estimation of the installed RES power by 2030 [44]. These factors illustrate the estimated expansion of RES in the entire region by 2030. The considered region comprises four municipalities with a total of eight MV grids and the examined MV is one of these eight grids. The total power of RES installed in the entire region by 2030 was, thus, calculated depending on the installed power by 2017 and the scaling factors. The additional RES capacity was then calculated as the difference between the total estimated capacity by 2030 and the power already installed in 2017. In a further step, the additional RES capacity was evenly distributed over the MV grids of the considered region.

Table 3-4 Scaling factors adopted for PV, wind and biomass capacities in the entire region, according to the scenario 2030 [44]

	PV	Wind	Biomass
2017	1	1	1
2030	1.86	4.63	1.06

After that, the time series for PV, wind and biogas power on the nodes of the examined MV grid was calculated for the scenario 2030. The calculation was realized depending on both the installed power in the grid in 2017 and the additional RES power by 2030, as well as on the normalized reference time series according to the RES type.

$$P_{RES,i,2030,t} = \frac{(P_{RES,add,T,2030} + P_{RES,T,2017})}{P_{RES,T,2017}} \cdot P_{RES,i,2017} \cdot P_{RES,Ref,t} \quad (6)$$

$$\forall\, i \in N, \forall\, t \in T_{year,q}$$

$P_{RES,i,2030,t}$ Injection power of RES on a node i at time step t for the scenario 2030 in MW

$P_{RES,add,T,2030}$ Additional RES power installed in the grid connected to the transformer T for the scenario 2030 in MW

$P_{RES,i,2017}$ RES power installed on a node i for the scenario 2017 in MW

Table 3-5 summarizes the PV and wind power installed as well as the load installed for the scenario 2030.

Table 3-5 PV, wind and load installed in the modelled MV grid

Installed PV power by 2030 / MW	30.25 (connected to 76 nodes)
Installed Wind power by 2030 / MW	19.44 (connected to 1 node)
Installed load / MW	23.8

Figure 3-3 shows the active power injection values of all PV power plants in the grid for all days of the considered year, according to the feed-in scenario 2030. The maximal active power injection of PV on one node is around 2 MW. Figure 3-4 shows the active power injection of the wind plants connected to the grid via node 2 for all days of the considered year. The maximal active power injection according to the scenario 2030 amounts to about 19.4 MW on this node.

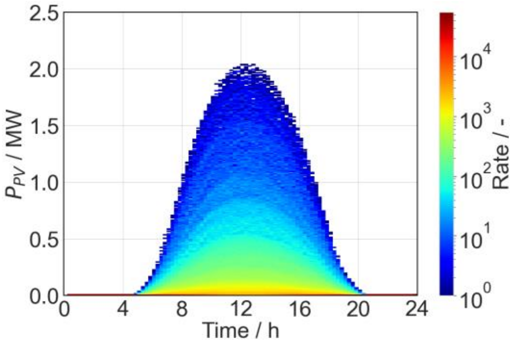

Figure 3-3 Histogram of the active power injection of all PV plants for the scenario 2030

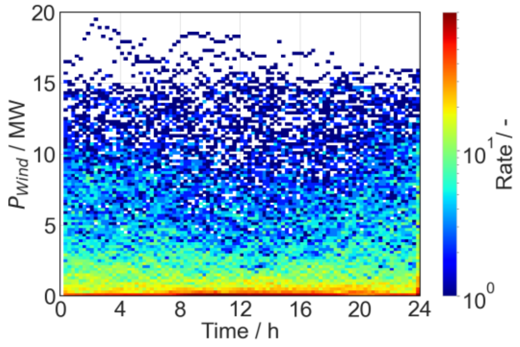

Figure 3-4 Histogram of the active power injection of the wind plants for the scenario 2030

Figure 3-5 shows the active power of all loads connected to the grid for all days of the year. It can be seen from the figure that the maximal load reached on one node is about 2.3 MW. Figure 3-6 represents the residual loads on all nodes of the MV grid for all days of the considered year 2030. The residual load values on the MV nodes are steadily below 2.3 MW, but can reach negative values of −19.4 MW on the connection node of the wind plants (node 2) at certain points in time.

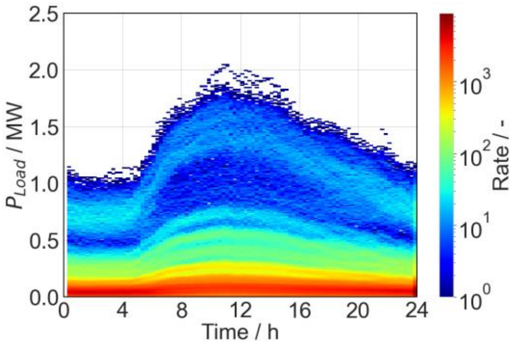

Figure 3-5 Histogram of the active power of the loads connected to the grid

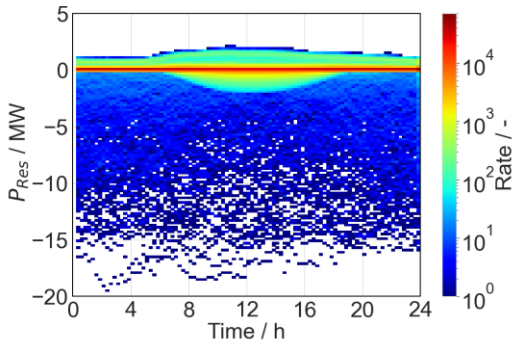

Figure 3-6 Histogram of the active residual load on all nodes of the grid

The reactive power injection of loads, PV and wind plants was considered subject to a constant power factor $\cos\varphi$ delivered for every plant and load in the input data [44].

3.2.3 Implementation of the Grid Components

The modelling of the MV grid was realized according to the parameters of the grid components, including buses (nodes), loads, generators and power lines. The solver PYPOWER was used for the modelling of the grid components and the LFC. PYPOWER is a solver that can be applied for power flow and optimal power flow calculations. The open-source software is a driven version from MATPOWER and supports the programming language Python. The parameters of the grid have to be assigned to the solver in definite matrix form for loads (bus), power lines (branch) and generators (gen).

3.2.4 Linearization of the Load Flow Calculation

The linearized LFC for MV grids adopted in this work is based on the Newton-Raphson load flow method. The principles of the LFC according to the Newton-Raphson method are described in the following sections [45, 46]. An outline of the methodology adopted for the linearization of the LFC is then given. After that, the quality of the linearization method is evaluated.

3.2.4.1 Load Flow Calculation according to the Newton-Raphson Method

Assuming a function $f(x)$, the tangent $t_0(x)$ of the function at the point x_0 can be written as:

$$t_0(x) = f(x_0) + f'(x_0) \cdot (x - x_0) \tag{7}$$

As shown in Figure 3-7, the tangent $t_0(x)$ represents the best linear approximation of the function $f(x)$ at point x_0. Based on that, the Newton-Raphson method approximates iteratively the root of the function $f(x)$ to the roots of its tangents, which delivers for the first iteration beginning with the tangent $t_0(x)$ of the function at the point x_0:

$$t_0(x_1) = f(x_0) + f'(x_0) \cdot (x_1 - x_0) = 0 \ \approx f(x_1) \tag{8}$$

$$\Rightarrow \ x_1 = \ x_0 - \frac{f(x_0)}{f'(x_0)} \tag{9}$$

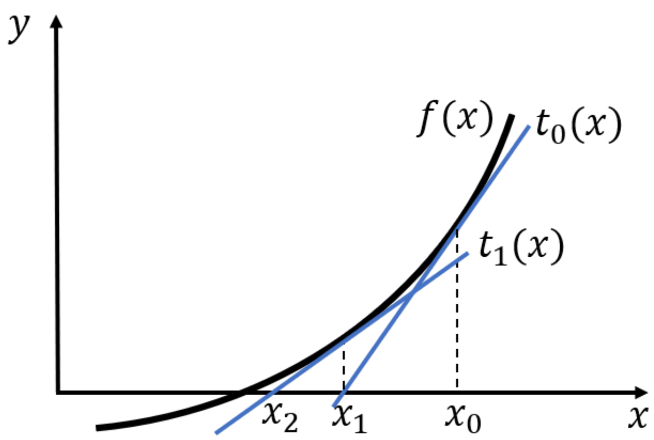

Figure 3-7 Newton-Raphson approximation method of the root of a single-variable function

The better approximated root of the function at every iteration is then used as the starting point in the next iteration.

$$x_{n+1} = x_n - \frac{f(x_n)}{f'(x_n)} \tag{10}$$

Assuming a multivariable function $f(x_1, x_2, \dots, x_n)$ with n variables, where $x_1^*, x_2^*, \dots, x_n^*$ represent the starting point for the iterative approximation of the function's root, and $x_1^{**}, x_2^{**}, \dots, x_n^{**}$ represent the root of the function's tangent at that point. The function at that starting point could be then written for the first iteration as follows:

$$-f(x_1^*, x_2^*, \dots, x_n^*) = \frac{\partial f}{\partial x_1}(x_1^*) \cdot \Delta x_1 + \frac{\partial f}{\partial x_2}(x_2^*) \cdot \Delta x_2 + \dots + \frac{\partial f}{\partial x_n}(x_n^*) \cdot \Delta x_n \tag{11}$$

$$\text{with } \Delta x = x^{**} - x^*$$

In relation to the LFC, the multivariable function $f(x_1, x_2, \dots, x_n)$ is assumed to be the difference between the set injection power and the injection power value calculated on a node i subject to the node voltage magnitudes and voltage angles of all the nodes of the grid in the per-unit system:

$$\Delta p_i = p_{set,i} - p_i(\vartheta, u) = p_{set,i} - u_i \sum_{j=1}^{n} y_{ij} \cdot u_j \cdot cos\left(\vartheta_i - \vartheta_j - \alpha_{ij}\right) \tag{12}$$

$$\forall\, i \in \{1,2,\dots,n\}$$

$$\Delta q_i = q_{set,i} - q_i(\vartheta, u) = q_{set,i} - u_i \sum_{j=1}^{n} y_{ij} \cdot u_j \cdot sin(\vartheta_i - \vartheta_j - \alpha_{ij}) \tag{13}$$

$$\forall\, i \in \{1,2,\dots,n\}$$

$p_{set,i}$	Set active injection power at a node i in pu
$q_{set,i}$	Set reactive injection power at a node i in pu
$p_i(\vartheta, u)$	Active injection power calculated at a node i in pu
$q_i(\vartheta, u)$	Reactive injection power calculated at a node i in pu
Δp_i	The difference between the set active injection power and the active injection power value calculated at a node i in pu
Δq_i	The difference between the set reactive injection power and the reactive injection power value calculated at a node i in pu
ϑ_i	Voltage angle on a node i in rad
u_i	Voltage magnitude at a node i in pu

y_{ij} Admittance value of the line between node i and j in pu

α_{ij} Admittance angle of the line between node i and j in rad

With the help of the Newton-Raphson approximation as described above, the equations (12) and (13) can then be stated for the first iteration as follows:

$$\Delta p_i = \sum_{j=1}^{n-1} \frac{\partial p_i}{\partial \vartheta_j}(\vartheta_j) \cdot \Delta\vartheta_j + \sum_{j=1}^{n-1} \frac{\partial p_i}{\partial u_j}(u_j) \cdot \Delta u_j \text{ , } \forall\, i \in \{1,2,\dots,n-1\} \tag{14}$$

$$\Delta q_i = \sum_{j=1}^{n-1} \frac{\partial q_i}{\partial \vartheta_j}(\vartheta_j) \cdot \Delta\vartheta_j + \sum_{j=1}^{n-1} \frac{\partial q_i}{\partial u_j}(u_j) \cdot \Delta u_j \text{ , } \forall\, i \in \{1,2,\dots,n-1\} \tag{15}$$

Where n is the number of the nodes in the grid including the slack node, whose node voltage value and voltage angle are assumed to be known. Therefore, the equations (14) and (15) are not considered for the slack node. For the rest of the n-1 nodes, the equations can be written in the form of the following matrix system [45]:

$$\begin{pmatrix} (\Delta p) \\ (\Delta q) \end{pmatrix} = (J) \cdot \begin{pmatrix} (\Delta\vartheta) \\ (\Delta u) \end{pmatrix} \tag{16}$$

Where (J) is the Jacobian matrix containing all the first-order partial derivations of (Δp) and (Δq) in the function of the node voltage magnitudes and voltage angles

$$\begin{pmatrix} (\Delta p) \\ (\Delta q) \end{pmatrix} = \begin{pmatrix} \begin{pmatrix} \frac{\partial p_1}{\partial \vartheta_1} & \cdots & \frac{\partial p_1}{\partial \vartheta_{n-1}} \\ \vdots & \ddots & \vdots \\ \frac{\partial p_{n-1}}{\partial \vartheta_1} & \cdots & \frac{\partial p_{n-1}}{\partial \vartheta_{n-1}} \end{pmatrix} & \begin{pmatrix} \frac{\partial p_1}{\partial u_1} & \cdots & \frac{\partial p_1}{\partial u_{n-1}} \\ \vdots & \ddots & \vdots \\ \frac{\partial p_{n-1}}{\partial u_1} & \cdots & \frac{\partial p_{n-1}}{\partial u_{n-1}} \end{pmatrix} \\ \begin{pmatrix} \frac{\partial q_1}{\partial \vartheta_1} & \cdots & \frac{\partial q_1}{\partial \vartheta_{n-1}} \\ \vdots & \ddots & \vdots \\ \frac{\partial q_{n-1}}{\partial \vartheta_1} & \cdots & \frac{\partial q_{n-1}}{\partial \vartheta_{n-1}} \end{pmatrix} & \begin{pmatrix} \frac{\partial q_1}{\partial u_1} & \cdots & \frac{\partial q_1}{\partial u_{n-1}} \\ \vdots & \ddots & \vdots \\ \frac{\partial q_{n-1}}{\partial u_1} & \cdots & \frac{\partial q_{n-1}}{\partial u_{n-1}} \end{pmatrix} \end{pmatrix} \cdot \begin{pmatrix} (\Delta\vartheta) \\ (\Delta u) \end{pmatrix} \tag{17}$$

The correction of the node voltage magnitudes and voltage angles can be calculated for the n-1 nodes at every iteration with the help of the inverse of the Jacobian matrix

$$\begin{pmatrix} (\Delta\vartheta) \\ (\Delta u) \end{pmatrix} = (J^{-1}) \cdot \begin{pmatrix} (\Delta p) \\ (\Delta q) \end{pmatrix} \tag{18}$$

And the better approximation of the voltage angles and magnitudes can be, hence, determined iteratively

$$\vartheta_i{}^{(\nu+1)} = \vartheta_i{}^{(\nu)} + (\Delta\vartheta_i)^{(\nu)}, \forall\, i \in \{1,2,\dots,n-1\} \tag{19}$$

$$u_i^{(\nu+1)} = u_i{}^{(\nu)} + (\Delta u_i)^{(\nu)}, \forall\, i \in \{1,2,\dots,n-1\} \tag{20}$$

where ν is an iteration count. The Jacobian matrix and the power mismatch in each new iteration are recalculated depending on the latest approximated voltage and angle values. The iterative process is carried on until the power mismatch falls below a predefined accuracy level ε:

$$\Delta p < \varepsilon \text{ and } \Delta q < \varepsilon$$

3.2.4.2 Linearization of the Voltage Calculation

Hereafter, the linearization method of the LFC adopted in this work for MV grids is described. First of all, the load flow in the modelled grid was calculated for one chosen operating point according to the Newton-Raphson LFC, as described in 3.2.4.1. The column vector containing the better approximations of the voltage angles and magnitudes was determined after reaching the predefined accurate level of $\varepsilon = 10^{-8}$ in three iterations:

$$\begin{pmatrix}(\vartheta)\\(u)\end{pmatrix}^{(3)} = \begin{pmatrix}(\Delta\vartheta)\\(\Delta u)\end{pmatrix}^{(2)} + \begin{pmatrix}(\vartheta)\\(u)\end{pmatrix}^{(2)} = (J^{-1})^{(2)} \cdot \begin{pmatrix}(\Delta p)^{(2)}\\(\Delta q)^{(2)}\end{pmatrix} + \begin{pmatrix}(\vartheta)\\(u)\end{pmatrix}^{(2)} \tag{21}$$

The column vector of the power mismatch can be split into the column vector of the set injection power and that of the calculated power, so that the equation (21) can be written as follows:

$$\begin{pmatrix}(\vartheta)\\(u)\end{pmatrix}^{(3)} = (J^{-1})^{(2)} \cdot \begin{pmatrix}(p_{set})\\(q_{set})\end{pmatrix} - (J^{-1})^{(2)} \cdot \begin{pmatrix}p\big((\vartheta,u)^{(2)}\big)\\q\big((\vartheta,u)^{(2)}\big)\end{pmatrix} + \begin{pmatrix}(\vartheta)\\(u)\end{pmatrix}^{(2)} \tag{22}$$

In order to linearize the LFC and speed it up, a one-step calculation was adopted based on equation (22). Accordingly, the following parts of the equation were assumed to be constant:

$$(A) = (J^{-1})^{(2)} \tag{23}$$

$$(C) = -(J^{-1})^{(2)} \cdot \begin{pmatrix}p\big((\vartheta,u)^{(2)}\big)\\q\big((\vartheta,u)^{(2)}\big)\end{pmatrix} + \begin{pmatrix}(\vartheta)\\(u)\end{pmatrix}^{(2)} \tag{24}$$

The calculation of the voltage magnitudes and angles was simplified, resulting in the linear equation system (25), where the variables of the system are the set values of the active and reactive injection power (p_{set}) and (q_{set}), respectively:

$$\begin{pmatrix}(\vartheta)\\(u)\end{pmatrix} = (A) \cdot \begin{pmatrix}(p_{set})\\(q_{set})\end{pmatrix} + (C) \tag{25}$$

(p_{set}) Column vector of the set active power injection at the grid nodes in pu

(q_{set}) Column vector of the set reactive power injection at the grid nodes in pu

3.2.4.3 Linearization of the Current Flow Calculation

Hereafter, the calculation of the current flow through the lines of the grid was linearized according to [47, 48, 49]. The complex current flowing through a line from node i to node j is calculated depending on the complex voltages of the nodes and the line admittance in the per-unit system as follows:

$$\underline{i}_{ij} = \underline{y}_{ij} \cdot \left(\underline{u}_i - \underline{u}_j\right) \tag{26}$$

$\underline{i}_{ij}$ Current flow through a line connected between node i and j in pu

$\underline{y}_{ij}$ Complex admittance of the line connected between node i and j in pu

By expressing the admittance as a function of the conductance g_{ij} and the susceptance b_{ij} of the line, and by expressing the complex voltages depending on the voltage magnitude and angle, the apparent current flow can be written as:

$$\underline{i}_{ij} = (g_{ij} + jb_{ij}) \cdot \left(u_i \cdot (cos(\vartheta_i) + j\,sin(\vartheta_i)) - u_j \cdot (cos(\vartheta_j) + j\,sin(\vartheta_j))\right) \tag{27}$$

b_{ij} Susceptance of the line connected between node i and j in pu

g_{ij} Conductance of the line connected between node i and j in pu

Assuming that the voltage angles of the grid nodes are generally smaller than 30°, the small-angle approximation can be applied for every node i of the grid as follows:

$$\begin{aligned} cos(\vartheta_i) &\approx 1 \\ sin(\vartheta_i) &\approx \vartheta_i \end{aligned} \tag{28}$$

The equation (27) can, thus, be simplified to:

$$\underline{i}_{ij} = (g_{ij} + jb_{ij}) \cdot \left(u_i + j \cdot u_i \cdot \vartheta_i - u_j - j \cdot u_j \cdot \vartheta_j\right) \tag{29}$$

Assuming, furthermore, that the voltage magnitude on the nodes is near 1 pu and has a maximum deviation of 5 % in the MV grid, the following simplification was adopted for every node i of the grid:

$$u_i \cdot \vartheta_i \approx \vartheta_i \tag{30}$$

The equation (29) could, hence, be further simplified as follows:

$$\begin{aligned} \underline{i}_{ij} &= (g_{ij} + jb_{ij}) \cdot \left(u_i + j \cdot \vartheta_i - u_j - j \cdot \vartheta_j\right) \\ &= \left[g_{ij} \cdot (u_i - u_j) - b_{ij} \cdot (\vartheta_i - \vartheta_j)\right] + j \cdot \left[b_{ij} \cdot (u_i - u_j) + g_{ij} \cdot (\vartheta_i - \vartheta_j)\right] \end{aligned} \tag{31}$$

The complex current $\underline{i}_{ij}$ can be split into a real part $i_{ij,p}$ and an imaginary part $i_{ij,q}$:

$$\begin{aligned} i_{ij,p} &= g_{ij} \cdot (u_i - u_j) - b_{ij} \cdot (\vartheta_i - \vartheta_j) \\ i_{ij,q} &= b_{ij} \cdot (u_i - u_j) + g_{ij} \cdot (\vartheta_i - \vartheta_j) \end{aligned} \tag{32}$$

$i_{ij,p}$ Real part of the current flow through a line connected between node i and j in pu

$i_{ij,q}$ Imaginary part of the current flow through a line connected between node i and j in pu

3.2.4.4 Quality of the Linear Approximation

The linearized LFC method has been applied to the modelled MV grid, described in 3.2.1, in order to evaluate its accuracy. Accordingly, the Newton-Raphson method was calculated initially for one operating point in order to determine the constant matrix (A) and the constant column vector (C), according to (23) and (24). The linearized system, as in (25), was then used to calculate the voltage magnitudes and angles of the grid nodes for all time steps of the considered year with 15 minutes time resolution. The time series used for the active and reactive power injection (P_N) and (Q_N) were generated based on the 2030 scenario, as described in 3.2.2.

The feed-in power of the wind plants according to the 2030 scenario is too high to be connected to the grid over one node and one power line. This would represent an impermissible operation state. Due to the high wind power feed-in, the resulting approximation of the voltage magnitude and angle on this node diverges considerably from the reference values of the Newton-Raphson method. Therefore, the results of the voltage magnitude and angle at node 2 and the results of the power flow through line 1 were not considered hereafter in the evaluation of the linear approximation quality. In what follows, the results of the linearized LFC are compared with the results of the Newton-Raphson LFC for the rest of the grid nodes and lines.

Figure 3-8 and 3-9 show the absolute frequency of occurrence of the linearized voltage magnitude and voltage angle error, respectively. The absolute error frequency was calculated for all nodes and all time steps of the year. The figures show that the linearized LFC approximates the Newton-Raphson LFC well, because the majority of the error values for voltage magnitude and angles are around zero. The number of equal-width bins adopted in the range of x of the histograms amounts to 100 bins.

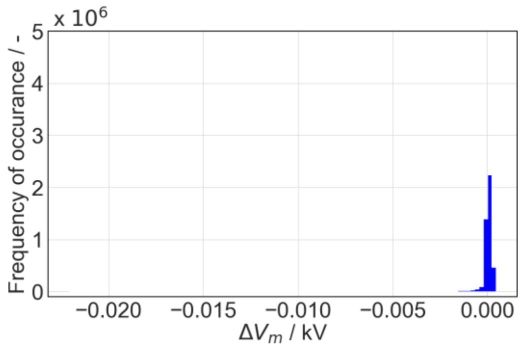

Figure 3-8 Absolute error frequency of the linear approximated voltage magnitude

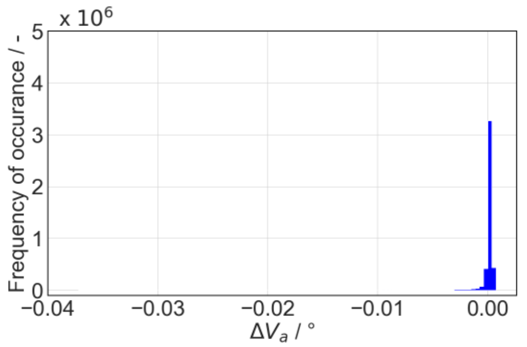

Figure 3-9 Absolute error frequency of the linear approximated voltage angle

In a further step, the linearized system (33) was applied in order to calculate the current flow through the power lines. Figure 3-10 and 3-11 show the absolute error frequency of the real and imaginary parts of the linearized currents, respectively. The error frequency here was also calculated for all lines of the grid and all time steps of the year. The number of equal-width bins adopted in the range of x of the histograms here also equals 100 bins. It can be observed from the figures that the real and imaginary parts of the currents were approximated quite well through the linear LFC. Especially the error values of the real part of the approximated current are predominantly around zero.

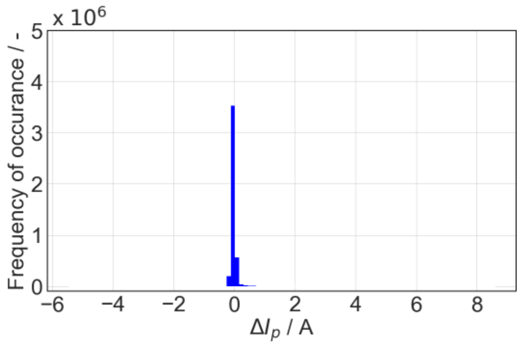

Figure 3-10 Absolute error frequency of the real part of the linear approximated current

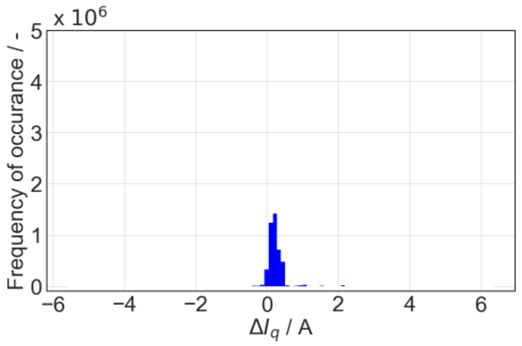

Figure 3-11 Absolute error frequency of the imaginary part of the linear approximated current

Furthermore, the mean absolute error AE_{mean} and the maximum absolute error AE_{max} were calculated for the voltage angle and voltage magnitude values as well as for the real and imaginary parts of the current values, considering all time steps of the year. Using the example of the voltage magnitude, the mean absolute error AE_{mean} and the maximum absolute error AE_{max} were calculated as follows:

$$AE_{mean} = \frac{\sum_{i=1}^{N_{nodes}} \sum_{t=1}^{N_{steps,q}} \left| U_{NR,i,t} - U_{lin,i,t} \right|}{N_{nodes} \cdot N_{steps,q}} \tag{33}$$

$$AE_{max} = max\{|U_{NR,i,t} - U_{lin,i,t}|\} \tag{34}$$

$$\forall\, i \in N, \forall\, t \in T_{year,q}$$

$U_{lin,i,t}$ Resulting voltage magnitude value from the linearized LFC for node i at time step t in kV

$U_{NR,i,t}$ Resulting voltage magnitude value from the Newton-Raphson LFC for node i at time step t in kV

Table 3-6 presents the calculated mean and maximum absolute errors of the linearized LFC based on (33) and (34). The maximum absolute error of the approximation amounts to 0.022 kV for the voltage magnitude and 0.037° for the voltage angle. Moreover, the mean absolute error amounts to 0.0002 kV for the voltage magnitude and 0.0004° for the voltage angle. These values indicate a very good approximation of the voltage magnitude and angle values. The approximation of the real and imaginary parts of the currents in the MV power lines is also very acceptable, since the maximum absolute error of the approximation amounts to 8.6 A for the real part and 6.37 A for the imaginary part of the current. The mean absolute error values are also acceptable with 0.022 A for the real part and 0.23 A for the imaginary part of the current. Altogether, it can be deduced that the linear LFC constitutes an accurate approximation of the Newton-Raphson LFC for MV grids and can, thus, be applied to model the grid restrictions in the linear optimization.

Table 3-6 Comparison of the linearized LFC results with the results of the Newton-Raphson LFC

	Mean Absolute Error	**Maximum Absolute Error**
Voltage magnitude U_i / kV	0.0002	0.022
Voltage angle ϑ_i / °	0.0004	0.037
Real current part I_p / A	0.022	8.6
Imaginary current part I_q / A	0.23	6.37

4 Development of the Optimized Grid Planning Method

In the context of this research work, a planning algorithm of the distribution grid was developed and tested on HV and MV grids. The planning algorithm aims at the expansion of the grid in accordance with the planning fundamentals at minimal costs. The following chapters give an outline of the mathematical optimization method used in the planning algorithm and a detailed description of its functioning for the planning of HV and MV grids.

4.1 Mathematical Optimization Used

This subchapter gives an overview of the general functioning of the mathematical optimization and solver used in the grid planning algorithm.

4.1.1 Mixed-Integer Linear Programming

The optimization implemented in the planning algorithm has the structure of an MILP problem. An optimization problem containing both discrete (integer) and non-discrete (continuous) decision variables is designated as a mixed-integer programming (MIP) problem. In the case where the objective function of the optimization problem and all its constraints are linear, the mixed-integer problem is a MILP problem [50]. The standard MILP formulation is as follows.

$$min\{c^T \cdot x\} \tag{35}$$

$$s.t.\, A \cdot x \begin{Bmatrix} \leq \\ = \\ \geq \end{Bmatrix} b\,,\;\; x_{min} \leq x \leq x_{max} \tag{36}$$

4.1.2 Branch and Bound

The solver used in this work for solving the implemented MILP problems of the grid planning algorithm is the Gurobi Optimizer [51]. This solver applies the branch and bound approach, which is a mathematical method commonly used to find the optimal solution of MILP problems. This method divides the initial problem iteratively into smaller subproblems and determines the lower and upper bounds of the subproblems. Based on these bounds, some subproblems are discarded if they do not contain efficient solutions to the problems [52]. In what follows, an outline of the branch and bound solving process of MILP problems is presented. In a first step, all the integrality restrictions of the original MILP problem are removed. The resulting MILP problem, which is called the linear-programming relaxation of the original problem, is then solved. After solving the linear-programming relaxation, some variables that were initially restricted to integer solutions now have fractional solutions. Considering among these a variable x, which has, for example, among these variables the fractional solution 7.6 after solving the linear-programming relaxation, this fractional solution is then excluded and further constraints are implemented instead in order to consider the integrality restrictions. Assuming that the original MILP problem is termed P_0, the newly added restrictions, in this case $x \geq 8$ and $x \leq 7$, are implemented separately in the initial problem, thus, creating two new subproblems, P_1 and P_2, that would replace the initial problem P_0. The variable x is here called a branching variable. As illustrated in Figure 4-1, the solving process is then repeated for the newly created subproblems, generating, hence, a search tree whose root is the original MILP problem. The newly created MILP subproblems are called nodes of the tree and the nodes which have not yet been solved are called the leaves of the tree. The solving process is carried on until all leaves are solved or discarded. At that point, the original MILP is solved and the best solution is chosen as the optimal solution of the original problem [51].

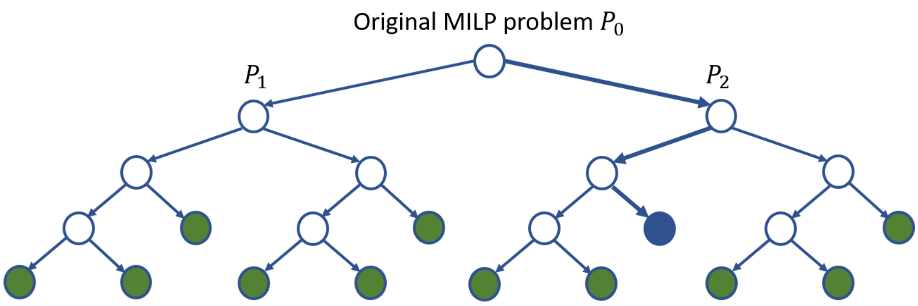

Figure 4-1 Simplified illustration of the branch and bound approach

Assuming a specific minimization problem, the best integer solution found for the problem, at any time point during the solving process, is designated as the incumbent. If, at a later point in time, a better solution is found, then the incumbent takes the value of the better new integer solution. The current incumbent, therefore, represents an upper bound of the optimal problem, since only solutions with lower values than the incumbent value will be accepted. On the other hand, the minimum of the optimal objective values of all current leaf nodes, at any time point during the solving process, is referred to as the lower bound. The best solution of the problem can only be greater or equal to the lower bound. The solver terminates when the gap between the incumbent objective value Z_{inc} and the lower bound Z_{lb} reaches a predefined set value gap_{opt} [51]:

$$gap = \frac{|Z_{inc} - Z_{lb}|}{|Z_{inc}|} \leq gap_{opt} \tag{37}$$

The default preset value of the gap in the Gurobi Optimizer amounts to 10^{-4}. In order to save solving time, the set value gap_{opt} has been chosen in this work for some planning variants by 10^{-2}.

4.1.3 Linear Programming Algorithms

The Gurobi Optimizer applied in this work uses two main optimization algorithms and their variants to solve continuous models and continuous relaxations of mixed-integer models. These algorithms are the barrier and the simplex algorithms [53].

4.2 Planning Algorithm for HV Grids

The functioning principle of the implemented planning algorithm is illustrated in Figure 4-2. In a first step, the grid lines are divided into LSs. The user of the algorithm can then select the desired planning instruments, including the CGE with OHLs or with UGCs, the application of BSS and the use of DPC. These instruments can be used separately or combined. In a further step, a linear mixed-integer optimization is solved, whose main target is to minimize the total costs of the planning instruments used. The required grid restrictions were considered here as linear constraints according to the planning fundamentals for HV grids. The considered grid restrictions correspond to the compliance with the current-carrying capacity of power lines in the (n-0) and (n-1) states. The application of BSS and DPC to prevent grid congestion assumes, in this work, a perfect prognosis of the load consumption and RES feed-in power as well as the controllability of the RES by the grid operator.

The objective functions and the constraints implemented will be described extensively in what follows.

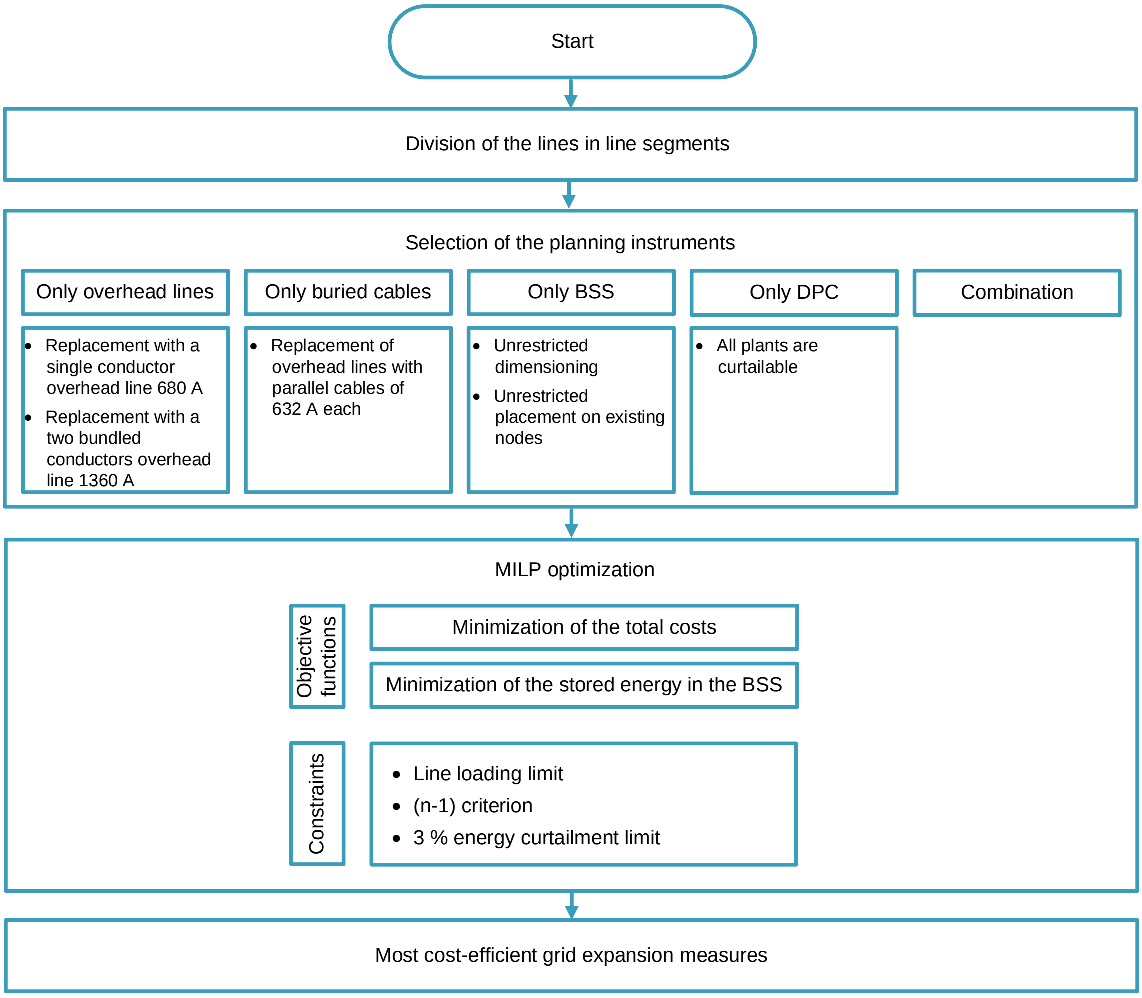

Figure 4-2 Operating principle of the planning algorithm for HV grids

4.2.1 Objective Functions

The implemented optimization comprises more than one linear objective function. The approach adopted here regarding the objective functions is the hierarchical objective method. In this approach, a priority is assigned to each objective and the objectives are then optimized in decreasing priority order, so that the solution found for the current objective at each step would not degrade the solution found for the previous objectives with higher priority [54].

The main objective function is that with the highest priority assigned in the optimization of the planning algorithm. The aim of the main objective function is to minimize the total costs of the chosen planning instruments over a specific economic life. The considered costs are, therefore, those of the CGE, BSS and DPC:

$$min\{Cost_{CGE} + Cost_{BSS} + Cost_{DPC}\} \tag{38}$$

$Cost_{CGE}$ Costs of the CGE measures in $EUR\ million$ (optimization variable)

$Cost_{BSS}$ Costs of the BSS application in $EUR\ million$ (optimization variable)

$Cost_{DPC}$ Costs of the DPC application over the economic life in $EUR\ million$ (optimization variable)

The second implemented objective function (39), with less priority than the main objective function, minimizes the energy amount stored $E_{s,t}$ at every time step. This ensures the discharge of the storages when no grid congestion is prognosticated and, thus, minimizes the number of battery cycles performed. Furthermore, maintaining the battery discharged when no grid congestion is prognosticated enables the use of this free capacity for market-based applications. The higher the free capacity of the storage, the more trade possible and the higher profits it could generate.

$$min\left\{\sum_{s=1}^{N_{nodes}}\sum_{t=1}^{N_{steps,q}} E_{s,t}\right\} \tag{39}$$

$E_{s,t}$ Storage energy of a BSS s at time step t in MWh (optimization variable)

The energy amount stored $E_{s,t}$ at every time step depends on the storage power, the charge and discharge efficiency factor of the BSS, and the time step duration, as follows:

$$E_{s,t} = (\eta_{BSS} \cdot P_{s,c,t} - \frac{1}{\eta_{BSS}} \cdot P_{s,d,t}) \cdot \Delta t_{step} + E_{s,t-1} \tag{40}$$

$$P_{s,t} = P_{s,c,t} - P_{s,d,t} \tag{41}$$

$$min\{P_{s,c,t}, P_{s,d,t}\} = 0 \tag{42}$$

$$with\ P_{s,c,t} \geq 0\ , P_{s,d,t} \geq 0\ \ \forall\ s \in S, \forall\ t \in T_{year,q}$$

η_{BSS} Charge and discharge efficiency factor of the BSS

$P_{s,c,t}$ Charging power of the BSS s at time step t on the grid side in MW (optimization variable)

$P_{s,d,t}$ Discharging power of the BSS s at time step t on the grid side in MW (optimization variable)

$P_{s,t}$ Storage power of the BSS s at time step t in MW (optimization variable)

Note that the optimization variables $P_{s,c,t}$ and $P_{s,d,t}$ were implemented according to (42) such that one of the two variables always equals 0 at every time step. Consequently, the resulting storage power $P_{s,t}$ equals $P_{s,c,t}$ or $-P_{s,d,t}$ at every time step.

When the BSS is used for grid-supporting purposes, the application of a charge and discharge efficiency factor η_{BSS} below 1 within the optimization leads the linear optimization to an excessive increase of the charging and discharging losses. The increase of these losses reduces the overload on the grid and leads to less storage capacity being necessary and, thus, to reduced costs. In order to avoid this excessive use of the storage losses, a charge and discharge efficiency factor equal to 1 was considered for the calculation of the energy amount stored during the optimization. The stored energy values resulting from the optimization were then corrected with the real charge and discharge efficiency factor, according to (40) after completion of the optimization. Since the application of an efficiency factor below 1 leads to a reduced storage capacity, the charge and discharge efficiency factor η_{BSS} was considered within the optimization problem for the calculation of the investment costs and the replacement costs of battery cells.

In what follows, a detailed description of the cost allocation and its modelling in the linear optimization are presented.

4.2.1.1 Costs of the CGE

The CGE measures considered in this work represent the replacement or reinforcement of existing power lines in the grid. The costs of the CGE $Cost_{CGE}$ comprise the investment in the new power lines $I_{CGE,line}$, new outgoing feeder panels $I_{CGE,panel}$ as well as new compensation reactors $I_{CGE,comp}$ and Peterson coils $I_{CGE,grounding}$ in case of cable application, and the ongoing operating costs $K_{CGE,op}$ of the new lines.

$$Cost_{CGE} = I_{CGE,line} + I_{CGE,panel} + I_{CGE,comp} + I_{CGE,grounding} + K_{CGE,op} \tag{43}$$

$I_{CGE,line}$	Investment costs of new lines in $EUR\ million$ (optimization variable)
$I_{CGE,panel}$	Investment costs of new feeder panels in $EUR\ million$ (optimization variable)
$I_{CGE,comp}$	Investment costs of new compensation reactors in $EUR\ million$ (optimization variable)
$I_{CGE,grounding}$	Investment costs of new Peterson coils in $EUR\ million$ (optimization variable)
$K_{CGE,op}$	Total ongoing operating costs in $EUR\ million$ (optimization variable)

4.2.1.1.1 Investment Costs in New Power Lines

The investment costs in new power lines $I_{CGE,line}$ for a particular power grid depend on the technology adopted for the new lines, namely, OHLs or UGCs, and the applied CGE variants. In the following, the modelling of the line investment costs in the objective function of the MILP is described in detail based on the technology and variants used.

Investment Costs of New Lines by the Application of OHLs

The HV circuits in Germany are generally constructed and operated in parallel systems, such that one electricity pylon generally carries two and sometimes several independent parallel circuit systems. An LS can, thus, comprise several parallel OHL systems (generally two), which are carried by the same electricity pylons. In addition, an LS includes conductors, an earth line and insulators. The start and end point of each LS can, in this instance, be a transformer substation or a power line branching. In case of an overload of one line, the line expansion is realized for all parallel lines of the same LS identically in order to ensure a uniform static load on electricity pylons. Using the example of a simplified HV grid in Figure 4-3, LS1 comprises two parallel OHL systems. The expansion of one OHL system located in this segment implies the expansion of the other parallel OHL system and the reinforcement or even the replacement, as appropriate, of the pylons located in this segment. Both line systems are reinforced identically [12].

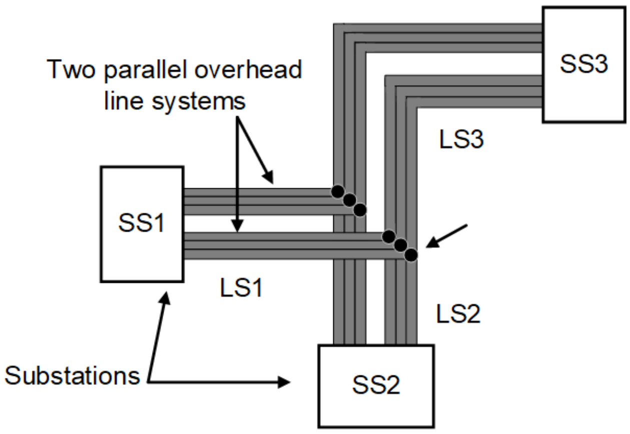

Figure 4-3 Exemplary structure of power line systems in a HV grid

The CGE variants considered in this work when planning the HV grid with OHLs are:

- CGE variant 1: Replacement construction utilizing a single conductor OHL with a current-carrying capacity of 680 A. The existing OHL is replaced here by a single new conductor OHL, with a higher current-carrying capacity (ampacity) of 680 A. This power line expansion could be associated with the reinforcement of electricity pylons.

- CGE variant 2: Replacement construction utilizing an OHL based on two bundled conductors with a current-carrying capacity of 1360 A. The existing OHL is replaced here by a new OHL with two bundled conductors and a higher total current-carrying capacity of 1360 A. This variant is always associated with a reinforcement of electricity pylons.

The addition of a second identical parallel OHL with the same current-carrying capacity as proposed in [7, 8] has not been considered in this work as a possible variant, due to the lack of knowledge about place availability on the electricity pylons.

As described previously, the expansion of an OHL system implies the expansion of the parallel OHL systems included in the same LS. This aspect has been considered in the optimization by modelling the LSs associated to the OHLs. The total investment in the new OHLs $I_{CGE,line}$ has been calculated depending on the specific costs of the employed CGE variant and the length of the LS.

$$I_{CGE,line} = \sum_{m=1}^{N_{Seg}} \sum_{v=1}^{2} b_{m,v} \cdot K_v \cdot l_m \cdot 10^{-6} \tag{44}$$

$b_{m,v}$	Binary variable associated to the LS m and the CGE variant v (optimization variable)
K_v	Specific costs of the CGE variant v in EUR/km
l_m	Length of the LS m in km

The optimization variables $b_{m,v}$ are of a binary type and can have only two values, 0 or 1, at the end of the optimization. Each variable is associated with one LS m and one CGE variant v, and describes whether or not the LS m should be expanded according to the CGE variant v. Depending on the least expensive CGE measures determined by the optimization, the variable $b_{m,v}$ at the end of the optimization is then equal to 1 if the CGE variant v for the LS m belongs to the optimal planning solution. If it does not, then the variable $b_{m,v}$ has the value 0. The CGE variant $v = 0$ corresponds here to the case where no expansion is required for the considered LS and is, therefore, not taken into account in the cost calculation.

It should be noted that in the case of OHLs, the total length of an LS is equal to the length of one line system of the segment, since the specific costs considered are meant for a whole LS per km. The electricity pylons generally make up the biggest part of the costs of CGE with OHLs [12].

Investment Costs in New Lines by the Application of Underground Cables

In this work, the CGE with UGCs is meant to replace the existing OHLs on which grid congestion is prognosticated with the appropriate cables that would prevent the prognosticated congestion for all (n-1) states. In this case, the parallel line systems of the same LS are also replaced by the appropriate cables. The CGE variants considered in this work when planning the HV grid with UGCs are the following:

- CGE variant 3: Replacement construction of the OHL system utilizing one UGC with a higher current-carrying capacity of 632 A.
- CGE variant 4: Replacement construction of the OHL system utilizing two parallel UGCs with a current-carrying capacity of 632 A each, enabling a higher total current-carrying capacity of 1264 A.
- CGE variant 5: Replacement construction of the OHL system utilizing three parallel UGCs with a current-carrying capacity of 632 A each, enabling a higher total current-carrying capacity of 1896 A.

In the case where an LS comprises two parallel OHL systems, both systems are replaced with as many cables as necessary to stand the prognosticated load flow through each line. Thereby, each OHL of the LS is considered apart in order to size the cables required to replace that line, according to the prognosticated load flow. The biggest part of the costs is made up here by the excavation and ground work [12]. The objective function (44) has been adapted in the case of CGE with the cable technology as follows:

$$I_{CGE,line} = \sum_{l=1}^{N_{lines}} \sum_{v=3}^{N_{var}} b_{l,v} \cdot K_v \cdot l_l \cdot F_D \cdot 10^{-6} \tag{45}$$

$b_{l,v}$ Binary variable associated to the line l and the CGE variant v (optimization variable)

l_l Length of the line l in km

F_D Detour factor

The CGE variant $v = 0$ corresponds to the case where no expansion is required for the considered line and is, therefore, not taken into account in the cost calculation. The detour factor F_D describes the deviation of the cable length from the OHL length when switching from the OHL to the UGC technology, due to the devious route adopted. Overhead lines can be laid straight in rural areas, traversing impassable sites, rivers or roads [55]. The new cables, however, cannot always be laid straight on the same route as the OHLs, especially when it comes to traverse obstacles [56]. Underground cables are mostly laid along public roads to facilitate access for high-load transporters for maintenance and repair [57]. Depending on the topographical conditions and the obstacles encountered, the length of the laid cables could, thus, be longer than the original OHL length. For the calculation of the investment costs for new cables, a detour factor of 1.3 was assumed in this work.

Table 4-1 presents the specific costs of the CGE variants that were applied for the calculation of the CGE costs in this work.

Table 4-1 Specific costs of the CGE variants considered in the HV grid

CGE Variant	Description	Equipment	Specific Costs / TEUR/km
1	Single conductor overhead line 680 A	Overhead lines, Double line system pylons	715 [12]
2	Two bundle conductor line 1360 A	Overhead lines, Double line system pylons	1100 [12]
3	One underground cable of 632 A	One cable, Ground work	1210 [12]
4	Two parallel underground cables of 632 A each	Two cables, Ground work	2420 [12]
5	Three parallel underground cables of 632 A each	Three cables, Ground work	3630 [12]

4.2.1.1.2 Investment Costs in New Outgoing Feeder Panels

The CGE of power lines is associated with the expansion of transformer substations. By increasing the current-carrying capacity of an existing power line system to more than 680 A, the transformer station, to which the line is connected, must also be expanded with a further outgoing feeder panel of 680 A.

<u>Investment Costs of New Feeder Panels by Applying OHLs</u>

In the case of CGE based on OHLs, the investment expenses for adding further outgoing feeder panels $I_{CGE,panel}$ were considered in the main objective function for the CGE variant 2 only, since this variant would require new feeder panels:

$$I_{CGE,panel} = \sum_{m=1}^{N_{Seg}} K_{panel} \cdot n_{panel,m} \cdot b_{m,2} \cdot 10^{-6} \tag{46}$$

K_{panel} Specific investment costs of a new outgoing feeder panel in transformer stations $EUR/unit$

$n_{panel,m}$ Number of feeder panels connected to the LS m in units

Investment Costs of New Feeder Panels by Applying UGCs

The CGE of power lines with UGCs is also associated with the expansion of transformer substations. The investment expenses for adding further outgoing feeder panels $I_{CGE,panel}$ were considered here in the main objective function for the CGE variants 4 and 5, since these variants would require new feeder panels:

$$I_{CGE,panel} = \sum_{l=1}^{N_{lines}} K_{panel} \cdot n_{panel,l} \cdot (b_{l,4} + 2 \cdot b_{l,5}) \cdot 10^{-6} \tag{47}$$

$n_{panel,l}$ Number of feeder panels connected to the line l in units

The CGE variants 1 and 3 were not considered in the calculation of the investment in new outgoing feeder panels, since the existing panels were assumed to be sufficient for line systems with current-carrying capacities less or equal to 680 A. In the case of variant 5, which represents the replacement of the OHL system with three UGCs with a current-carrying capacity of 632 A each, two more outgoing feeder panels in addition to the one already existing would be required in order to connect the three new cables. Table 4-2 presents the specific costs of the new outgoing feeder panels in the calculation.

Table 4-2 Specific costs of new outgoing feeder panels in the HV grid

Equipment	**Specific Costs / TEUR/unit**
One outgoing feeder panel of 680 A	770 [12]

4.2.1.1.3 Investment Costs of Compensation Reactors and Peterson Coils

The use of reactors for the reactive power compensation and Peterson coils for the resonant grounding were considered in this work only in the case of CGE with UGCs. Due to the high insulator capacitance of the cables, high reactive power is induced reducing the active power flow capacity of the cables. Therefore, compensation reactors are used to compensate the capacitive reactive power of the UGCs. Assuming a 100 % compensation, the capacitive reactive power that must be compensated was calculated in the main objective function as follows [45, 58]:

$$Q_{comp} = \sum_{l=1}^{N_{lines}} U_N^2 \cdot \omega \cdot C' \cdot l_l \cdot (b_{l,3} + 2 \cdot b_{l,4} + 3 \cdot b_{l,5}) \cdot 10^{-6} \tag{48}$$

Q_{comp} Capacitive reactive power induced by the underground cables in $Mvar$ (optimization variable)

U_N Nominal voltage of the grid in V

ω Angular frequency in rad/s

C' Insulator capacitance of one underground cable in F/km

The investment costs in compensation reactors have been considered depending on the capacitive reactive power of the cables and the specific investment costs of the reactors [59].

$$I_{CGE,comp} = Q_{comp} \cdot K_{Reactor} \tag{49}$$

$K_{Reactor}$ Costs of the compensation reactors in $EUR/Mvar$

In addition to the reactors for the reactive power compensation, Peterson coils are required to compensate for or reduce the capacitive fault current in case of a single line to ground fault. These coils are then connected between the neutral point of transformers and the earth (Peterson coil grounding). The capacitive fault current that must be neutralized was determined, depending on the insulator capacity of the cables and their lengths [45, 58]:

$$I_{CF} = \sum_{l=1}^{N_{lines}} 3 \cdot \frac{U_N}{\sqrt{3}} \cdot \omega \cdot C' \cdot l_l \cdot (b_{l,3} + 2 \cdot b_{l,4} + 3 \cdot b_{l,5}) \tag{50}$$

I_{CF} Capacitive fault current in case of a single line to ground fault in A (optimization variable)

The investment costs of the Peterson coils were considered in the planning algorithm depending on the capacitive fault current and the specific costs of Peterson coils [59]:

$$I_{CGE,grounding} = I_{CF} \cdot K_{Peterson} \tag{51}$$

$K_{Peterson}$ Costs of the Peterson coils in EUR/A

Standard cables with a 800 mm2 cross-section are often used in the 110 kV grid [12]. For the calculation of the capacitive reactive power and the capacitive fault current, the insulator capacitance, presented in Table 4-3, was adopted for one UGC.

Table 4-3 Insulator capacitance adopted for one standard UGC

Parameter	Designation	Unit	Value
$\boldsymbol{C'}$	Insulator capacitance per unit	nF/km	211 [60]

Table 4-4 shows the specific costs adopted for the calculation of the investment costs of compensation reactors and Peterson coils in the case of cable application.

Table 4-4 Specific costs of compensation reactors and Peterson coils

Equipment	Specific Costs
Compensation reactor	3500 $EUR/Mvar$ [12]
Peterson coils	2450 EUR/A [12]

4.2.1.1.4 Operating Costs

The annual operating costs here represent the inspection, maintenance and repair costs of the new CGE measures. These costs have been estimated at 2 % of the total initial investment [61]. The annual operating costs over the considered economic life were then discounted to the present value of the total operating costs at the initial investment year.

$$K_{CGE,Op} = 2\% \cdot \left(I_{CGE,line} + I_{CGE,panel} + I_{CGE,comp} + I_{CGE,grounding}\right) \cdot PVF \quad (52)$$

The present-value factor (PVF) for the considered economic life was calculated as follows:

$$PVF = \frac{(1+r)^{N_{years}} - 1}{r \cdot (1+r)^{N_{years}}} \quad (53)$$

PVF Present-value factor

r Interest rate

N_{years} Economic life considered in yr

4.2.1.2 Costs of the BSS Application

The costs of the battery systems $Cost_{BSS}$ include the initial investment costs $I_{BSS,ini}$, the replacement costs $I_{BSS,rep}$ and the ongoing operating costs $K_{BSS,op}$.

$$Cost_{BSS} = I_{BSS,ini} + I_{BSS,rep} + K_{BSS,op} \quad (54)$$

$I_{BSS,ini}$ Initial investment costs of the BSS project in $EUR\ million$ (optimization variable)

$I_{BSS,rep}$ Replacement investment in battery cells and converters in $EUR\ million$ (optimization variable)

$K_{BSS,op}$ Total operation costs of the BSS in $EUR\ million$ (optimization variable)

4.2.1.2.1 Initial Investment Costs in BSS

The initial investment costs of battery systems $I_{BSS,ini}$ in the first investment year were calculated depending on the total capacity of the BSS and the specific investment costs for large-scale battery storage projects.

$$I_{BSS,ini} = K_{BSS,spec} \cdot 10^{-6} \cdot \sum_{s=1}^{N_{nodes}} E_{max,s} \tag{55}$$

$$E_{max,s} = max\left\{E_{s,t_1}, E_{s,t_2}, \dots, E_{s,t_{N_{steps,q}}}\right\} \tag{56}$$

$E_{max,s}$ Capacity of the BSS s in MWh (optimization variable)

$K_{BSS,spec}$ Specific investment costs of BSS projects in EUR/MWh

It has been assumed in the optimization that all nodes of the grid represent potential placements of the BSS. Therefore, every optimization variable modelling the BSS application, such as the storage capacity $E_{max,s}$, is assigned initially to each node s of the grid before the beginning of the optimization. The user can also reduce the potential nodes for the placement of BSS in the grid at the beginning in order to reduce the computing time of the optimization.

By minimizing the total costs depending on the optimization variables for storage capacity and power, the optimal capacity and rated power of the BSS can be determined as results of the optimization. In addition, the minimization of the costs leads to the exclusion of the nodes that have negligible contribution to preventing congestion from all initial nodes. This leads to the optimal placement of the grid-supporting BSS in the grid.

The specific investment costs $K_{BSS,spec}$ were deduced from the total costs of existing large-scale battery projects in Germany and worldwide, divided by the total capacity of the battery system. Consequently, they cover the capacity-specific expenses, such as the cost of the battery cells, connectors, battery monitoring systems, sensors, housing and shelves. The investment costs also cover the power-specific expenses, such as the cost of inverters and circuit breakers. They additionally comprise the costs of installation and land.

4.2.1.2.2 Ongoing Operating Costs

The annual ongoing operating costs of the BSS were estimated at 0.5 % of the initial investment costs. The annual costs were then discounted regarding the considered interest rate over the N_{years} economic life, to the total present value at the initial investment year.

$$K_{BSS,op} = 0.5\% \cdot I_{BSS,ini} \cdot PVF \quad (57)$$

4.2.1.2.3 Replacement Investments

The replacement investments $I_{BSS,rep}$ accrue when system components, such as battery cells or converters, must be exchanged at their end of life. In this work, replacement investments in battery cells $I_{rep,batt}$ and converters $I_{rep,conv}$ were considered. The total replacement investments, therefore, represent the sum of all new investments in battery cells and converters during the considered economic life, discounted to the present value.

$$I_{rep,batt} = \sum_{i=1}^{N_{rep,Batt}} \frac{K_{batt,i} \cdot \sum_{s=1}^{N_{nodes}} E_{max,s}}{(1+r)^{i \cdot N_{life,batt}}} \cdot 10^{-6} \quad (58)$$

$$I_{rep,conv} = \sum_{i=1}^{N_{rep,Conv}} \frac{K_{conv,i} \cdot \sum_{s=1}^{N_{nodes}} P_{max,s}}{(1+r)^{i \cdot N_{life,conv}}} \cdot 10^{-6} \quad (59)$$

$$I_{BSS,rep} = I_{rep,batt} + I_{rep,conv} \quad (60)$$

$I_{rep,batt}$	Replacement investment of battery cells in $EUR\ million$ (optimization variable)
$I_{rep,conv}$	Replacement investment of converters in $EUR\ million$ (optimization variable)
$K_{batt,i}$	Specific costs of battery cells at the time of the investment i in EUR/MWh
$K_{conv,i}$	Specific costs of converters at the time of the investment i in EUR/MW
$P_{max,s}$	Rated power of the BSS s in MW (optimization variable)
$N_{life,batt}$	Service life of battery cells in yr
$N_{life,conv}$	Service life of converters in yr
$N_{rep,batt}$	Number of required replacements of battery cells
$N_{rep,conv}$	Number of required replacements of converters

The calculation of the costs described above, accruing through the use of large-scale BSS, were determined based on assumptions which stem from existing stationary battery projects in Germany and worldwide and from current studies. Table 4-5 shows the specific expenses adopted for the first investment in the BSS project and the specific costs for the replacement investments in battery cells and converters at their end of life. The specific expenses for the first investment in BSS projects were calculated as the average of the specific cost values of existing stationary battery projects [62–67].

Table 4-5 Specific investment costs for BSS projects, battery cells and converters

Investment Type	**Specific Costs**
Investment costs for big stationary battery plants	489 EUR/kWh
Replacement investments in battery cells as of 2030	70 EUR/kWh [68]
Replacement investments in converters	65 EUR/kW [69]

Table 4-6 shows the technical parameter of the BSS adopted for the cost calculation. The assumed economic life thereby amounts to 40 years and represents the expected service life of an OHL conductor.

Table 4-6 Assumptions adopted for the cost calculation of BSS

Input Data	**Value**
Charge and discharge efficiency factor of the battery system	90 % [70]
Depth of discharge (DoD)	100 % [71]
Service life of battery cells	20 a [72], [73]
Service life of converters	15 a [74]
Economic life	40 a [75]
Interest rate	8 %

4.2.1.3 Costs of the DPC

The time series-based DPC is a variant of the PC which can be applied temporarily, goal-oriented and selective to PV and wind plants in order to avoid grid congestion [37]. The application of the DPC implies the possibility of controlling the power plants by the responsible grid operators. In this work, it was assumed that this possibility is given for all PV and wind plants connected to the grid in question and to the subordinate grids. The DPC of RES was considered in the planning algorithm as a further planning instrument.

The curtailment costs $Cost_{DPC}$ represent the compensation costs paid to RES operators for the curtailed amount of power. The curtailment costs incurring in the simulated year were calculated depending on the curtailed PV and wind energy E_{DPC} and the specific curtailment costs $K_{DPC,spec}$. For the purposes of simplification, the curtailment costs incurring in the simulated year were assumed to be constant yearly over the economic life and discounted to the total present value at the initial investment year:

$$Cost_{DPC} = K_{DPC,spec} \cdot E_{DPC} \cdot PVF \cdot 10^{-6} \tag{61}$$

E_{DPC} Total curtailed energy during the simulated year in MWh/a (optimization variable)

$K_{DPC,spec}$ Specific costs of the PC in EUR/MWh

The total curtailed energy during the simulated year is calculated depending on the amount of PV and wind power curtailed on every node i at every time step t.

$$E_{DPC} = \sum_{t=1}^{N_{steps,q}} \sum_{i=1}^{N_{nodes}} (\Delta P_{PV,i,t} + \Delta P_{Wind,i,t}) \cdot \Delta t_{step} \tag{62}$$

$\Delta P_{PV,i,t}$ PV active power curtailed on node i at time step t in MW (optimization variable)

$\Delta P_{Wind,i,t}$ Wind active power curtailed on node i at time step t in MW (optimization variable)

Δt_{step} Duration of a time step t in h

Table 4-7 shows the adopted specific curtailment costs which have been deduced from the total compensation costs levied for feed-in management of RES in the German distribution grid in 2018 [76].

Table 4-7 Specific costs assumed for the curtailment of RES

Cost Type	**Specific Costs**
Compensation costs for the curtailment of RES power	97.2 EUR/MWh [76]

4.2.2 Linear Constraints

In addition to the objective functions, linear constraints were implemented in the optimization in order to consider the grid restrictions according to the planning principles for HV grids, as described in 2.1.3.1.

4.2.2.1 Linear Constraints Regarding the Planning Principles in the Case of OHL Application

In order to fulfil the grid planning principles, the linear constraints (63) were implemented combining the contribution of CGE, BSS and DPC to prevent line overloads for the (n-0) state and all (n-1) states of the grid. Considering a line l in the grid, which is included in an LS m, the linear constraints (63) state that the power flow value through the line must be maintained within the power-carrying capacity $S_{max,l,v}$ of that line for every time step t and every line outage a. The instruments available to fulfil these constraints are the control of the BSS power ($P_{S,t}$) or the reduction of the PV and wind power ($\Delta p_{PV,t}$) and ($\Delta p_{Wind,t}$), respectively [29, 32, 33, 34, 35]. Another available instrument is the increase of the power-carrying capacity of the line $S_{max,l,v}$ by line expansion according to the CGE variant v. Based on these planning instruments, the linear optimization determines the best combination of measures that must be taken to fulfil the constraints (63) for all time steps of the year and all lines at minimal cost.

$$If\ b_{m,v} = 1, then:$$

$$\begin{cases} (NACLODF)^{(a)}[l;N] \cdot ((P_{N,t}) + (P_{S,t}) + (\Delta P_{PV,t}) + (\Delta P_{Wind,t})) \leq S_{max,l,v} \\ (NACLODF)^{(a)}[l;N] \cdot ((P_{N,t}) + (P_{S,t}) + (\Delta P_{PV,t}) + (\Delta P_{Wind,t})) \geq -S_{max,l,v} \end{cases} \quad (63)$$

$$\forall\, m \in M\,, \forall\, l \in L \mid l \in m, \forall\, a \in A, \forall\, t \in T_{years,q}, v \in \{0,1,2\}$$

$(NACLODF)^{(a)}[l;N]$	The l^{th} row of the matrix $(NACLODF)$ for the line state a
$S_{max,l,v}$	Power-carrying capacity of line l in the case of CGE variant v in MVA

Variant 0 corresponds to the case where no new CGE measures are required. This means that $S_{max,l,0}$ corresponds to the original power-carrying capacity of the line l without CGE. The calculation of the load flow in the constraints (63) is based on the simplified assumption that the matrix $(NACLODF)$ remains constant. In reality, the values of the matrix can change depending on the new CGE measures applied, which can lead to deviations in the calculated power flow values.

4.2.2.2 Linear Constraints Regarding the Planning Principles in the Case of UGC Application

In the case of UGC application, further linear constraints according to (64) were implemented. The constraints ensure that in case an overloaded OHL must be replaced by UGCs to prevent the overload, then the parallel lines included in the same LS must be also replaced by the appropriate UGCs. If the overload can be prevented without CGE, then the parallel OHLs of the same LS will not be expanded.

$$if\ \ N_{m,lines} \geq 2, then\ b_{l_i,0} = b_{l_j,0} \quad (64)$$

$$\forall\, m\ \in M, \forall \left\{l_i, l_j\right\} \subset m \mid i \neq j$$

Whereas l_i and l_j are two arbitrary parallel lines comprised in the same LS m, and $b_{l_i,0}$ and $b_{l_j,0}$ are binary variables associated to the lines l_i and l_j, respectively, in the case of the CGE variant 0.

By analogy with the CGE based on OHLs, the linear constraints (65) were implemented in the case of CGE with UGCs. Contrary to (63), these constraints allow the application of different CGE variants to the parallel lines of the same LS m, based on the UGC technology.

$$If\ b_{l,v} = 1, then:$$

$$\begin{cases} (NACLODF)^{(a)}[l;N] \cdot ((P_{N,t}) + (P_{S,t}) + (\Delta P_{PV,t}) + (\Delta P_{Wind,t})) \leq S_{max,l,v} \\ (NACLODF)^{(a)}[l;N] \cdot ((P_{N,t}) + (P_{S,t}) + (\Delta P_{PV,t}) + (\Delta P_{Wind,t})) \geq -S_{max,l,v} \end{cases} \tag{65}$$

$$\forall\ l \in L\ , \forall\ a \in A\ , \forall\ t \in T_{years,q}, v \in \{0,3,4,5\}$$

4.2.2.3 Further Linear Constraints Implemented

In order to ensure, that only one CGE variant is chosen for each LS among all possible considered CGE variants, the following linear constraints were implemented in the case of CGE with OHLs:

$$b_{m,0} + b_{m,1} + b_{m,2} = 1 \tag{66}$$

$$\forall\ m \in M$$

In the case of CGE with UGCs, the following constraints were implemented to ensure only one CGE variant is chosen for each line:

$$b_{l,0} + b_{l,3} + b_{l,4} + b_{l,5} = 1 \tag{67}$$

$$\forall\ l \in L$$

In order to model a realistic operation of the BSS, the constraints (68) regarding the positive sign of the amount of energy stored in the BSS at every time step have been implemented:

$$E_{s,t} \geq 0 \tag{68}$$

$$\forall\ s \in S, \forall\ t \in T_{year,q}$$

In addition, further linear constraints concerning the correct use of the DPC in the grid planning were considered. As described in 2.2.2, the curtailed energy of a PV or wind power plant in a year must not exceed 3 % of the total prognosticated energy of the plant [3]. Therefore, the total PV and wind energy curtailable by the planning algorithm on every node of the grid was limited to 3 % of the total prognosticated PV and wind energy, respectively, per node.

$$\begin{cases} E_{curt,PV,i} = \sum_{t=1}^{N_{steps,q}} \Delta P_{PV,i,t} \cdot \Delta t_{step} \leq 0.3 \cdot \sum_{t=1}^{N_{steps,q}} P_{PV,i,t} \cdot \Delta t_{step} \\ E_{curt,Wind,i} = \sum_{t=1}^{N_{steps,q}} \Delta P_{Wind,i,t} \cdot \Delta t_{step} \leq 0.3 \cdot \sum_{t=1}^{N_{steps,q}} P_{Wind,i,t} \cdot \Delta t_{step} \end{cases} \tag{69}$$

$$\forall\, i \in N$$

$E_{curt,PV,i}$	PV energy curtailed on node i in a year in MWh (optimization variable)
$E_{curt,Wind,i}$	Wind energy curtailed on node i in a year in MWh (optimization variable)
$P_{PV,i,t}$	PV power on node i at time step t in MW
$P_{Wind,i,t}$	Wind power on node i at time step t in MW

In addition, the PV and wind power curtailable on every node i was restricted to the maximal prognosticated power at every time step t:

$$\begin{cases} 0 \leq \Delta P_{PV,i,t} \leq P_{PV,i,t} \\ 0 \leq \Delta P_{Wind,i,t} \leq P_{Wind,i,t} \end{cases} \tag{70}$$

$$\forall\, i \in N, \forall\, t \in T_{years,q}$$

4.2.3 Costs of the Power Losses

During the operation of the grid, power losses accrue steadily for all adopted grid expansion solutions. However, the choice of the applied expansion instruments, whether OHLs, UGCs, BSS, DPC or a combination of these instruments, has a different influence on the power losses in the grid. The power losses incurred can be significant, especially at higher voltage grid levels, due to the high load flows. These losses must be compensated by grid operators through a transparent, market-oriented and nondiscriminatory manner [3]. In order to evaluate the impact of every planning variant on the grid losses, the total energy losses incurred in the grid were calculated in this work for all considered planning variants after completion of the optimization. This means that the energy losses were not considered in the planning algorithm as a deciding criterion for the grid planning and could not, hence, influence the planning results. The total energy losses and their estimated costs were merely calculated based on the grid planning algorithm results after completion of the optimization as a further evaluation parameter of the planning variants. The types of losses considered in this work are the storage and grid losses. The storage losses accrue in the BSS and reflect a storage efficiency less than 1. The grid losses accrue in the power lines and transformers. Only grid losses accruing in the grid lines were considered in this work. These losses are divided into current-dependent losses, voltage-dependent losses and compensation losses in the case of UGCs and compensation reactor application [58, 61, 71, 72, 73]. The costs of the total losses over the economic life were calculated as follows:

$$Cost_{Loss} = K_{Loss,BSS} + K_{Loss,I} + K_{Loss,U} + K_{Loss,Comp} \tag{71}$$

$Cost_{Loss}$	Total costs of incurred losses in the lines and the BSS in $EUR\ million$
$K_{Loss,BSS}$	Costs of the losses incurred in the BSS in $EUR\ million$
$K_{Loss,I}$	Costs of the current-dependent losses incurred in the power lines in $EUR\ million$
$K_{Loss,U}$	Costs of the voltage-dependent losses incurred in the power lines in $EUR\ million$
$K_{Loss,Comp}$	Costs of the compensation losses in $EUR\ million$

4.2.3.1 Costs of the Storage Losses

The energy-efficiency factor is the ratio between the energy taken from the battery and the energy supplied to the battery for a given time slice. It is also the product of the Coulombic efficiency factor and the voltage-dependent efficiency factor of the battery [80]. A deviation of the Coulombic efficiency factor from 1 is caused in lithium ion batteries by irreversible side reactions resulting from aging effects, such as corrosion or passivation layers. These reactions are uncritical in lithium ions batteries. The voltage-dependent factor reflects occurring overvoltages. The losses between the energy taken from the battery and the that supplied to the battery are, to a great extent, converted into heat [81]. The energy losses incurred in the BSS over the simulation year were calculated in this work depending on the charge and discharge efficiency factor η_{BSS} as:

$$E_{Loss,BSS} = \sum_{t=1}^{N_{steps,q}} \sum_{s=1}^{N_{BSS}} (1 - \eta_{BSS}) \cdot (P_{s,c,t} + \frac{1}{\eta_{BSS}} \cdot P_{s,d,t}) \cdot \Delta t_{step} \tag{72}$$

$E_{Loss,BSS}$	Energy losses incurred in the BSS over the simulated year in MWh

The costs of the energy losses incurred in the BSS over the considered economic life were calculated depending on the average value of the purchase price for the compensation energy and the present value factor.

$$K_{Loss,BSS} = E_{Loss,BSS} \cdot K_{CE} \cdot PVF \cdot 10^{-6} \tag{73}$$

K_{CE} Average value of the purchase price for the compensation energy in EUR/MWh

4.2.3.2 Costs of the Current-dependent Losses

The current-dependent losses occur in OHLs and UGCs depending on the current flow and the ohmic resistance of the line [58, 77]. The current-dependent energy losses incurred over one year were calculated for every considered planning variant, with the help of the time series-based modelling. The energy losses were, thus, calculated based on the resulting load flow from the planning algorithm after completion of the optimization, considering the new resistance of the lines in the case of a planning variant including CGE:

$$E_{Loss,I} = \sum_{t=1}^{N_{steps,q}} \sum_{l=1}^{N_{lines}} \frac{S_{l,t,max}^2}{U_N^2} \cdot R'_{l,v} \cdot l_l \cdot \Delta t_{step} \cdot 10^{-6} \tag{74}$$

$E_{Loss,I}$ Current-dependent energy losses over the simulated year in MWh

$S_{l,t,max}$ Maximum resulting power flow value through line l at time step t with respect to the possible line outages in VA

$R'_{l,v}$ Resistance per unit length of line l in the case of a CGE variant v in Ω/km

The resistance per unit length $R'_{l,v}$ of a line l corresponds to the resistance of one new OHL or cable multiplied by the number of the applied parallel bundles or cables respectively, according to the resulting CGE variant v.

Table 4-8 presents the adopted resistance values per unit length for one single conductor OHL and one cable. In the case where v is equal to 0, $R'_{l,v}$ corresponds to the original resistance of that line. In a further step, the costs of the current-dependent losses have been estimated based on the energy losses and the average purchase price of the compensation energy as follows:

$$K_{Loss,I} = E_{Loss,I} \cdot K_{CE} \cdot PVF \cdot 10^{-6} \tag{75}$$

4.2.3.3 Costs of the Voltage-dependent Losses

The voltage-dependent losses are due to the insulation permeability of the power line and occur as long as the line is under power, independent of the value of the current flow. The voltage-dependent losses were calculated for every planning variant depending on the nominal voltage and the resulting shunt conductance of the lines after completion of the optimization [77, 78]:

$$E_{Loss,U} = \sum_{l=1}^{N_{lines}} \sum_{v=0}^{5} U_N^2 \cdot G'_{l,v} \cdot l_l \cdot 8760\ h \cdot 10^{-6} \tag{76}$$

$E_{Loss,U}$ Voltage-dependent energy losses over the simulated in MWh

$G'_{l,v}$ Shunt conductance of line l per unit length in the case of a CGE variant v in S/km

It should be noted that the shunt conductance per unit length $G'_{l,v}$ of a line l corresponds to the shunt conductance of one new OHL or cable multiplied by the number of the applied parallel bundles or cables, respectively, according to the resulting CGE variant v from the planning algorithm.

Table 4-8 presents the adopted shunt conductance values per unit length for all variants v for one single conductor OHL and one cable. The costs of the voltage-dependent losses were calculated as follows:

$$K_{Loss,U} = E_{Loss,U} \cdot K_{CE} \cdot PVF \cdot 10^{-6} \tag{77}$$

4.2.3.4 Costs of the Compensation Losses

The compensation costs accrue in the case where UGCs are applied in the grid and compensation reactors are used to compensate the capacitive power due to the high insulator capacitance of the cables. The compensation losses occur in the ohmic resistance of the compensation reactors as long as they are under power, independent of the power flow value. These losses were calculated depending on the resulting cable capacitance after completion of the optimization, the quality factor of the compensation reactors and the grid voltage as follows [77, 78]:

$$E_{Loss,Comp} = \sum_{l=1}^{N_{lines}} \sum_{v=3}^{5} U_N^2 \cdot C'_{l,v} \cdot \omega \cdot l_l \cdot \frac{1}{g} \cdot 8760\ h \cdot 10^{-6} \tag{78}$$

$E_{Loss,Comp}$ Energy losses of the compensation reactors over the simulated year in MWh

$C'_{l,v}$ Insulator capacitance of the cable for line l in the case of the CGE variant v in F/km

g Quality factor of the compensation reactor

The compensation losses were considered in the planning algorithm only in the case of UGC application and, hence, only for the CGE variants 3, 4 and 5. In this case, the insulator capacitance per unit $C'_{l,v}$ corresponds to the capacitance per unit of one new cable multiplied by the number of the applied parallel cables according to the resulting CGE variant v from the planning algorithm. The costs of the compensation losses were calculated as follows:

$$K_{Loss,Comp} = E_{Loss,Comp} \cdot K_{CE} \cdot PVF \cdot 10^{-6} \tag{79}$$

Table 4-8 presents the adopted cable capacitance per unit length for one cable. The specific costs for the compensation of the energy losses were assumed to be 44.46 EUR/MWh, which is the average price of electricity on the EPEX Spot market in 2018 [82].

Table 4-8 Technical parameters assumed for the energy loss calculation

Parameter	Designation	OHL	UGC	Unit
$\boldsymbol{R_l'}$	Resistance per unit length	0.1095 [83]	0.0326 [60]	Ω/km
$\boldsymbol{G_l'}$	Shunt conductance per unit length	50 [56]	88 [78]	nS/km
$\boldsymbol{C_l'}$	Insulator capacitance per unit	-	0.211 [60]	$\mu F/km$
$\boldsymbol{g}$	Quality factor of the compensation reactor	-	470 [78]	-

4.3 Planning Algorithm for MV Grids

The functioning principle of the planning algorithm for MV grids is very similar to that for HV grids, as illustrated in Figure 4-4. In the case of MV grids, only UGCs are applied for the CGE and the grid restrictions considered are the compliance with the current-carrying capacity of the power lines and the voltage range limits allowed in the (n-0) state.

A description of the objective functions and constraints implemented in the planning algorithm for MV grids is given in the following sections.

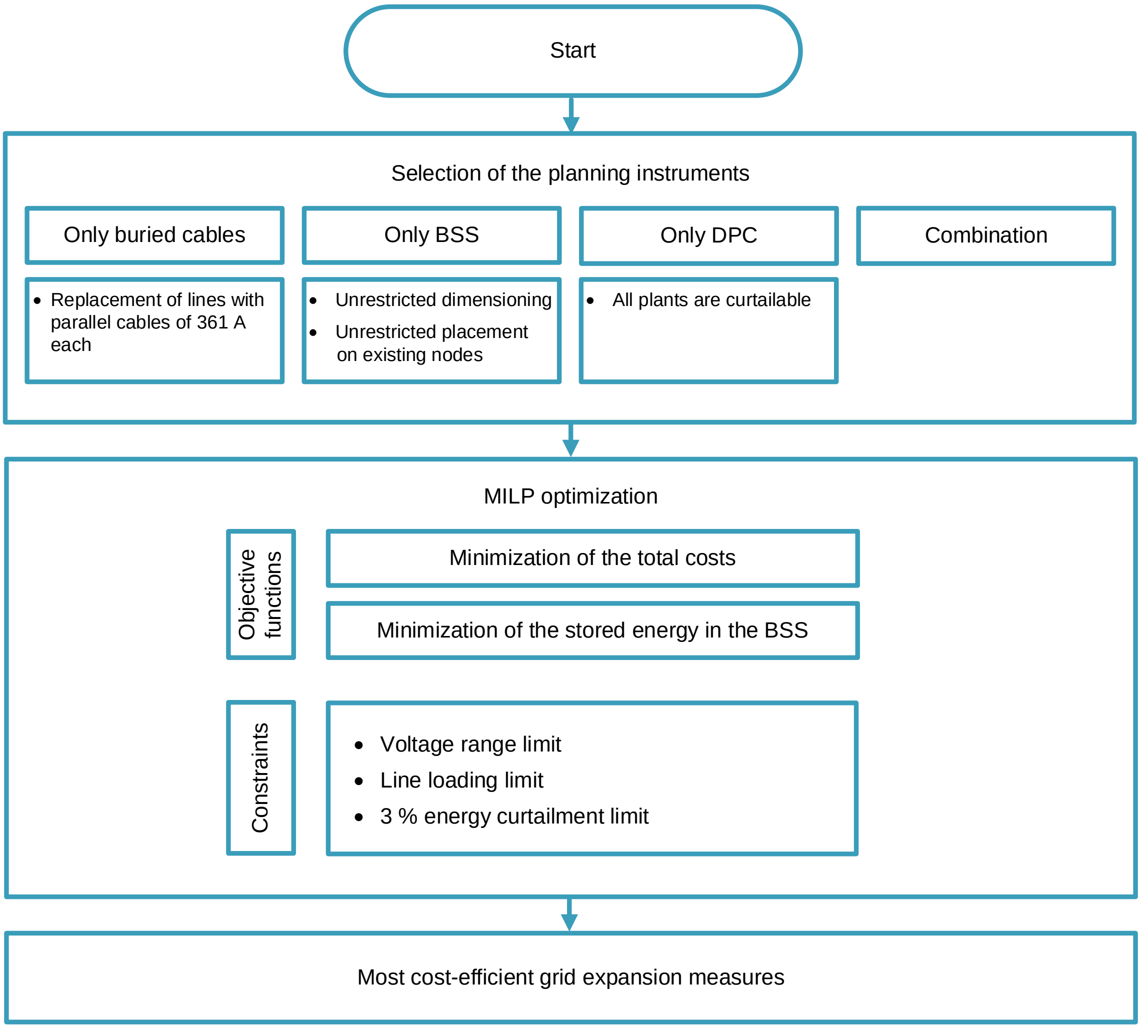

Figure 4-4 Functioning principle of the planning algorithm for MV grids

4.3.1 Objective Functions

The objective functions of the grid planning algorithm for MV grids were implemented in a similar way to the planning algorithm for HV grids (see 4.2.1). However, the CGE variants considered here are obviously different from the ones in HV grids.

The CGE variants considered for the planning of MV grids in this work are the following:

- CGE variant 1: Expansion construction utilizing a standard UGC with a current-carrying capacity of 361 A. If the existing power line is the latter, then a parallel cable of the same type is added, enabling a higher total current-carrying capacity of 722 A.
- CGE variant 2: Replacement construction utilizing a standard UGC with a current-carrying capacity of 361 A. If the current-carrying capacity of the existing line is less than 361 A, then the line is replaced by a standard UGC with a higher current-carrying capacity of 361 A.
- CGE variant 3: Replacement construction utilizing two standard UGCs each with a current-carrying capacity of 361 A, enabling a higher total current-carrying capacity of 722 A.
- CGE variant 4: Replacement construction utilizing three standard UGCs each with a current-carrying capacity of 361 A, enabling a higher total current-carrying capacity of 1083 A.

Unlike the HV grid, the CGE of MV grids nowadays in Germany is realized based on UGCs only [7, 44]. Therefore, the line expansion was considered in the optimization for each line separately.

The total investment cost of new cables $I_{CGE,line}$ was calculated depending on the specific costs of the employed CGE variant and the line length. A possible deviation of the new line length from the original one was not considered here, because the lines in the MV grid are shorter than in HV grids and a great part of the lines has already been laid with the cable technology.

$$I_{CGE,line} = \sum_{l=1}^{N_{lines}} \sum_{v=1}^{N_{var}} b_{l,v} \cdot K_v \cdot l_l \cdot 10^{-6} \tag{80}$$

$$v \in \{1,2,3,4\}$$

In the case where no CGE is required for a considered line of the grid, the variant 0 is chosen by the optimization algorithm and no incurred expenses are considered for that line. The expansion of power lines in the MV grid is also associated with the expansion of transformer substations. When increasing the current-carrying capacity of an existing power line that is connected to a transformer station to more than 361 A, the station is expanded with a further outgoing feeder panel. Therefore, the investment expenses for adding more outgoing feeder panels $I_{CGE,panel}$ was considered in the main objective function for the CGE variants 1, 3 and 4:

$$I_{CGE,panel} = \sum_{l=1}^{N_{lines}} K_{panel} \cdot n_{T,l} \cdot (b_{l,1} + b_{l,3} + 2 \cdot b_{l,4}) \cdot 10^{-6} \quad (81)$$

The specific investment costs K_{panel} are, hence, applied to the outgoing feeder panels added in transformer stations. Table 4-9 presents the specific investment costs of CGE measures adopted in MV grids. In the case of multiple parallel cables, a reduction of the investment costs of the cables has been taken into account. When replacing a power line by two parallel cables (CGE variant 3), the adopted investment costs of the new cables are equal to 1.5 times the investment costs of one cable. In the case where a line is replaced by three parallel cables (CGE variant 4), the adopted investment costs of the new cables equal twice the investment costs of one cable.

Table 4-9 Specific costs of the CGE measures in MV grids [7]

Equipment	**Description**	**Specific Costs**
One underground cable 361 A	cable, ground work, land, resonant neutral earthing	145 $TEUR/km$
One outgoing feeder panel 361 A	busbar (partly), coupling section, feeder panel, secondary system, land	90 $TEUR/unit$

4.3.2 Linear Constraints

In order to fulfil the grid restrictions required in MV grids, linear constraints were implemented in the planning algorithm. The expansion of power lines was applied here as a planning instrument to prevent overload problems. In the case of voltage violation on the grid nodes, the split of grid feeders, as described in 2.1.4.2, was not considered in the planning algorithm to prevent voltage congestion. Instead, the planning algorithm treats voltage congestion by the application of BSS or DPC, as explained in the following sections. Furthermore, the (n-1) criterion was not considered here for MV grids.

The constraints implemented in the planning algorithm combine the contribution of CGE, BSS and DPC to prevent voltage transgressions and line overloads in the (n-0) state. Only the provision of active power in the case of BSS application was considered here. In the case of DPC application, both active and reactive power are curtailed. The reactive power curtailed at each time step was implemented here depending on the curtailed active power and the phase change angle of the PV or wind power plant:

$$\Delta Q_{PV,i,t} = \Delta P_{PV,i,t} \cdot tan\, \varphi_{PV,i} \quad (82)$$

$$\Delta Q_{Wind,i,t} = \Delta P_{Wind,i,t} \cdot tan\, \varphi_{Wind,i} \quad (83)$$

$$\forall\, i \in N, \forall\, t \in T_{year,q}$$

$\Delta Q_{PV,i,t}$	PV reactive power curtailed on node i at time step t in $Mvar$ (optimization variable)
$\Delta Q_{Wind,i,t}$	Wind reactive power curtailed on node i at time step t in $Mvar$ (optimization variable)
φ_i	Phase change angle of the power plant connected to node i in °

The power plants of the same type connected to the same node i or to the underlying grids of the node were considered cumulatively as one plant connected to that node. The phase change angle φ_i is considered as a constant value for every PV or wind power plant and was deduced from the cumulated active and reactive power installed on the node. The linearized LFC method adopted for the planning of MV grids is different from that adopted for HV grids. In order to model the contribution of the BSS and DPC to fulfill the voltage constraints, the linear system (25) was expanded to include the column vector of the storage power and the column vectors of the curtailed PV and wind power in the per-unit system:

$$\begin{pmatrix} (\vartheta) \\ (u) \end{pmatrix} = (A) \cdot \begin{pmatrix} (p_{N,t}) + (p_{S,t}) + (\Delta p_{PV,t}) + (\Delta p_{Wind,t}) \\ (q_{N,t}) - (\Delta q_{PV,t}) - (\Delta q_{Wind,t}) \end{pmatrix} + (C) \quad (84)$$

Based on the equation system (84), linear constraints were implemented in the optimization, limiting the voltage deviation on every grid node i at every time step t to −1.5 % and +5 % of the nominal voltage, according to [7].

$$0.985\ pu \leq u_{i,t} \leq 1.05\, pu$$
$$\forall\, i \in N, \forall\, t \in T_{year,q} \quad (85)$$

Note that the use of CGE in the planning algorithm as the only planning instrument cannot satisfy the implemented voltage constraints, since the matrix (A) and the column vector (C) used for the linear LFC in the optimization are constant inputs and cannot, thus, be varied in order to fulfil the constraints. The variation of the injection power through the use of BSS or DPC is, therefore, required to satisfy the voltage constraints.

In order to ensure the safe operation of the power lines, the load flow must be steadily beneath the current-carrying capacity of the lines. Since the reactive current $I_{l,q}$ through the lines is relatively low compared to the active current $I_{l,p}$, the reactive current was neglected, leading to the adoption of the following simplification:

$$\underline{I}_{l,t} \cong \underline{I}_{p,l,t} \tag{86}$$

$$\forall\ l \in L, \forall\ t \in T_{year,q}$$

The simplified linear equations (32) were used to implement the restrictions for the maximal current flow value permitted through every line l connected between nodes i and j and at every time step t. The contribution of the CGE was, thereby, considered through the possibility of increasing the current-carrying capacity of the lines in the per-unit system depending on the considered CGE variants:

$$If\ b_{l,v} = 1, then: \begin{cases} (g_{ij} \cdot (u_{i,t} - u_{j,t}) - b_{ij} \cdot (\vartheta_{i,t} - \vartheta_{j,t})) \leq i_{max,l,v} \\ (g_{ij} \cdot (u_{i,t} - u_{j,t}) - b_{ij} \cdot (\vartheta_{i,t} - \vartheta_{j,t})) \geq -i_{max,l,v} \end{cases} \tag{87}$$

$$\forall\ l \in L, \forall\ t \in T_{year,q}, v \in\ \{0,1,2,3,4\}$$

$i_{max,l,v}$ Current capacity of line l in the case of the CGE variant v in pu

In order to ensure that only one CGE variant for each line is chosen from

considered, the following linear constraint was implemented:

$$b_{l,0} + b_{l,1} + b_{l,2} + b_{l,3} + b_{l,4} = 1 \tag{88}$$

$$\forall\ l \in L$$

5 Technical and Economical Results of the Grid Planning Algorithm

The results of the planning algorithm's application on the modelled HV and MV grids are presented in the following sections.

5.1 Application of the Planning Algorithm on a HV Grid

At first, the modelled HV grid, as described in 3.1, was analyzed based on the adopted linearized LFC before expanding the grid. Figure 5-1 presents the part of the grid which shows line overloads at some time points of the simulated year. The grey lines are the power lines which showed no overload for any (n-0) or (n-1) line state at no time point of the simulated year or which are too short to be considered. The red lines represent the power lines which showed an overload for at least one (n-0) or (n-1) line state at some time points of the simulated year. The black dots illustrate the junctions between two or three power lines. Ten lines of the considered HV grid part show an overload over the simulated year, as illustrated in the figure.

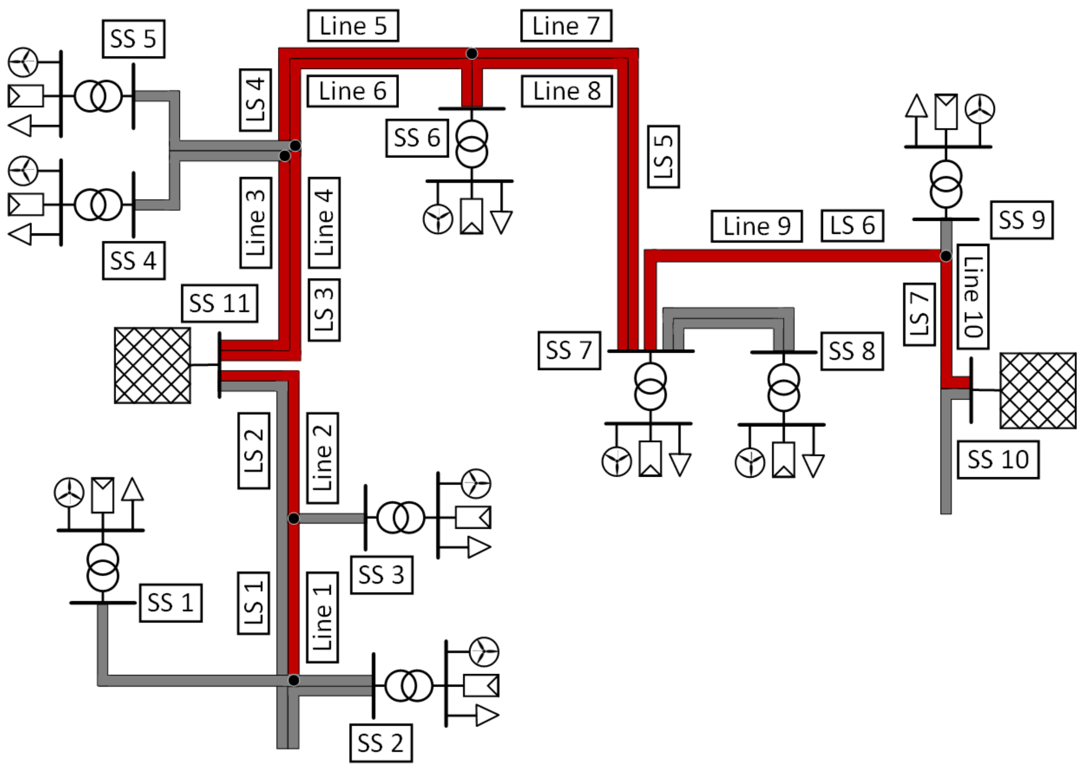

Figure 5-1 Overloaded lines of the modelled HV grid

Figure 5-2 illustrates the power flow through the overloaded lines in consideration of the (n-0) and all relevant (n-1) states, in the form of boxplots. For each considered line, the boxplot indicates the load values for 25, 50 and 75 % of the total calculated load states as well as the minimum and maximum reached load values. The dotted red line represents the power-carrying capacity of the lines in percent. It can be seen from the figure that the power flow at certain time points of the year could reach about 200 % of the thermal capacity of the line, as is the case for line 6. The aim of the planning algorithm is to expand the grid with minimal total costs in consideration of different expansion variants, in order to prevent all prognosticated congestion for all (n-1) states.

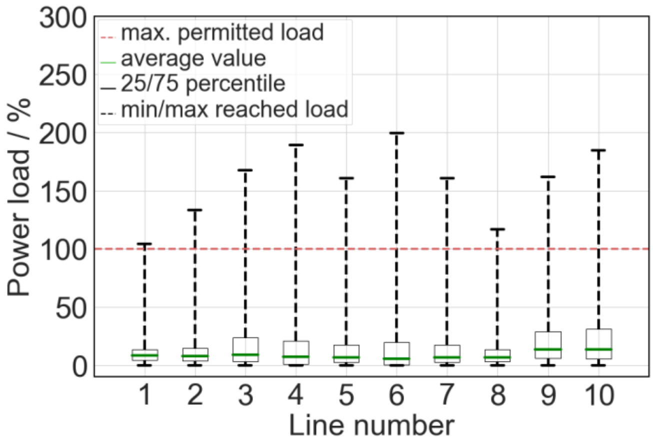

Figure 5-2 Line load of the endangered lines of the original HV grid

Table 5-1 presents the values of the maximum permitted and the maximum prognosticated load flow for each line of the HV grid part.

Table 5-1 Prognosticated load flow from the LFC and maximum permitted load flow of the lines

Lines	Maximum Load Flow Permitted / MVA	Maximum Load Flow Prognosticated / MVA
Line 1	101.9	106.3
Line 2	101.9	135.9
Line 3	129.5	217.2
Line 4	129.5	245.4
Line 5	101.9	164
Line 6	101.9	203.4
Line 7	101.9	164
Line 8	101.9	119.2
Line 9	120	194
Line 10	120	221.8

The maximum prognosticated load flow values in Table 5-1 have been derived from the linearized LFC considering the (n-0) and the relevant (n-1) states, as described in 3.1.

The planning algorithm has been applied to the modelled HV grid for different grid expansion variants. The applied expansion variants represent different combinations of the considered technologies:

- Overhead lines (OHL)
- Underground cables (UGC)
- Battery storage systems (BSS)
- Dynamic power curtailment (DPC)

The planning algorithm determines the optimal expansion measures for each considered variant that would prevent all prognosticated grid congestion and fulfil the (n-1) criterion over the simulated year and that, at the same time, ensures minimal total expansion costs. Due to the 3 % limit, the use of the dynamic curtailment as the only planning instrument has proven to be insufficient to prevent all prognosticated congestions in the considered HV grid. Therefore, this planning variant was not considered in the following evaluation.

5.1.1 Planning Results in the Case of OHL Application

When considering the CGE based on OHL, the expansion of one overloaded line system implies the expansion of the whole respective LS, including the parallel line systems. The results from the planning algorithm, by consideration of the CGE based on OHL as the only planning technology, has yielded the expansion of the LS LS1 according to variant 1 of the CGE and the expansion of the remaining LSs LS2 to LS7 according to the variant 2 of the CGE. Table 5-2 shows the resulting CGE measures from the planning algorithm depending on the LSs. As described in 4.2.1.1, variant 1 of the CGE represents a replacement construction with a single conductor OHL with a current-carrying capacity of 680 A. Variant 2 of the CGE represents a replacement construction utilizing an OHL based on two bundled conductors with a total current-carrying capacity of 1360 A. The resulting total line length of the CGE measures amounts to about 118.4 km.

Table 5-2 Results of the planning variant using CGE based on OHL

Line Segment	Parallel OHL Systems / units	Original Length / km	CGE Variant
LS1	2	9.8	1
LS2	2	5.2	2
LS3	2	2.4	2
LS4	2	21.4	2
LS5	2	11.8	2
LS6	1	14.2	2
LS7	1	2.9	2

Figure 5-3 shows the power flow through the same lines as in Figure 5-2 after CGE with OHLs, in the form of boxplots. The illustrated power flow values consider the (n-0) and all relevant (n-1) states for each line. The maximum values reached after CGE with OHLs are now under the power-carrying capacity for all lines. A significant transport capacity reserve is even available for most of the lines, enabling more integration of RES than that considered in the scenario 2030.

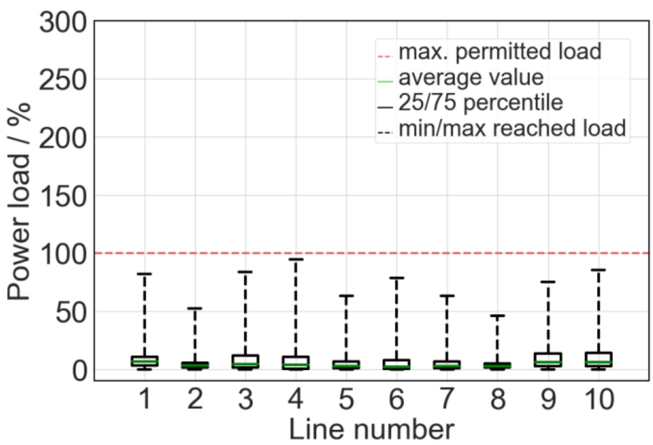

Figure 5-3 Line load of the HV lines after CGE based on OHL

The total costs of the resulting CGE measures are estimated at EUR 97.2 million. The investment costs of the new lines and feeder panels represent about 81 % of the total costs. The ongoing operating costs over the economic life of 40 years make up about 19.3 % of the total costs. Table 5-3 summarizes the distribution of the total costs.

Table 5-3 Resulting costs of the planning variant with OHL

Total Costs / EUR Million	Investment in OHL / %	Investment in Feeder Panels / %	Operating Costs / %
97.2	72.8	7.9	19.3

Based on the resulting CGE measures from the planning algorithm and the prognosticated load flow through the lines, the yearly accruing current and voltage-dependent losses were calculated. Assuming constant yearly losses over the economic life of 40 years, the total costs of the energy losses were then calculated, as described in 4.2.3. The total costs are estimated at EUR 5.2 million. Table 5-4 shows the yearly losses calculated and their repartitions between current-and voltage-dependent losses. As can be seen from the table, the current-dependent losses generally make up the significant part of the losses in the case of OHL applications.

Table 5-4 Resulting energy losses for the planning variant with OHL

Costs of Energy Losses / EUR Million	Yearly Energy Losses / GWh/a	Current Dependent Losses / %	Voltage Dependent Losses / %
5.2	9.8	88.3	11.7

5.1.2 Planning Results in the Case of OHL and DPC Application

When combining the CGE based on OHL with the dynamic curtailment as a further degree of freedom in the grid planning with consideration of the 3 % curtailment limit, the length of the required CGE measures was reduced to about 63 % compared to the application of OHLs alone. Consequently, only four LSs instead of seven must be expanded now. As illustrated in Table 5-5, the LSs affected by the CGE are, henceforth, LS4 and LS5 according to variant 1 as well as LS3 and LS7 according to variant 2 of the CGE. On the other hand, the curtailment energy of PV and wind plants required over the simulation year amounts to about 24.5 GWh.

Table 5-5 Results of the planning variant combining OHL and DPC

Line Segment	Parallel OHL / units	Original Length / km	CGE Variant	Curtailed Energy / GWh/a
LS3	2	2.4	2	24.5
LS4	2	21.4	1	
LS5	2	11.8	1	
LS7	1	2.9	2	

Figure 5-4 presents the power flow through the same lines as in Figure 5-2 after grid expansion with OHL and DPC, in the form of boxplots. The power flow values illustrated for each line consider the (n-0) and all relevant (n-1) states. Compared to the variant only with CGE, the expansion of the LSs LS1, LS2 and LS9 have now been completely replaced by the application of the dynamic curtailment. In addition, the expansion of LS4 according to variant 2 of the CGE has now been replaced by variant 1 of the CGE. This variant is sufficient to prevent the prognosticated overloads on line 5 but not on line 6, included in the same LS LS4. Therefore, the dynamic curtailment has been applied more in order to prevent the remaining prognosticated overloads on line 6. The contribution of the DPC to prevent the prognosticated overloads on lines 1, 2, 6 and 9 can be seen in Figure 5-4 from the accordance of the maximum load flow values reached on these lines with the power-carrying capacity.

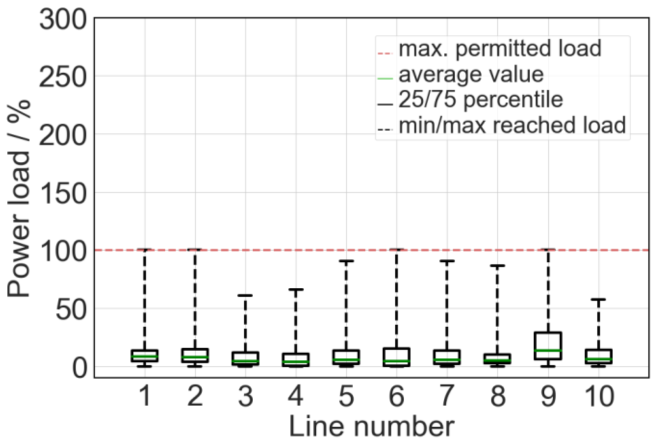

Figure 5-4 Load flow through the lines of the HV grid after grid expansion with OHL and DPC

The total costs of the combined application of OHL and DPC are estimated at about EUR 68 million, which is about 30 % lower than the costs of the grid expansion with only OHL. Table 5-6 shows the cost allocation of this variant, whereas the costs of OHL and line feeder panels constitute 47 % and the curtailment costs about 42 % of the total costs.

Table 5-6 Costs of the planning variant combining OHL and DPC

Total Costs / EUR Million	Investment in OHL / %	Investment in Feeder Panels / %	Operating Costs / %	Curtailment Costs / %
68	43.6	3.4	11.2	41.8

The yearly accruing current- and voltage-dependent losses were calculated, as described in 4.2.3.2 and 4.2.3.3. The total costs of the energy losses were subsequently determined, assuming constant yearly losses over the considered economic life. The total costs of the losses in the case of the grid expansion with OHL and DPC amount to EUR 8.1 million. Table 5-7 shows the calculated yearly losses and their repartitions between current- and voltage-dependent losses. As can be seen from the table, the yearly energy losses increased compared with the planning variant based only on OHL. This is due to the higher resistance of the power lines that have not been expanded.

Table 5-7 Resulting energy losses for the planning variant based on OHL and DPC

Costs of Energy Losses / EUR Million	Yearly Energy Losses / GWh/a	Current Dependent Losses / %	Voltage Dependent Losses / %
8.1	15.3	95.6	4.4

5.1.3 Planning Results in Case of UGC Application

The considered CGE with UGC in HV grids is meant to replace overloaded OHL with the appropriate cables that would prevent these overloads for all (n-1) states. In the case where an LS comprises two parallel OHLs and overloads are prognosticated on one of them, both lines would be replaced with as many UGCs as necessary to transport the prognosticated load flow through each line. Furthermore, it was assumed arbitrarily in this work that the detour factor amounts to 1.3 times the line length of the OHL. In this context, the planning algorithm determined the appropriate and cost optimized cable dimensioning to prevent the prognosticated overloads in the considered HV grid. Table 5-8 presents the original lengths of the overloaded OHLs according to Figure 5-1 and the resulting CGE variants. The lines parallel to line 1 and 2, despite not being affected by overloads and, hence, not presented in the table, were expanded according to variant 3 of the CGE, because they are included in the LSs LS1 and LS2. The expansion costs of these lines were also considered in the cost calculation. The total line length required in the case of CGE with UGCs represents here about 2.2 times the total required line length in the case of CGE with OHL.

Table 5-8 Resulting CGE measures with UGCs

Line	Original Length / km	CGE Variant
Line 1	9.8	3
Line 2	5.2	4
Line 3	2.4	4
Line 4	2.4	5
Line 5	21.4	4
Line 6	21.4	4
Line 7	11.8	4
Line 8	11.8	3
Line 9	14.2	4
Line 10	2.9	4

Figure 5-5 shows the power flow through the same lines as in Figure 5-2 after CGE based on UGCs, in the form of boxplots. The power flow values illustrated for each line consider the (n-0) and all relevant (n-1) states. The maximum values reached after application of the cables are now under the power-carrying capacity for all lines. The same as for CGE with OHLs, a transport capacity reserve is available for most of the lines, enabling more integration of RES than considered so far in the scenario 2030.

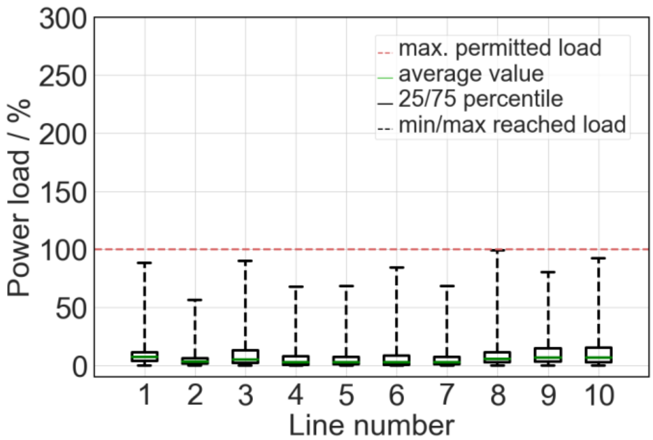

Figure 5-5 Load flow through the HV lines after CGE with UGC

The total costs of the CGE with cables, including the investments in cables, outgoing feeder panels, compensation reactors and operating costs over the economic life of 40 years, are presented in Table 5-9. These costs are estimated at about EUR 413.5 million, which represents about 4.3 times the total expansion costs with OHL.

Table 5-9 Costs of the planning variant using CGE with UGC

Total Costs / EUR Million	Investment in UGC / %	Investment in Feeder Panels / %	Investment in Reactors / %	Operating Costs / %
413.5	77.1	1.5	2.1	19.3

In addition to the current- and voltage-dependent losses, the compensation losses were calculated, as described in 4.2.3.4, in order to determine the yearly incurring energy losses. Based on that, the total costs of the energy losses over the considered economic life were estimated. As shown in Table 5-7, the total costs of the energy losses for this planning variant amount to EUR 5.5 million.

Table 5-10 Resulting energy losses for the planning variant with UGC

Costs of Energy Losses / EUR Million	Yearly Energy Losses / GWh/a	Current Dependent Losses / %	Voltage Dependent Losses / %	Compensation Losses / %
5.5	10.3	38	23.8	38.2

Although the yearly incurring energy losses, which amount to about 10.3 GWh, are, in total, a bit higher compared to the planning variant with OHL, the current-dependent losses are 55 % lower here than those of the OHL application. This is due to the conductor cross-section, which is generally bigger by cables than by OHLs, in order to enable the heat dissipation [77]. On the other hand, the voltage-dependent losses have a larger effect when applying UGCs than when applying OHLs due to the higher insulator conductance of cables. The compensation losses, which are negligible in the case of OHL application, make up, with 38.2 %, a considerable part of the losses in the case of the grid planning variant with cables.

5.1.4 Planning Results in the Case of UGC and DPC Application

When applying UGC in combination with the DPC, the required CGE measures were reduced. Table 5-11 shows the lines that still require CGE and the total energy curtailed over the simulated year. Compared with the variant based only on UGCs, the expansion of lines 1, 2 and 9, and those parallel to line 1 and 2 of the same LSs, was completely replaced here by the application of DPC. Furthermore, the expansion of lines 5 and 7 according to variant 4 of the CGE was replaced by variant 3 combined with the application of the DPC. In addition, the expansion of line 4 according to variant 5 of the CGE was replaced by variant 4, since the DPC led to the reduction of the RES power injection and, hence, to the reduction of the power flow through the considered lines, including line 4. Consequently, the total required cable length was reduced by the additional DPC application to about 51 % compared to only CGE with UGC.

Table 5-11 Results of the planning variant combining UGC and DPC

Line	Original Length / km	CGE Variant	Curtailed Energy / GWh/a
Line 3	2.4	4	22.8
Line 4	2.4	4	
Line 5	21.4	3	
Line 6	21.4	4	
Line 7	11.8	3	
Line 8	11.8	3	
Line 10	2.9	4	

Figure 5-6 presents the new power flow through the same lines as in Figure 5-2 after the combined application of UGC and DPC, in the form of boxplots. The power flow values illustrated for each line consider the (n-0) and all relevant (n-1) states. The contribution of the targeted DPC application to prevent the prognosticated overloads on lines 1, 2, 5, 7 and 9 can be demonstrated by the accordance of the maximum reached load flow value with the power-carrying capacity on these lines.

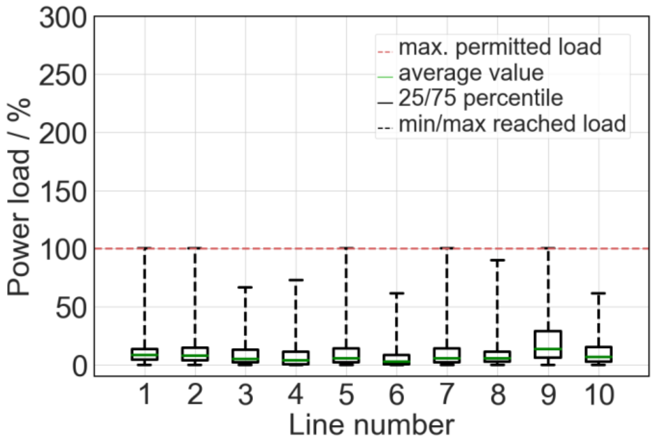

Figure 5-6 Load flow through the lines of the HV grid after grid expansion with UGC and DPC

The total costs of the grid expansion using UGC and DPC is estimated at about EUR 237.4 million, as shown in Table 5-12. The investment in cables has the highest share at about 68.6 %. The investment in feeder panels and compensation reactors is estimated at 3.2 %. The ongoing operating costs are estimated at 17.1 %. The curtailment costs constitute 11.1 % of the total costs, but lead to a reduction of the total costs to 57.4 % compared with the planning variant based only on UGCs.

Table 5-12 Costs of the planning variant combining UGC and DPC

Total Costs / EUR Million	Investment in UGC / %	Investment in Feeder Panels / %	Investment in Reactors / %	Operating Costs / %	DPC Costs / %
237.4	68.6	1.3	1.9	17.1	11.1

The current- and voltage-dependent losses as well as the compensation losses were calculated based on the planning algorithm results for this planning variant. The results of the loss calculation, shown in Table 5-13, reveal an increase of the yearly losses by this planning variant of about 17.5 % compared to the planning variant based only on UGCs.

Table 5-13 Resulting energy losses for the planning variant with UGC and DPC

Costs of Energy Losses / EUR Million	Yearly Energy Losses / GWh/a	Current Dependent Losses / %	Voltage Dependent Losses / %	Compensation Losses / %
6.4	12.1	71.2	12.25	16.55

Due to the DPC application, some OHLs have been kept in the grid and have not been replaced by cables. Given the fact that the resistance of OHL is greater than the resistance of UGC, the incurred current-dependent losses are, hence, higher when applying this planning variant than when applying only UGC and amount to about 71.2 % of the losses. The total costs of the losses over the considered economic life are estimated at about EUR 6.44 million.

5.1.5 Planning Results in the Case of BSS Application

When applying only BSS for the grid expansion, the planning algorithm, starting from nine possible nodes, determined six nodes that are appropriate for the placement and application of the BSS to prevent prognosticated line overloads. These nodes are SS2, SS3, SS5, SS6, SS7 and SS9. The total required capacity and rated power of the six BSS amount to about 2838 MWh and 260.4 MW, respectively. Table 5-14 shows the detailed repartition and dimensioning of the BSS.

Table 5-14 Results of the planning variant with BSS

Placement	Capacity / MWh	Rated Power / MW
SS2	5.2	4.4
SS3	134.8	29.6
SS5	38.8	11.2
SS6	1544.5	43.5
SS7	851.5	143.4
SS9	263.1	28.3

The total costs of such an application over the economic life of 40 years are estimated to about EUR 1520.1 million. Table 5-15 presents the allocation of the total costs, whereas the biggest part is due to the high storage capacity required in order to ensure the (n-1) conforming operation of the HV power lines. This planning variant based on BSS as the only planning instrument represents the least economic variant to prevent grid congestion and ensure the (n-1) criterion. On the other hand, such an application of BSS in the grid planning enables the entire avoidance of new CGE measures to prevent the prognosticated grid congestion.

Table 5-15 Resulting costs of the BSS variant

Total Costs / EUR Million	BSS Initial Investment / %	BSS Replacement Investment / %	BSS Operating Costs / %
1520.1	91.3 %	3.3 %	5.4 %

The incurred losses over the simulated year were calculated according to chapter 4.2.3, including storage losses as well as current- and voltage-dependent losses of the existing OHL. Table 5-16 presents the estimated total costs of the energy losses over the economic life of 40 years, as well as the calculated yearly energy losses and their repartition depending on the types of losses. Due to the application of BSS and the conservation of the existing OHL with high resistance in the power grid, the incurred yearly energy losses are relatively high compared to the planning variants based only on CGE. The current-dependent losses make up the biggest part of the losses with 61.7 %. The storage losses represent about 36.4 % of the total losses due to the frequent use of BSS to prevent grid congestion.

Table 5-16 Resulting energy losses for the planning variant with BSS

Costs of Energy Losses / EUR Million	Yearly Energy Losses / GWh/a	Storage Losses / %	Current Dependent Losses / %	Voltage Dependent Losses / %
17.6	33.2	36.4	61.7	1.9

5.1.6 Planning Results in the Case of BSS and DPC Application

When combining the use of BSS with DPC, the required BSS dimensioning decreases significantly. Consequently, only 2 of the 6 BSS are still required to prevent the grid congestion, and new CGE measures can still be avoided completely. As presented in Table 5-17 from the results of the planning algorithm, the appropriate nodes for the placement of the BSS are SS6 and SS9. The total capacity and rated power of the BSS amount in this case to about 347.1 MWh and 98.8 MW, respectively. The total curtailed energy over the simulated year accounts, thereby, for about 33.6 GWh.

Table 5-17 Results of the planning variant combining BSS and DPC

BSS Placement	BSS Capacity / MWh	BSS Rated Power / MW	Curtailed Energy / GWh/a
SS6	276.1	74.5	33.6
SS9	71	24.3	

The total costs of the combined use of BSS and DPC in the grid planning are estimated at about EUR 226.6 million. The allocation of these costs depending on the cost type is illustrated in Table 5-18. Due to the use of DPC, the storage capacity required for this planning variant amounts to about 12.2 % of the total capacity required when applying only BSS. The total costs have also decreased to about 15 % compared to that with only BSS application, although the curtailment costs represent only 17.2 % of the total costs. It is, thus, entirely reasonable to use the DPC in the case of the grid-supporting application of BSS.

Table 5-18 Resulting costs of the planning variant combining BSS and DPC

Total Costs / EUR Million	BSS Initial Investment / %	BSS Replacement Investment / %	BSS Operating Costs / %	DPC Costs / %
226.6	74.9	3.4	4.5	17.2

The energy losses over the simulated year were calculated based on the results of the planning algorithm. As shown in Table 5-19, the yearly energy losses decreased compared to the planning variant with only BSS due to the reduced use of BSS and, hence, the reduced storage losses, but are still relatively high compared with other planning variants. The current-dependent losses are still particularly high, since the existing OHLs have been kept in the grid. The total costs of the energy losses over the economic life amount to about EUR 13.4 million.

Table 5-19 Resulting energy losses for the planning variant with BSS and DPC

Costs of Energy Losses / EUR Million	Yearly Energy Losses / GWh/a	Storage Losses / %	Current Dependent Losses / %	Voltage Dependent Losses / %
13.4	25.4	21.1	76.4	2.5

5.1.7 Planning Results in the Case of OHL, BSS and DPC Application

The application of this planning variant in the planning algorithm delivered the same results as the planning variant based on OHL and DPC. Due to their high initial investment costs, BSS represent a more expensive planning instrument than OHL and DPC due to their high initial investment costs. Regarding the considered HV grid, the combined application of OHL and DPC represents the planning variant which prevents all prognosticated line congestion with the least costs.

5.1.8 Planning Results in the Case of UGC, BSS and DPC Application

The planning variant based on the combined application of BSS, DPC and UGC led to the reduction of the CGE measures and curtailed energy required to prevent the prognosticated grid congestion. By means of this variant, it is sufficient to replace line 6 with one cable (variant 3 of the CGE) instead of two parallel cables (variant 4 of the CGE) compared with the planning variant based on UGC and DPC. Consequently, this planning variant enables a reduction of the total required cable length to 40.5 % compared to the planning variant based on only CGE with cables. In addition to the CGE measures, the application of one BSS on the node SS6 with about 54 MWh capacity and 26 MW rated power, as well as a yearly curtailment of 22.4 GWh RES energy are required. Table 5-20 summarizes the resulting required expansion measures from the planning algorithm according to the considered planning variant.

Table 5-20 Results of the planning variant combining UGC, BSS and DPC

Line	Original Length / km	CGE Variant	Curtailed Energy / GWh/a	BSS Placement	BSS Capacity / MWh	BSS Power / MW
Line 3	2.4	4	22.4	SS6	54	26
Line 4	2.4	4				
Line 5	21.4	3				
Line 6	21.4	3				
Line 7	11.8	3				
Line 8	11.8	3				
Line 10	2.9	4				

As shown in Table 5-21, the total costs of this variant over the economic life of 40 years amount to about EUR 222.6 million. These costs represent 14.6 % of the BSS variant costs, and about 53.8 % of the cable variant costs. The combined use of BSS, DPC and UGCs is also more economical here than the combined use of BSS and DPC or the combined use of UGCs and DPC.

Table 5-21 Costs of the planning variant combining UGC, BSS and DPC

Total Costs / EUR Million	222.6
Investment in UGC / %	58
Investment in feeder panels / %	1.0
Investment in reactors / %	1.6
UGC operating costs / %	14.5
DPC costs / %	11.7
BSS investment / %	11.8
BSS Replacement investment / %	0.7
BSS operating costs / %	0.7

Table 5-21 shows the allocation of the total costs between CGE measures, BSS and DPC, whereas the costs of cables and feeder panels including investment and operating costs amount to about 75.1 % of the total costs. The DPC accounts for about 11.7 % and the BSS costs for about 13.2 %, including the initial investment, replacement investments and operating costs.

In a further step, the yearly accruing losses were calculated based on the resulting BSS scheduling and the prognosticated load flow through the lines. Table 5-22 shows the calculated yearly energy losses estimated at 13.6 GWh and their repartitions between storage losses, current- and voltage-dependent losses and compensation losses. As can be seen from the table, the current-dependent losses make up the significant part of the losses for this planning variant, since many existing OHLs have been maintained and were not replaced by cables. The total costs of the losses over the economic life of 40 years are estimated at EUR 7.2 million.

Table 5-22 Resulting energy losses for the planning variant with UGCs, BSS and DPC

Costs of Energy Losses / EUR million	Yearly Energy Losses / GWh/a	Storage Losses / %	Current Dependent Losses / %	Voltage Dependent Losses / %	Compensation Losses / %
7.2	13.6	9.7	69.6	9	11.7

5.1.9 Summary of the Grid Planning Results in the HV Grid

Table 5-23 ranks the considered planning variants in descending order based on the final total costs when summing the variant cost and the costs of the grid losses. In addition, the total length of the CGE measures required for every planning variant is indicated in the table. According to variant ranking, the planning variant combining OHLs and DPC represents the most economical planning variant to prevent grid congestion and ensure the (n-1) criterion. Furthermore, this planning variant enables a significant reduction of the required CGE measures compared to only CGE application.

The application of UGCs is still many times more expensive than the application of OHLs. In combination with BSS and DPC, the total costs of the grid expansion with UGCs can be significantly reduced but it is still more expensive than grid expansion with OHLs.

Additionally, it can be deduced from the results of the planning algorithm that the application of BSS alone in the grid planning of the considered HV grid represents the less economic planning variant. The use of BSS as the only planning tool to prevent all prognosticated congestion and fulfil the (n-1) criterion is technically feasible and enables the entire avoidance of CGE measures. However, this variant requires high storage capacities to store the RES surplus and also leads to the highest grid losses. This application is, therefore, economically inefficient.

When combining the BSS with the use of DPC, the total costs and the grid losses can be reduced significantly. This planning variant is more able to compete with other planning variants, such as the one with UGCs and DPC, than the variant based only on BSS.

The use of OHLs is still generally more economical than the use of BSS or UGCs. However, the application of OHLs in the grid planning can encounter low acceptance within society in some regions in Germany. This can slow the authorization process for OHL application and, hence, slow the integration of more RES into the grid. In that case, the planning variant combining BSS, UGCs and DPC could be a turnaround solution for the expansion of the power grid at relatively acceptable costs and could, thus, enhance the integration of renewables into the grid. Furthermore, this variant could enable a reduction in the required CGE measures compared with only a CGE application.

Table 5-23 Ranking of the planning variants based on the resulting costs and the CGE length

Planning Variant	Expansion Variant Costs / EUR Million	Costs of Energy Losses / EUR Million	Total Final Costs / EUR Million	Length of CGE Measures / km
OHL and DPC	68	8.1	76.1	74.3
OHL	97.2	5.2	102.4	118.4
UGC, BSS and DPC	222.6	7.2	229.8	106.6
BSS and DPC	226.6	13.4	240	0
UGC and DPC	237.4	6.4	243.8	134.5
UGC	413.5	5.5	419	263.5
BSS	1520.1	17.6	1537.7	0

In order to evaluate the necessary computing effort of the optimization for each planning variant, the computing time, the internal memory of the computer (RAM) used, and the variables and constraints of the MILP optimization were determined. Table 5-24 summarizes the results of these parameters. The indicated memory of the RAM used in the table is calculated in percent in relation to the total available RAM memory of 78 GB after the termination of the optimization. It should be noted that for the sake of simplification of the optimization problem and reduction of the computing time, the following simplifications were adopted:

- In the case of the planning variants without application of BSS, only days which show an overload or a violation of the (n-1) criterion over at least 15 minutes of the day have been considered in the optimization.
- In the case of variants with BSS application, all the days which show an overload or a violation of the (n-1) criterion over at least 15 minutes of the day

have been considered in the optimization. In addition, some following days were also considered in order to enable the discharging of the BSS into the grid on these days in consideration of the grid restrictions.

- In the case of the variant with only BSS application and the variant with BSS and DPC application, six relevant nodes in the grid were selected initially and implemented into the planning algorithm as potential nodes for the placement of the BSS.
- In the case of the variant with BSS, DPC and UGCs, only two nodes were selected initially as potential nodes for the placement of BSS. These two nodes were chosen based on the planning results for the variant BSS and DPC, where six nodes were initially selected for the placement of BSS, but only two of them were chosen from the optimization as appropriate for the placement of BSS. Furthermore, the curtailable PV and wind plants were restricted to relevant plants. These simplifications were made for the variant based on BSS, DPC and UGCs in order to reduce the number of optimization variables.
- In order to evaluate the computing effort, documented in Table 5-24, the subordinate optimization function (39), described in 5.1.9, was neglected here because its main contribution is to discharge the storages when no grid congestion is prognosticated in order to use the free capacity for market-based applications. This function has no influence on the resulting costs and the nodes chosen for the placement of BSS.

Table 5-24 Evaluation of the computing effort of the MILP optimization

Planning Variant	Computing Time / min	Variables	Constraints	Memory / %
OHL	2.4 min	32	13	4.2
OHL and DPC	370.6 min	473586	473692	5.4
UGC	2.6 min	55	22	4.2
UGC and DPC	534.1	473611	473703	5.1
BSS	61 min	145193	1403147	4
BSS and DPC	61 min	615293	1843420	4.9
Cable, BSS and DPC	2150 min	248157	225337	4.9

It can be deduced from the analysis of the computing effort that the planning variants based on only OHLs or UGCs require less computing effort since they are using only a few optimization variables of type binary that are restricted to 0 or 1. The planning variants using BSS or BSS and DPC are based on a lot more optimization variables of type continuous. The solver, therefore, requires more computing time to solve the optimization problem. When combining continuous with binary optimization variables, the complexity of the problem increases and the solver requires even more computing time to solve the integrality restrictions of the MILP problem using the branch and bound approach described in chapter 4.1.2. This is the case for the planning variant combining UGCs, BSS and DPC. It should be noted that the number of variables and constraints of this planning variant is reduced in comparison to the planning variant using BSS and DPC due to the simplifications described above.

5.2 Application of the Grid Planning Algorithm on a MV Grid

The linearized LFC of the modelled MV grid, as described in 3.2.4, delivered the voltage magnitudes and angles as well as the power flow in the grid. Figure 5-7 shows the voltage magnitude at 6 out of 132 nodes of the considered MV grid, in the form of box plots. The node number 2 represents the node where the wind plants are connected. The high value of the power injection from the wind plants led to high-voltage magnitude values on that node, which exceeded at certain points the +5 % voltage transgression limits, illustrated by the dotted red lines in the figure. The LFC of the MV grid also revealed that some lines of the grid were overloaded due to the high feed-in of RES before grid expansion. Figure 5-8 illustrates the loading of 4 out of 131 lines in relation to their current-carrying capacities, in the form of boxplots. These lines show an overload at certain time points of the simulated year. The boxplots indicate the loading values on every power line for 25, 50 and 75 % of the total calculated loading states as well as the minimum and maximum reached loading values. The dotted red line represents the current-carrying capacity of the lines.

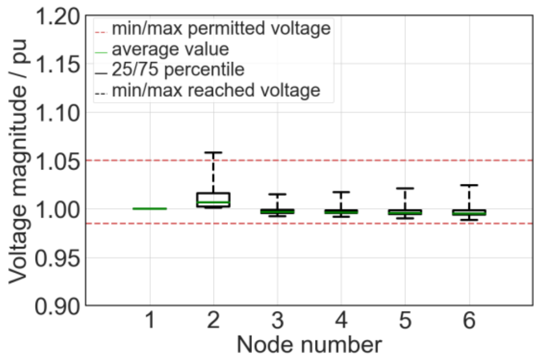

Figure 5-7 Voltage magnitude on the nodes which are connected to the overloaded lines of the MV grid

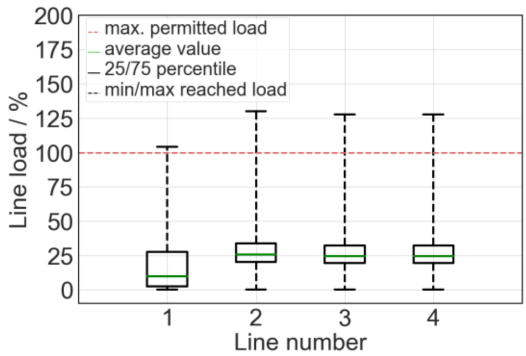

Figure 5-8 Line load on the overloaded lines of the MV grid

It can be deduced from Figure 5-7 and 5-8 that the scenario 2030 would lead to some congestions in the considered MV grid if no grid expansion measures are applied. The congestion, although infrequent during the year, could endanger the energy supply security. In what follows, the planning algorithm, as described in chapter 4, was applied to prevent these grid congestions by the use of conventional and innovative grid expansion instruments. The conventional expansion instruments considered here are UGCs, and the innovative expansion instruments are the BSS and the DPC. These measures were used in the planning algorithm separately and combined in order to compare the resulting expansion measures and the total costs incurred for each planning variant. Thereby, the energy losses were neglected for the grid planning of MV grids and the specific costs indicated in chapter 4 have been adopted for the calculation of the total costs.

5.2.1 Planning Results in the Case of UGC Application

The following considered planning variant consists of the CGE based on UGCs. This planning variant is implemented in the planning algorithm such that it can prevent power line overloads and contribute to the voltage magnitude reduction on the grid nodes, but cannot totally ensure the prevention of eventual voltage transgression on grid nodes. As described in 3.2.4.2 and 4.3.2, the matrix (A) representing the inverse of the Jacobean matrix and the column vector (C) were assumed to be constant in the linearized LFC. This means that the variation of the voltage magnitude and angle in the optimization problem according to (25) can only be done through the variation of the injection power $(\tilde{p})$ and $(\tilde{q})$. Therefore, the planning variant based only on CGE with UGCs cannot on its own satisfy the implemented constraints (85) that limit the voltage boost on the grid nodes to -−1.5 % and +5 % of the nominal voltage. To evaluate the planning variant with only UGCs, the voltage constraints (85) were omitted and only constraints regarding the current-carrying capacity of the lines were considered. Table 5-25 shows the original length of each overloaded line before grid expansion and the resulting CGE measures from the planning algorithm to prevent the line overloads.

Table 5-25 Results of the planning variant with UGC

Line	Length / km	CGE Variant
Line 1	13.8	3
Line 2	0.253	2
Line 3	0.498	2
Line 4	0.456	2

According to the planning results, the lines 2, 3 and 4, which each originally had a current-carrying capacity of 175 A, should each now be replaced by a cable with a current-carrying capacity of 361 A (variant 2 of the CGE). Furthermore, the 537 A cable of line 1, which connects the wind plant to the 20 kV substation busbar, should be replaced by two parallel cables each of 361 A, thus, allowing a combined current-carrying capacity of 722 A (variant 3 of the CGE). The total length of the required CGE measures amounts to about 28.8 km.

The total costs of these CGE measures over the considered economic life of 40 years are estimated at about EUR 4.1 million. Table 5-26 shows the cost allocation between investment in UGCs and feeder panels as well as ongoing operating costs.

Table 5-26 Resulting costs of the planning variant with UGC

Total Costs / EUR Million	Investment in UGC / %	Investment in Feeder Panels / %	Operating Costs / %
4.1	78.5	2.2	19.3

Based on the CGE with UGCs, the original lines of the MV grid are replaced by standard cables with higher current-carrying capacity. Figure 5-9 and 5-10 show the injected power from the wind plant and the resulting current flow through the line 1, respectively, connected to the power plants, before CGE (blue traces) and after CGE (dotted green traces). As illustrated by the figures, the line connecting the wind plants to the grid with a current-carrying capacity of 537 A was replaced with two parallel standard cables by the planning algorithm, enabling a total current-carrying capacity of 722 A. The dotted red line in Figure 5-10 represents the thermal current-carrying capacity of the original line, and the dotted purple line illustrates the current-carrying capacity of 722 A of the new parallel cables in the case of CGE.

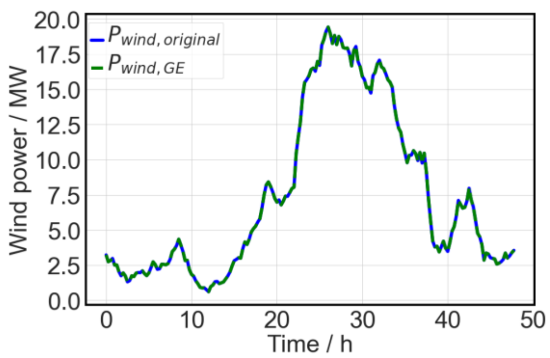

Figure 5-9 Injected power of the wind plants initially (blue) and after CGE (green)

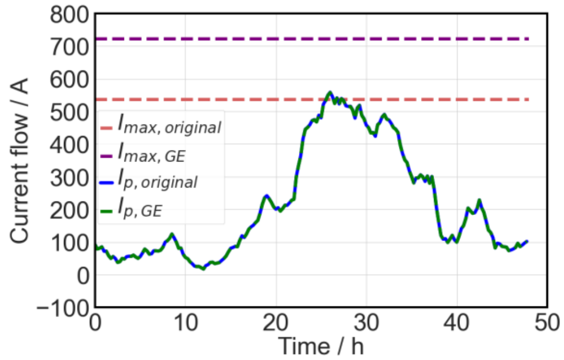

Figure 5-10 Current flow through the line 1 originally (blue) and after CGE (green)

5.2.2 Planning Results in the Case of BSS Application

When choosing BSS as the only possible grid expansion instrument, the results of the planning algorithm show that two BSS are required to prevent the prognosticated grid congestion with 12.2 MWh total capacity and 4.5 MW total rated power. Table 5-27 shows the location and dimensioning of the BSS. By means of this planning variant, new CGE measures can be completely avoided.

Table 5-27 Results of the planning variant with BSS

BSS Placement	BSS Capacity / MWh	BSS Rated Power / MW
Node 2	6.3	2.7
Node 6	5.9	1.8

The costs of this planning variant amount to EUR 6.6 million. Almost 90 % of these costs accrue at the initial investment. The remaining 10 % are due to the ongoing operating costs of the BSS and the replacement investments in battery cells and converters at the end of their service life.

Table 5-28 Resulting costs of the BSS planning variant

Total Costs / EUR Million	BSS Initial Investment / %	BSS Replacement Investment / %	BSS Operating Costs / %
6.6	90	4.6	5.4

The placement of a BSS on the connection node of the wind plants (Node 2) is part of the resulting expansion measures. In addition to the dimensioning and costs, the planning algorithm also delivers the power scheduling of the BSS over the simulated year. As demonstrated in Figure 5-11 for two exemplary days of the simulated year, the BSS would charge the surplus power at times of high feed-in wind power and discharge it later when the power injection decreases (green line). If the BSS is not applied, the totality of the wind power would be injected into the grid (blue line) causing grid congestion. Figure 5-12 shows the charging and discharging power of the BSS (blue line) and the stored energy (orange line).

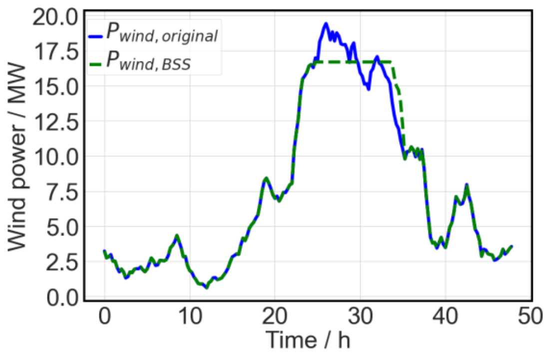

Figure 5-11 Injection power of the wind plants originally (blue) and after application of the BSS (green)

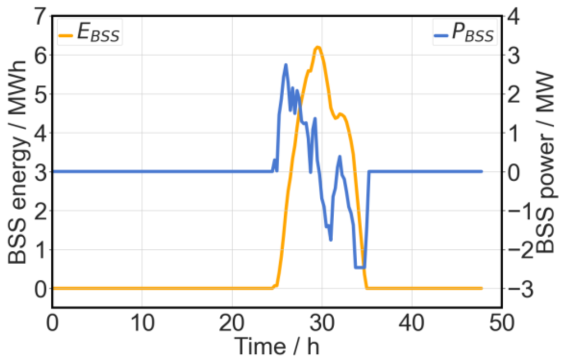

Figure 5-12 Charging and discharging power (blue) and stored energy (orange) of the BSS

In order to prevent grid congestion, the planning algorithm calculates the exact amount of power that should be charged by the BSS at every time step, depending on the prognosticated injection power. The prognosticated injection power is given as input to the planning algorithm in the form of time series for every node and represents the time series calculated in this work, as described in 3.2.2. Figure 5-13 shows the compliance of the resulting voltage magnitude values (green line) on the connection node of the wind plants with the permitted voltage limit (dotted red line) due to the charging of the surplus power. The blue line in the figure shows the transgression of the voltage magnitude limit if no grid expansion is realized. Since the voltage constraints, in this particular case, are more conservative than the load flow constraints, the amount of power charged in the BSS to fulfill the maximum permitted voltage magnitude is higher than the necessary power amount to satisfy the thermal current-carrying capacity of the line that connects the wind plants to the grid. As shown in Figure 5-14, the current flow values (green line) of the line is clearly below its current-carrying capacity (dotted red line). Once no grid congestion is prognosticated, the BSS discharges the power into the grid taking into account the voltage and current constraints.

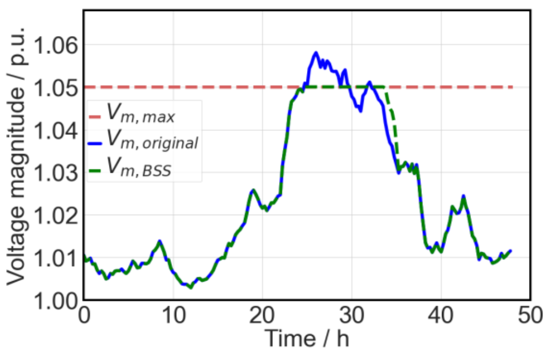

Figure 5-13 Voltage magnitude on node 2, originally (blue) and by BSS application (green)

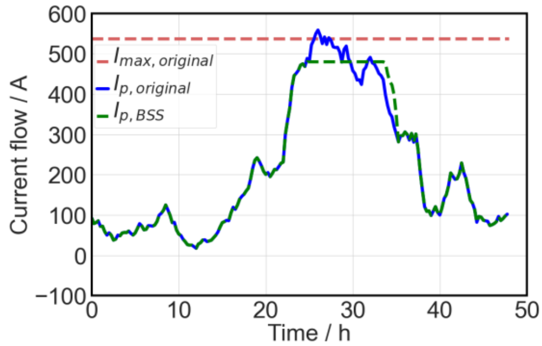

Figure 5-14 Current flow through the line 1 before (blue) and after BSS application (green)

5.2.3 Planning Results in the Case of DPC Application

When using the DPC as the only planning instrument, an amount of about 47 MWh must be curtailed from the RES feed-in energy in order to prevent the prognosticated grid congestion during the simulation year. As shown in Table 5-29, this corresponds to about 0.069 % of the total prognosticated RES energy in a year. Consequently, the dynamic curtailment variant is sufficient to prevent all prognosticated congestion for the considered MV grid.

Table 5-29 Results of the planning variant with DPC

Plants	Total Prognosticated Energy / GWh/a	Curtailed Energy / MWh/a
PV	38.9	30.1
Wind	29.1	16.8

For the calculation of the DPC costs, the yearly amount of curtailed energy in the simulation year and the specific costs of the DPC were assumed to be constant over the economic life of 40 years. As shown is Table 5-30, the total costs of this planning variant are estimated at around EUR 0.054 million. The DPC variant is, consequently, more economical than the CGE or BSS variant.

Table 5-30 Resulting costs of the DPC variant

Total Costs / EUR Million
0.054

In addition to the costs, the planning algorithm delivers the power scheduling of the RES over the simulated year taking into account the DPC applied. Figure 5-15 shows the feed-in power of the wind plants originally (blue line) and after application of the DPC (green line), based on the same conditions and exemplary days as in Figure 5-11.

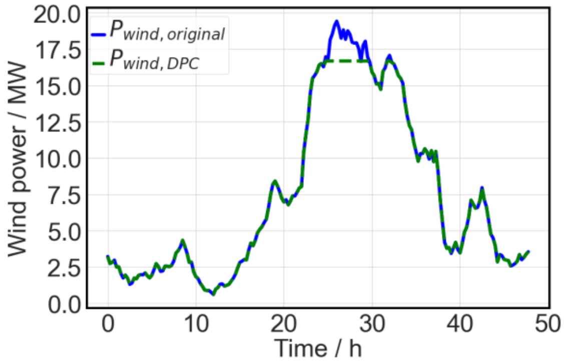

Figure 5-15 Injection power of the wind plants originally (blue) and after application of the DPC (green)

As illustrated by Figure 5-16 and 5-17, the wind power peak was reduced by the application of the DPC so that the prognosticated voltage and current congestion (blue lines) could be prevented (green lines). The use of the DPC follows almost the same principle as the application of the BSS, with the difference, however, that the surplus power curtailed is definitely unexploited.

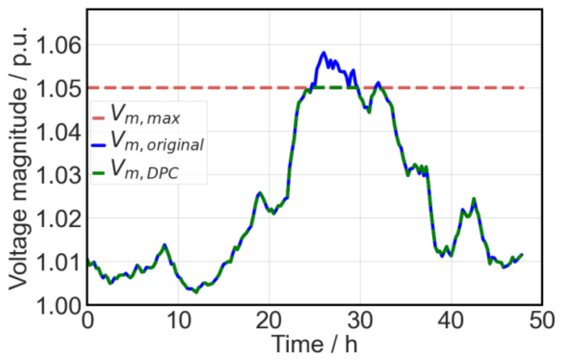

Figure 5-16 Voltage magnitude on node 2 originally (blue) and by the application of DPC

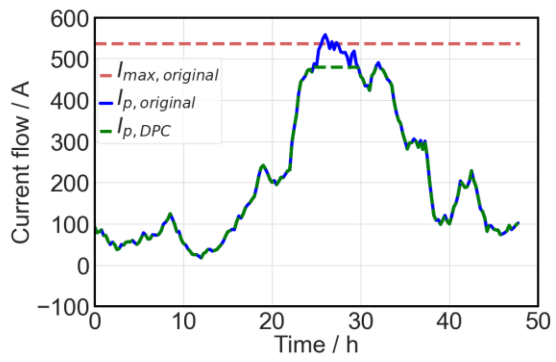

Figure 5-17 Current flow through the line 1 originally (blue) and by the application of DPC

5.2.4 Planning Results in the Case of UGC and BSS Application

In a further step, the planning algorithm was applied choosing a combination of BSS and UGCs for the grid planning. According to the results of the planning algorithm, the use of the BSS allowed the fulfilment of the current constraints on line 1 and the voltage constraints on node 2. As presented in Table 5-31 and 5-32, line 1 was not replaced by new cables. Instead, one BSS with a capacity of 6.3 MWh and a rated power of 2.7 MW was applied to node 2, connecting the wind plant to the grid. On the other hand, the lines 2, 3 and 4 were each replaced by a cable with a current-carrying capacity of 361 A. The total length of the required CGE measures was, thus, reduced to about 4.2 % compared to the planning variant with only CGE.

Table 5-31 Results of the BSS dimensioning for the planning variant combining BSS and UGC

BSS Placement	BSS Capacity / MWh	BSS Rated Power / MW
Node 2	6.3	2.7

Table 5-32 Results of the cable dimensioning for the planning variant combining BSS and UGC

Line	Length / km	CGE Variant
Line 2	0.253	2
Line 3	0.498	2
Line 4	0.456	2

The total costs of this variant are estimated at around EUR 3.65 million. Table 5-33 shows the cost allocation between BSS and UGCs. Consequently, the planning variant combining BSS and UGC is by 11 % more economical than the planning variant based only on UGCs and by 44.7 % more economical than the planning variant based only on BSS.

Table 5-33 Resulting costs of the grid expansion based on BSS and UGC

Total Costs / EUR Million	**3.65**
BSS investment / %	84.4
BSS replacement investment / %	4.6
BSS operating costs / %	5
UGC investment / %	4.8
Feeder panel investment / %	0
UGC operating costs / %	1.2

5.2.5 Summary of the Grid Planning Results in the MV Grid

Table 5-34 ranks the considered planning variants of the MV grid in descending order based on the total costs of the variants. In addition, the total length of the required CGE measures for every planning variant is indicated in the table. It can be deduced from the evaluation of the results that the DPC is the most economical variant for the planning of the considered MV grid. Since the prognosticated congestion in the grid is infrequent, the targeted curtailment of PV and wind power peaks would be sufficient to prevent this congestion without the application of CGE measures and without even using the totality of the 3 % curtailment limit for each plant. However, the disadvantage of this variant is that curtailed power is definitely wasted.

The second most economical planning variant according to the planning algorithm is the combination of UGCs with BSS. The power line expansion was applied on three lines of the grid in order to prevent their overload and the BSS was applied on the connection node of the wind plants to the grid, in order to prevent voltage transgression on the connection node and the overload of the connecting line. The combination of BSS with UGCs in the grid planning proved to be more economical than using UGCs or BSS separately. Furthermore, this variant enables a significant reduction of the required CGE measures.

The use of BSS as the only grid expansion instrument has shown to be the most expensive solution and not economically reasonable in particular to prevent very high prognosticated line overloads as is the case for lines 2, 3 and 4 of the considered MV grid. Nevertheless, the application of the BSS can be reasonable for preventing voltage congestion and moderate overloads as is the case for node 2 and line 1 which connect the wind plants to the grid.

Table 5-34 Ranking of the planning variants based on the total resulting costs

Planning Variant	Total Costs / EUR Million	Length of CGE Measures / km
DPC	0.054	0
UGC and BSS	3.65	1.2
UGC	4.1	28.8
BSS	6.6	0

Figure 5-18 presents the loading on lines 1, 2, 3 and 4 after the application of BSS in the form of boxplots. These power lines originally showed an overload at certain points of the simulated year. As demonstrated by the figure, the optimized application of BSS enables the operation of the lines in consideration of their current-carrying capacity at each point in time of the simulated year with 15 minutes time resolution. The application of CGE, however, generally leads to an over-dimensioning of the grid, as shown in Figure 5-19. This enables a certain reserve that can be used to integrate more RES or in case of deviating prognoses.

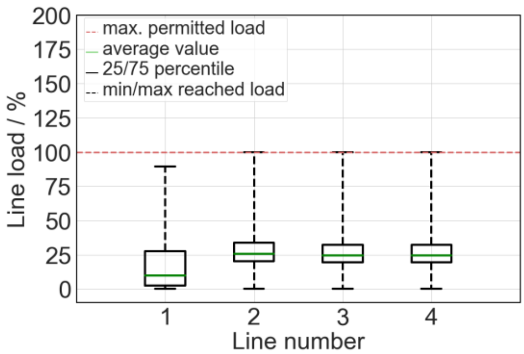

Figure 5-18 Line load of the originally overloaded lines after application of BSS

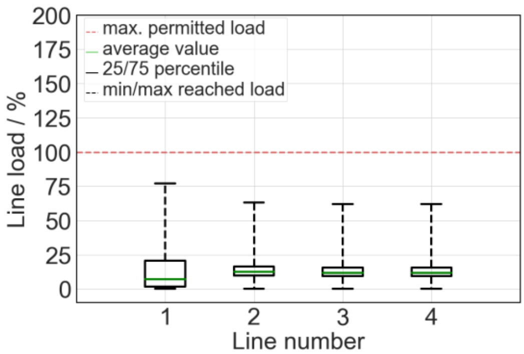

Figure 5-19 Line load of the originally overloaded lines after CGE

In order to evaluate the computing effort of the optimization that is needed for each planning variant, the computing time, the internal memory of the computer used (RAM), as well as the variables and constraints of the MILP optimization were determined. Table 5-35 summarizes the results of these parameters. The indicated memory of the RAM used in the table is calculated in percent in relation to the total available RAM memory of about 78 GB after the termination of the optimization. It should be noted that for the sake of simplification of the optimization problem and reduction of the required computing time, the following simplifications were adopted:

- All the days which show a line overload or a violation of the voltage limits over at least 15 minutes of the day were considered in the optimization for all the considered variants. In addition, the day following each determined day with overloads was also considered in order to enable the discharging of the BSS into the grid on these days considering the grid restrictions.

- For all variants where BSS are applied, five relevant nodes in the grid were selected initially and implemented in the planning algorithm as potential nodes for the placement of the BSS.
- The curtailable PV and wind plants were restricted to relevant plants near the grid congestion.

Table 5-35 Evaluation of the computing effort of the MILP optimization

Planning Variant	Computing Time / min	Variables	Constraints	Memory / %
UGC	0.328	36893	36876	4.9 %
DPC	1.12	137385	228977	5.1 %
BSS	6.45	213718	244229	5.1 %
UGC and BSS	20.6	213738	203536	4.8 %

Analogously to the results of the HV grid, the higher the number of variables and constraints in the optimization, the higher the computing effort required. In addition to the number of variables and constraints, the type of the optimization variables also has an influence on the required computing effort. The optimization of the planning variant with only UGCs is based on a few binary optimization variables that can only have the value 0 or 1. This reduces the computing effort required to solve the MILP problem using the branch and bound approach, as described in chapter 4.1.2. It should be noted that this planning variant also comprises continuous variables, which reproduce the voltage magnitude and angles of the grid nodes. Therefore, the number of variables for this planning variant is high compared with the equivalent planning variant applied in the HV grid.

The planning variants using DPC or BSS require a lot more optimization variables of type continuous than the CGE variant. Consequently, the solving of the MILP problem requires more computing effort for these planning variants. The planning variant using UGC and BSS comprises binary and continuous optimization variables. This leads to more required optimization variables and, at the same time, increases the complexity of the optimization problem.

6 Development of a Multiuse Concept for the BSS

The power flow value through a line can be extremely variable depending, *inter alia*, on the fluctuating feed-in power of RES into the grid and the grid state meaning (n-0) or (n-1) state. Based on the 2030 RES expansion scenario, the grid congestion was determined in the considered HV grid on 33 % of the days of the simulated year. This means that the modelled BSS would stay unused in two-thirds of the simulated year if only a grid-supporting use is envisaged. In order to reduce the total costs of the grid planning when using BSS, a multiuse concept of the BSS was followed. Within this concept, the BSS dimensioned according to chapter 5, would participate in the EPEX Day-Ahead market to trade electricity at times when they are not required for grid-supporting purposes. Due to the unbundling requirements, the market-based application is, in this case, only possible if performed from a third party other than the grid operator. The concept adopted for multiuse BSS and the gains resulting from this concept are presented in what follows.

6.1 Concept Adopted for Multiuse BSS

In order to determine the maximal possible profits from the electricity trade, a linear optimization was implemented to maximize the profits over the simulated year. Thereby, the following assumptions were considered in the optimization:

- The operation of the BSS for the electricity trade must be steady in accordance with the storage dimensioning resulting from the planning algorithm
- The overriding objective of the BSS application is the prevention of grid congestion. Therefore, the capacity and rated power amounts required for the grid-supporting application must be set aside at the time of prognosticated overloads and not used for the electricity trade.
- Only the exact storage capacity and power amounts required to prevent prognosticated grid congestion were set aside. This implies a perfect prognosis of the grid congestion and, hence, of the consumption and feed-in power in the grid.
- The electricity trade within the electricity market must conform with the grid restrictions and the (n-1) criterion in the case of HV grids.
- The optimization of the profit from the EPEX Day-Ahead market is based in this work on a perfect market prognosis such that the BSS operator has a

perfect prognosis of the electricity prices on the delivery day and can optimally decide about the bids to submit on the day before. This also implies that the submitted bids are always accepted.

- The electricity prices used in the profit optimization represent the real resulting market clearing prices in the EPEX Day-Ahead market in 2018.

In this work, perfect prognoses of the grid congestion and the market behavior were assumed for the grid planning and the estimation of the profits from the electricity market. However, an appropriate security margin must be applied for the real operation of BSS in the grid or the electricity market, in order to consider forecast uncertainties. Hereafter, the implemented linear optimization to maximize the profits from the electricity market is described in detail.

The main objective for using the BSS is to prevent grid congestion. At times when they are not required for grid-supporting purposes, the BSS can be applied to participate in the spot market in order to make profits. When the electricity price is low, the energy is bought and stored, and when the price increases, the stored energy in the BSS is sold. The operation of the BSS in the EPEX Day-Ahead market was optimized in this research work such that the profits from the electricity trade are maximized and eventual grid congestion due to this operation is prevented. The yearly profits $Gain_{Spot,a}$ are calculated depending on the revenues and expenses arising at every hour of the year.

$$max\left\{Gain_{Spot,a}\right\} = min\left\{\sum_{s=1}^{N_{BSS}} \sum_{t=0}^{N_{steps,h}} K_{trade,s,t} + K_{tax,s,t} + K_{fee,s,t}\right\} \tag{89}$$

$Gain_{Spot,a}$	Yearly profits from the participation of the BSS in the Day-Ahead Market in $EUR\ /a$ (optimization variable)
$K_{trade,s,t}$	Expenses or revenues of the BSS s occurring from the electricity trade at time step t in EUR (optimization variable)
$K_{tax,s,t}$	Tax expenses occurring by charging the electricity from the grid into the BSS s at time step t in EUR (optimization variable)
$K_{fee,s,t}$	Stock market fees occurring at time step t due to the participation of the BSS s in the Day-Ahead market in EUR (optimization variable)

The optimization variable $K_{trade,s,t}$ is calculated subject to the charging or discharging power $P_{market,s,t}$ of the BSS and the electricity price $Price_{market,t}$ at every hour t of the year. By charging the electrical power from the grid, the BSS power is positive according to the passive sign convention. By discharging into the grid, the BSS power is negative. If the BSS is charging power from the grid for a specific hour of the day and the electricity price is positive, it means that the electricity is being bought and charged into the BSS. For this specific hour t, $K_{trade,t}$ is, thus, positive and represents the expenses for buying the electricity on the Spot market. If the BSS is discharging power into the grid and the electricity price is positive, it means that the electricity is being sold. $K_{trade,t}$ is, thus, negative and represents the revenues from selling the electricity on the Spot market. The electricity price on the spot market can be either positive or negative in response to prevailing supply and demand. In all cases, if $K_{trade,t}$ is negative for a specific hour t, it represents a revenue. If it is positive, it represents an expense.

$$K_{trade,s,t} = P_{market,s,t} \cdot \Delta t_{market} \cdot Price_{market,t} \tag{90}$$

$$\forall\, s \in S, \forall\, t \in T_{year,h}$$

$P_{market,s,t}$	Charging or discharging power of the BSS s for the electricity trade at time step t in MW (optimization variable)
Δt_{market}	Time step of the transactions which equals 1 hour on the Day-Ahead market in h
$Price_{market,t}$	The electricity price on the EPEX Spot market at time step t in EUR/MWh

The BSS power $P_{market,s,t}$ depends on the charging power $P_{market,c,s,t}$ and the discharging power $P_{market,d,s,t}$ on the grid side:

$$P_{market,s,t} = P_{market,c,s,t} - P_{market,d,s,t} \tag{91}$$

$$\forall\, s \in S, \forall\, t \in T_{year,h}$$

$P_{market,c,s,t}$	Charging power of the BSS s for the electricity trade at time step t in MW
$P_{market,d,s,t}$	Discharging power of the BSS s for the electricity trade at time step t in MW

The following constraint was implemented in order to ensure that the BSS is not charging and discharging simultaneously:

$$min\{P_{market,c,s,t}, P_{market,d,s,t}\} = 0 \tag{92}$$

$$\forall\, s \in S, \forall\, t \in T_{year,h}, P_{market,c,s,t} \geq 0, P_{market,d,s,t} \geq 0$$

The tax expenses $K_{tax,t}$ accrue when charging energy from the grid, since it behaves in this case as a connected load into the grid. The tax expenses were calculated in the optimization as follows:

$$K_{tax,t} = P_{market,c,s,t} \cdot \Delta t_{market} \cdot Tax_{Batt} \tag{93}$$

Tax_{Batt} Specific tax costs by charging the BSS from the grid in EUR/MWh

The transaction fees represent the charges levied for the realization of transactions and registration of contracts through the market platform. They were considered in the linear optimization as follows:

$$K_{fee,t} = \left|P_{market,s,t}\right| \cdot \Delta t_{market} \cdot Fee_{Transaction} \tag{94}$$

$Fee_{Transaction}$ Specific levied fees for the use of the market platform in EUR/MWh

The stored energy amount $E_{market,s,t}$ due to the electricity trade was calculated depending on the charging and discharging power and on the charge and discharge efficiency factor of the BSS:

$$E_{market,s,t} = (P_{market,c,s,t} \cdot \eta_{BSS} - \frac{P_{market,d,s,t}}{\eta_{BSS}}) \cdot \Delta t_{step} + E_{market,s,t-1} \tag{95}$$

$$\forall\, s \in S, \forall\, t \in T_{year,h}$$

$E_{market,s,t}$ Resulting energy amount from the electricity trade in the BSS s at time step t in MWh

Additionally, further linear constraints were implemented in the optimization in order to set aside the power amount required for the management of the grid congestion at the time of prognosticated overloads and separate it from the power amount applied for the electricity trade. The sum of both absolute values must be less or equal to the rated power of the BSS.

$$0 \le \left|P_{market,s,t}\right| + \left|P_{s,t}\right| \le P_{max,s} \tag{96}$$

$$\forall\, s \in S, \forall\, t \in T_{year,h}$$

The same applies to the respective energy amounts at every time step.

$$0 \le E_{market,s,t} + E_{s,t} \le E_{max,s} \tag{97}$$

$$\forall\, s \in S, \forall\, t \in T_{year,h}$$

Managing the prognosticated congestion in the grid is the prime purpose of the BSS application. Therefore, the electricity trade also has to be carried out considering the restrictions of the grid and the (n-1) criterion in the case of HV grids. For this purpose, further linear constraints were implemented in the optimization to constrain the power ($P_{Market,S,t}$) of the BSS for electricity trade, as illustrated by (98) for the HV grid. Hereby, the storage power for the congestion management ($P_{S,t}$) and the curtailed power amount ($\Delta P_{RES,t}$) are considered as known values and no longer as optimization variables, since they have already been calculated in the BSS scheduling optimization for grid congestion management, as described in chapter 4.

$$\begin{cases} (NACLODF)^{(a)}[l;N] \cdot ((P_{N,t}) + (P_{S,t}) + (\Delta P_{RES,t}) + (P_{Market,S,t})) \leq S_{max,l} \\ (NACLODF)^{(a)}[l;N] \cdot ((P_{N,t}) + (P_{S,t}) + (\Delta P_{RES,t}) + (P_{Market,S,t})) \geq -S_{max,l} \end{cases} \tag{98}$$

$$\forall\, l \in L, \forall\, a \in A, \forall\, t \in T_{year,h}$$

Battery systems should only reach a limited full cycle number N_{cycle} by charging and discharging the electrical energy. Therefore, the number of full cycles due to the grid-supporting and market-based operations of the BSS in the optimization was constrained to the maximum number of cycles N_{cycle} of the BSS.

$$\sum_{t=1}^{N_{steps,h}} (E_{market,s,t} + E_{s,t}) \leq \frac{N_{cycle}}{N_{life,batt}} \cdot E_{s,max} \tag{99}$$

$$\forall\, s \in S$$

N_{cycle} Maximum full cycle number of the BSS

The profit made over the simulated year was assumed to be constant yearly over the economic life of 40 years. The yearly profits were then discounted over the economic life in consideration of the adopted interest rate to the present value of the total gains $Gain_{tot}$ at the initial investment year.

$$Gain_{tot} = Gain_{Spot,a} \cdot \frac{(1+r)^{N_{years}} - 1}{r \cdot (1+r)^{N_{years}}} \cdot 10^{-6} \tag{100}$$

$Gain_{tot}$ Total profits from the participation of the BSS in the Day-Ahead Market over the economic life of 40 years in $EUR\ million$

Table 6-1 presents the specific costs and input data adopted for the calculation of the yearly profits $Gain_{Spot,a}$ from the EPEX Spot market, as described above. Thereby, the adopted specific tax cost Tax_{Batt} was estimated in this work based on the electricity taxes levied in Germany in 2018, from which BSS are not exempt. The levied taxes include the concession tax, the tax for offshore wind energy, the tax for interruptible loads and the tax according to paragraph 19 of the regulation ordinance [78].

Table 6-1 Input data adopted for the calculation of the profits from the EPEX Spot market

Input Data	Value
Specific tax costs	2.2 EUR/MWh
Specific transaction fees in the EPEX Spot market	0.0075 EUR/MWh [85]
Electricity price in the EPEX Spot market	Historic data of the year 2018 [82]
Charge/discharge cycles	5000 [86]

6.2 Resulting Gains from the Multiuse BSS

The participation of the BSS in the Day-Ahead trade of the EPEX Spot market concerns only the planning variants in which BSS are applied. This market-based application of the BSS involves outgoing costs for the purchase of the electricity as well as for the taxes and charges levied. On the other hand, selling the stored electricity of the BSS leads to revenues. The application of the linear optimization, as described in 6.1, maximizes the total profit from the electricity trade over the considered year. Thereby, the grid-supporting application of the BSS takes precedence over the market-based application. The results of the BSS application for electricity trade in the HV and MV grids are presented in what follows.

6.2.1 Resulting Gains from the Multiuse BSS in the HV Grid

In order to compare the total costs of the planning variants using BSS with the total gains from the electricity trade, the yearly optimized market costs and revenues were discounted regarding the interest rate adopted over the economic life to the total present values at the initial investment year. Table 6-2 presents the total electricity purchase costs, the total charges and taxes levied, and the total revenues from the electricity trading over the economic life of 40 years, depending on the planning variant considered. In addition, the table shows the reduction of the total costs presented in 5.1 based on the profits from the electricity market calculated in percent.

Table 6-2 Results of the electricity trade using BSS in the HV grid

	BSS	BSS and DPC	BSS, UGG and DPC
Purchase costs / EUR Million	155.8	22.8	2.3
Charges and taxes / EUR Million	11.5	1.8	0.2
Revenues / EUR Million	251.7	41.9	5.3
Total profits / EUR Million	84.4	17.3	2.8
Reduced amount of the total costs / %	5.5	7.6	1.2

Figure 6-1 and 6-2 show the storage energy and power of a BSS by grid-supporting and market-based applications, respectively, over one exemplary day of the simulated year. The BSS with 71 MWh capacity and 24.3 MW rated power is one of the two BSS resulting from the planning algorithm when planning the grid using BSS and DPC, as described in 5.1.6. The red dotted lines in the figures represent the capacity and the rated power, respectively, of the considered BSS. The green lines in both figures illustrate the optimized scheduling of the storage energy and power for the grid-supporting application, respectively. This optimized grid-supporting scheduling was calculated by the planning algorithm in order to prevent the prognosticated grid congestion. The blue lines in the figures represent the optimized scheduling of the storage energy and power for the market-based application, respectively, in order to make profits from the electricity trade, as described in 6.1. The dotted purple line depicts the hourly market price on the Day-Ahead market in EUR/MWh. At times when the market price is low or negative, the electricity is bought and the BSS is charged. The bought energy is then stored until the price rises. Only then is the stored energy sold and the BSS discharged. Historical data of the market prices were used as perfect prognosticated market prices for the optimization of the profit from the electricity trade.

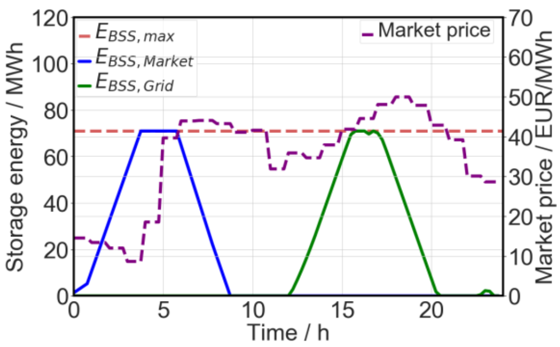

Figure 6-1 Storage energy scheduling for grid-supporting (green line) and market-based (blue line) applications over one exemplary day

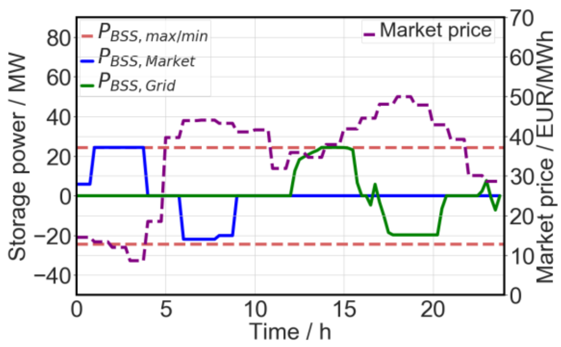

Figure 6-2 Storage power scheduling for grid-supporting (green line) and market-based (blue line) applications over one exemplary day

6.2.2 Resulting Gains from the Multiuse BSS in the MV Grid

Analogously to the multiuse concept of BSS in the HV grid, the profits from the electricity trade using BSS in the MV were optimized over the considered year. Assuming the same yearly market costs and revenues over the economic life of 40 years, the yearly market costs, revenues, and profits were discounted regarding the adopted interest rate to the corresponding total present values at the initial investment year. Table 6-3 shows the results of the electricity trade for every planning variant using BSS.

Table 6-3 Results of the electricity trade using BSS on the Spot market

	BSS	BSS and UGC
Purchase costs / EUR Million	1.13	0.58
Charges and taxes / EUR Million	0.09	0.05
Revenues / EUR Million	2.05	1.08
Total profits / EUR Million	0.83	0.45
Reduced amount of the total costs / %	12.6	12.3

It can be deduced from Table 6-3 that the planning variant using only BSS is still the most expensive variant for the expansion of the MV grid. Despite the profits made from the electricity trade, the resulting reduced total costs of this variant still exceed the total costs of the other planning variants. However, the planning variant combining BSS and UGC is more profitable for the considered MV grid than the application of the BSS or UGC separately. The most profitable planning variant for the considered MV grid is still the DPC, even though the electricity trade is not applicable for this variant.

Figure 6-3 and 6-4 show the storage energy and power of a BSS, respectively, by grid-supporting and market-based applications, over two exemplary days of the simulated year. The BSS with 5.9 MWh capacity and 1.8 MW rated power is one of the BSS resulting from the planning algorithm when planning the grid using only BSS.

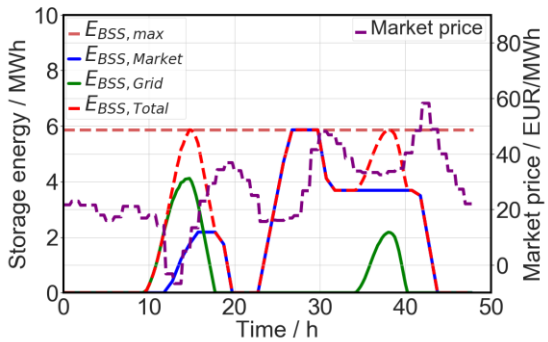

Figure 6-3 Storage energy scheduling for grid-supporting (green line) and market-based (blue line) applications over two exemplary days

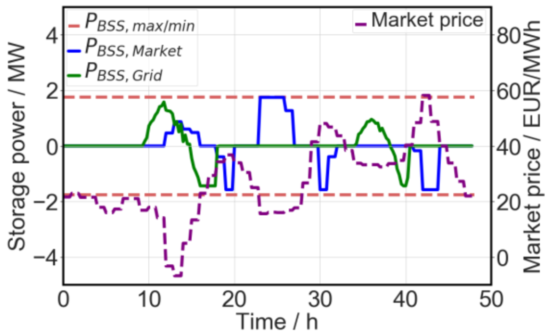

Figure 6-4 Storage power scheduling for grid-supporting (green line) and market-based (blue line) applications over two exemplary days

7 Sensitivity Analysis

The grid expansion using CGE, BSS and DPC, to manage prognosticated grid congestion raises costs over the considered economic life. Within the scope of a sensitivity analysis, the values of different input parameters were varied in order to examine the influence of these parameters on the total costs. Thereby, only one input parameter was varied concurrently. For the rest of the input parameters, the values of the reference scenario, described in chapters 3, 4 and 5, were adopted. The considered output variable represents the total costs for the grid expansion of an HV grid using OHLs, BSS and DPC. The total costs were calculated as an output parameter according to the approach described in 4.2 for an economic life of 40 years. The grid adopted for the sensitivity analysis is, hereby, the same HV grid considered for the evaluation of the planning algorithm in 5.1, whereas only one planning variant was considered here which is the combined application of OHLs, BSS and DPC. For the sake of simplicity, the CGE based on UGCs was not considered in this sensitivity analysis.

7.1 Parameters Considered in the Sensitivity Analysis

The calculation of the total costs as an output parameter is based on different input parameters, including the specific costs of the technologies used and the network conditions. The specific costs of the technologies used are, *inter alia*, the initial investment costs for OHLs and BSS, replacement investments for battery cells and converters, operating costs of the power lines and BSS, and DPC costs. However, the network conditions represent the characteristics of the network, which could be the length of the overloaded lines, the installed PV power or the installed wind power.

Hereafter, the parameters that have been varied within the sensitivity analysis and whose influence on the total costs have been analyzed are listed:

- The length of the OHL
- The installed power of PV
- The installed power of wind plants
- Investment costs of OHL
- Investment costs of BSS
- Specific costs of the DPC

The Length of the Power Lines

The length of the power lines represents a characteristic of the grid topology. In order to analyze the influence of the line lengths on the planning results, the planning algorithm described in 4.2 was run for different line lengths. The variation of the line lengths was realized by multiplication of the original lengths by a factor F_{length}. Table 7-1 shows the factors adopted for the variation of the lines' length by the calculation of the total costs. The scenario in which the multiplication factor is equal to 1 represents the reference scenario with the original line lengths described in Table 5-2.

Table 7-1 Factors adopted for the variation of the power lines' length

$\boldsymbol{F_{length}}$	0.25	0.5	1	1.5	2

The Installed PV Power

The PV power installed in the grid has a direct impact on the prognosticated grid congestion and, hence, on the results of the planning algorithm. In order to analyze the impact of different expansion scenarios of PV on the planning results, the installed PV power was multiplied by a different factor F_{PV} for each expansion scenario. Table 7-2 presents the factors adopted for the variation of the PV power installed in the grid. Factor 1 corresponds, hereby, to the PV expansion scenario of 2030 described in Table 3-1.

Table 7-2 Factors adopted for the variation of the PV power installed in the grid

$\boldsymbol{F_{PV}}$	0.25	0.5	1	1.5	2

The Installed Wind Power

Analogously, the wind power installed in the grid was varied in the same manner as that described for the installed PV power. Table 7-3 shows the factors adopted for the variation of the wind power installed in the grid. Factor 1 also corresponds here to the wind expansion scenario of 2030 described in Table 3-1.

Table 7-3 Factors adopted for the variation of the wind power installed in the grid

$\boldsymbol{F_{Wind}}$	0.25	0.5	1	1.5

Investment Costs of OHLs

Overhead lines are nowadays the technology most commonly used for the expansion of HV grids. The investment costs adopted in the planning algorithm reflect the present costs on the market. In order to examine its impact on the planning results and on the total costs, the adopted investment costs of new OHLs and new feeder panels were multiplied by a factor F_{GE} according to Table 7-4.

Factor 1 corresponds, thereby, to the specific costs adopted for OHLs in the reference scenario presented in Table 4-1.

Table 7-4 Factors adopted for the variation of the investment costs in OHL

$\boldsymbol{F_{GE}}$	0.25	0.5	1	1.5	2

Investment Costs of BSS

The BSS still represent a relatively new technology compared to OHLs. However, intensive research is increasingly undertaken nowadays in the field of batteries which can enable the reduction of their costs and the improvement of their efficiency and service life. Within the sensitivity analysis, the initial investment costs of the BSS were varied according to the multiplication factor F_{BSS} in order to examine their effect on the planning results and total costs. The adopted values here are presented in Table 7-5. Factor 1 corresponds, thereby, to the specific costs for BSS adopted in the reference scenario presented in Table 4-5.

Table 7-5 Factors adopted for the variation of the initial investment costs of BSS

$\boldsymbol{F_{BSS}}$	0.25	0.5	1	1.5	2

Specific Costs of DPC

The power curtailment of RES can be applied by grid operators in order to prevent grid congestion in return for financial compensation. In order to examine the impact of the DPC costs' variation on the total costs, the adopted specific compensation costs have been varied according to a multiplication factor F_{DPC} as shown in Table 7-6. The factor 1 corresponds thereby to the adopted specific costs for DPC in the reference scenario as presented in Table 4-7.

Table 7-6 Adopted factors for the variation of the compensation costs for DPC

$\boldsymbol{F_{DPC}}$	0.25	0.5	1	1.5	2

7.2 Results of the Sensitivity Analysis for the HV Grid

In what follows, the results of the sensitivity analysis are described in detail and compared for each parameter with the reference scenario. These results include the optimized grid expansion measures required to prevent the prognosticated grid congestion and the total costs occurring over the economic life of 40 years. These results were provided by the planning algorithm which has been applied for each considered scenario of the sensitivity analysis. The calculation of the load flow within the implemented linear optimization is based on the simplified assumption that the matrix $(NACLODF)$ remains constant. In reality, the values of the matrix can change depending on the expanded lines.

Influence of the Length of Power Lines

The variation of the line lengths does not influence the occurring line loading but influences the grid expansion costs. As shown in Table 7-7 and 7-8, the longer the line lengths, the more expensive the application of OHLs for the grid expansion. In the reference scenario where the line lengths have not been varied ($F_{length} = 1$), the planning results from the planning algorithm show that four LSs must be expanded according to variants 1 and 2 of the CGE. In the case where the lines are one and a half times or twice as long as in the reference scenario, the CGE with OHL was applied to only three LSs. Instead, more DPC energy and two further BSS were used, because this combination, in these cases, is more economical than only CGE with OHL. On the other hand, more OHL and less DPC were applied in the case where the line lengths of the grid are shorter than in the reference scenario, since the CGE with OHL becomes cheaper and more profitable.

Table 7-7 Planning results for different line lengths

F_{length}	Line Segments	CGE Variant	Curtailed Energy / GWh/a	BSS Placement	BSS Capacity / MWh	BSS Power / MW
0.25	LS2, LS5	1	3.4	-	0	0
	LS3, LS4, LS6, LS7	2				
0.5	LS2, LS5	1	3.4	-	0	0
	LS3, LS4, LS6, LS7	2				
1	LS4, LS5	1	24.5	-	0	0
	LS3, LS7	2				
1.5	LS4	1	25.2	SS7, SS9	18	14.2
	LS3, LS7	2				
2	LS4	1	25.2	SS7, SS9	18	14.2
	LS3, LS7	2				

Table 7-8 Results of the total costs for different line lengths

F_{length}	Total Costs / EUR Million	CGE Costs / %	BSS Costs / %	DPC Costs / %
0.25	27.3	85.7	0	14.3
0.5	45.1	91.35	0	8.65
1	68	58.2	0	41.8
1.5	81.4	51.9	12.3	35.8
2	94.5	58.5	10.6	30.9

Influence of the Installed PV Power

The variation of the PV power installed in the grid influences the line loading and, thus, the grid expansion measures required to prevent overloads. As shown in Table 7-9 and 7-10, the higher the installed PV power is, the more line expansions according to the variant 2 of the CGE are required. The CGE based on OHLs would be, in this case, the most economical solution to apply in order to cope with the higher feed-in power from PV. On the other hand, less PV power installed in the grid would lead to less required CGE measures and DPC. In both cases, the application of OHLs combined with DPC is more economical than the application of only BSS.

Table 7-9 Planning results for different PV power values installed in the grid

F_{PV}	Line Segments	CGE Variant	Curtailed Energy / GWh/a	BSS Placement	BSS Capacity / MWh	BSS Power / MW
0.25	LS4, LS7	1	4.4	-	0	0
	LS3	2				
0.5	LS4	1	8	-	0	0
	LS3, LS7	2				
1	LS4, LS5	1	24.5	-	0	0
	LS3, LS7	2				
1.5	LS2	1	1.9	-	0	0
	LS3, LS4, LS5, LS6, LS7	2				
2	LS2	1	9.9	-	0	0
	LS3, LS4, LS5, LS6, LS7	2				

Table 7-10 Results of the total costs for different PV power values installed in the grid

F_{PV}	Total Costs / EUR Million	CGE Costs / %	BSS Costs /%	DPC Costs / %
0.25	31.8	84.1	0	15.9
0.5	38.4	75.8	0	24.2
1	68	58.2	0	41.8
1.5	87.3	97.5	0	2.5
2	96.6	88.1	0	11.9

<u>Influence of the Installed Wind Power</u>

The wind power installed in the grid has a great impact on the grid loading and the expansion measures required. Table 7-11 and 7-12 show the required expansion measures and the resulting total costs, respectively, for different wind power values installed in the grid. Already from a factor of 1.5 times the power installed in the reference scenario, all considered lines must be replaced by OHLs with two bundled conductors in addition to the DPC application. On the other hand, reducing the wind power installed in the grid by half leads to a significant relief of the grid, so that all prognosticated overloads could be prevented through the application only of DPC. The CGE with OHLs is no longer necessary in that case. When reducing the wind power installed in the grid by one quarter, no line congestion is then expected and the CGE is, thus, no longer necessary.

Table 7-11 Planning results for different wind power values installed in the grid

F_{Wind}	Line Segments	CGE Variant	Curtailed Energy / GWh/a	BSS Placement	BSS Capacity / MWh	BSS Power / MW
0.25	-	1	0	-	0	0
	-	2				
0.5	-	1	1.4	-	0	0
	-	2				
1	LS4, LS5	1	24.5	-	0	0
	LS3, LS7	2				
1.5	-	1	9.5	-	0	0
	LS2, LS3, LS4, LS5, LS6, LS7	2				

These results show the strong influence of the installed wind plants on the line loading and the required grid expansion measures, which is more significant than in the case of PV plants.

Table 7-12 Results of the total costs for different wind power values installed in the grid

F_{Wind}	Total Costs / EUR Million	CGE Costs / %	BSS Costs / %	DPC Costs / %
0.25	0	0	0	0
0.5	1.6	0	0	100
1	68	58.2	0	41.8
1.5	99.5	89	0	11

Influence of the Investment Costs of OHLs

The variation of the specific investment costs of OHLs does not have any influence on the line load, but rather on the total costs and the chosen grid expansion measures. Table 7-13 and 7-14 show the resulting grid expansion measures and the total costs, respectively, for different specific OHL costs. In the case where the specific costs increase to one and a half times or twice the costs of the reference scenario, fewer CGE measures were applied by the planning algorithm compared with the reference scenario. Instead, more DPC and BSS were used, since this combined application is more profitable than the application only of OHLs. Only LS3, LS4 and LS7 were expanded for these scenarios. Due to the high overload on these LSs, their expansion is still worthwhile despite the high specific OHL costs.

When decreasing the specific OHL costs by a factor of 0.5 or 0.25 compared to the reference scenario, more LSs were expanded using OHLs with two bundled conductors and less DPC was applied. The BSS are comparatively too expensive to be applied in these cases.

Table 7-13 Planning results for different specific costs of OHL

F_{GE}	Line Segments	CGE Variant	Curtailed Energy / GWh/a	BSS Placement	BSS Capacity / MWh	BSS Power / MW
0.25	LS2	1	0.02	-	0	0
	LS3, LS4, LS5, LS6, LS7	2				
0.5	LS2, LS5	1	3.4	-	0	0
	LS3, LS4, LS6, LS7	2				
1	LS4, LS5	1	24.5	-	0	0
	LS3, LS7	2				
1.5	LS4	1	25.2	SS7, SS9	18	14.2
	LS3, LS7	2				
2	LS4	1	25.2	SS7, SS9	18	14.2
	LS3, LS7	2				

Table 7-14 Results of the total costs for different specific costs of OHL

F_{GE}	Total Costs / EUR Million	CGE Costs / %	BSS Costs / %	DPC Costs / %
0.25	21.3	99.9	0	0.1
0.5	42.2	90.8	0	9.2
1	68	58.2	0	41.8
1.5	82.8	52.7	12.1	35.2
2	97.4	59.7	10.3	30

Influence of the Investment Costs of BSS

The variation of the specific costs of BSS also has an impact on the total costs and, hence, on the expansion measures applied to prevent grid congestion. Table 7-15 and 7-16 show the resulting grid expansion measures and the total costs, respectively, for different specific costs of BSS. It can be deduced from these results that the application of BSS can only become economically viable compared to OHL and DPC when the specific costs of BSS decrease by half or more compared to the reference scenario costs.

Table 7-15 Planning results for different specific costs of BSS

F_{BSS}	Line Segments	CGE Variant	Curtailed Energy / GWh/a	BSS Placement	BSS Capacity / MWh	BSS Power / MW
0.25	LS4	1	20.9	SS7, SS9	40.6	20.8
	LS3, LS7	2				
0.5	LS4	1	23.97	SS7, SS9	22	15.4
	LS3, LS7	2				
1	LS4, LS5	1	24.5	0	0	0
	LS3, LS7	2				
1.5	LS4, LS5	1	24.5	0	0	0
	LS3, LS7	2				
2	LS4, LS5	1	24.5	0	0	0
	LS3, LS7	2				

Table 7-16 Results of the total costs for different specific costs of BSS

F_{BSS}	Total Costs / EUR Million	CGE Costs / %	BSS Costs /%	DPC Costs / %
0.25	59.7	48.7	10.8	40.5
0.5	63.3	45.9	10.2	43.9
1	67.9	58.3	0	41.7
1.5	68	58.2	0	41.8
2	68	58.2	0	41.8

Influence of the DPC Costs

Within the sensitivity analysis, the planning algorithm was applied to the grid for different specific costs of the DPC. Table 7-17 and 7-18 present the resulting grid expansion measures and the total costs, respectively, for different specific costs of the DPC. It can be deduced from the tables that the DPC costs in the reference scenario are already low enough to be deployed in the grid planning combined with OHLs. When decreasing the specific costs of DPC by a factor of 0.5 or 0.25, it is not possible to curtail more RES energy due to the 3 % limit implemented in the planning algorithm. Therefore, CGE measures are still required to prevent grid congestion.

Table 7-17 Planning results for different specific costs of DPC

F_{DPC}	Line Segments	CGE Variant	Curtailed Energy / GWh/a	BSS Placement	BSS Capacity / MWh	BSS Power / MW
0.25	LS4, LS5	1	24.5	-	0	0
	LS3, LS7	2				
0.5	LS4, LS5	1	24.5	-	0	0
	LS3, LS7	2				
1	LS4, LS5	1	24.5	-	0	0
	LS3, LS7	2				
1.5	LS5	1	5.6	-	0	0
	LS3, LS4, LS6, LS7	2				
2	LS2, LS5	1	3.4	-	0	0
	LS3, LS4, LS6, LS7	2				

In the case where the specific costs of DPC increase by a factor of one and a half times or twice compared with the reference scenario, less DPC and, instead, more CGE measures with OHL were deployed to prevent the grid congestion. Even in these scenarios, the DPC is still economically viable to prevent low and infrequent overloads, as it is the case for LS1. The application of BSS in these scenarios is still not economically reasonable compared to OHLs and DPC.

Table 7-18 Results of the total costs for different specific costs of DPC

F_{DPC}	Total Costs / EUR Million	CGE Costs / %	BSS Costs / %	DPC Costs / %
0.25	46.7	84.8	0	15.2
0.5	53.8	73.6	0	26.4
1	68	58.2	0	41.8
1.5	81.8	88.1	0	11.9
2	84.4	90.8	0	9.2

Figure 7-1 summarizes the results of the sensitivity analysis by summarizing the variation of the total grid expansion costs depending on the variation of the considered input parameters. The input and output values are, thereby, given in relation to the respective values of the reference scenario. It can be deduced from the figure that the most influential parameters regarding the resulting expansion measures and, hence, the total planning costs for the considered grid are the wind and PV power installed in the grid. Especially a high wind power share leads to high load flow values, which results in more transport capacity being needed in order to prevent grid congestion. In this case, the CGE based on OHLs is economically the most reasonable expansion instrument to integrate the wind plants. In addition to the installed wind and PV power, the total costs also depend largely on the investment costs of OHLs and, secondarily, on the costs of the DPC. The variation of the specific costs of BSS has the least influence on the total costs than the other considered parameters. Only by decreasing the specific costs of BSS by half or more does the BSS become more competitive and can be deployed by the grid planning algorithm for the expansion of the HV grid combined with OHLs and DPC.

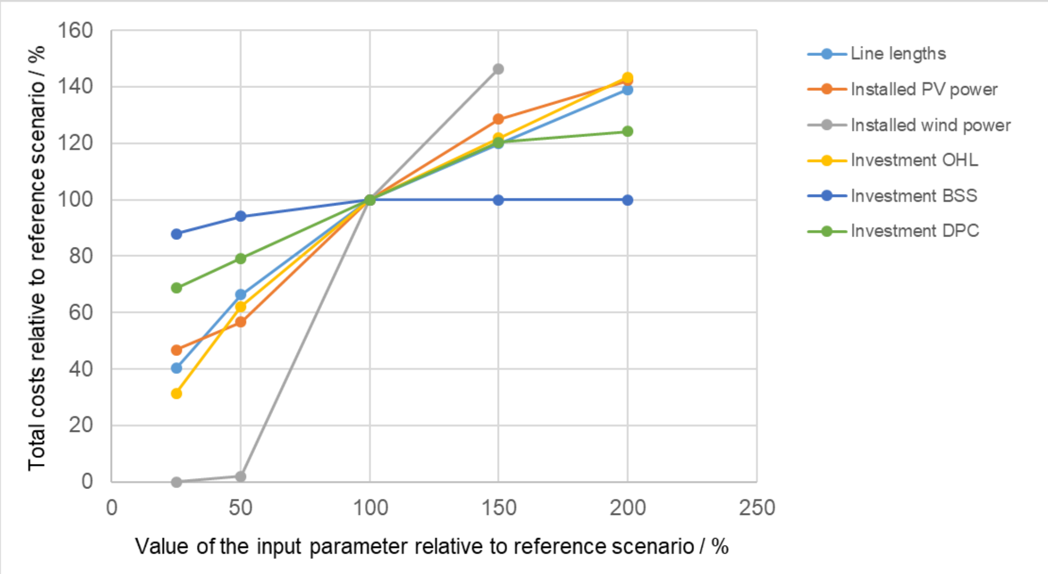

Figure 7-1 Sensitivity of the total grid expansion costs to the considered input parameter

8 Conclusion and Outlook

In the course of the German energy transition and the increasing integration of renewable energies into the distribution grid and due to the planned shutdown of nuclear and coal-fired power plants, the structure of the power system in Germany is undergoing continual change. To cope with these changes, the application of innovative technologies and planning concepts are currently required in addition to the need-oriented CGE. The aim of this application is to use the full potential of the existing grid and reduce additional conventional measures required for a safe power supply and integration of RES into the grid. The economic efficiency of the innovative and conventional measures must, hereby, also be taken into consideration.

In the context of this research work, a new grid planning method for distribution grids was developed combining CGE technologies based on OHLs and UGCs with innovative planning technologies, such as BSS and DPC. The aim of the method is to determine the most economical grid planning solution in compliance with the planning guidelines based on these different technologies. At the same time, the planning method intends to increase the utilization of the existing grid and avoid unnecessary CGE measures.

The functionality of the proposed planning method and its implementation in the form of a grid planning algorithm is described in chapter 4. The algorithm uses time series for load and RES power to determine the prognosticated grid congestion over a time range of a year. Depending on the prognosticated grid congestion and the investment and operating costs of the selected planning instruments, a MILP optimization is applied to determine the optimal combination of grid expansion measures required to prevent the congestion at minimum cost. The results of the optimization include the type and placement of CGE measures. They also include the storage capacity, rated power and placement of BSS, as well as the scheduling of BSS and DPC over the simulated year.

The planning algorithm is applicable for both HV and MV grids, whereby the linearized LFC method adopted for the planning of HV grids is different from that for MV grids, due to the different considered grid restrictions.

For the planning of HV grids, the planning principles considered within the algorithm reside in the compliance of the power flow with the power-carrying capacity of the lines for the (n-0) and (n-1) states. The planning instruments OHLs, UGCs, BSS and DPC were considered impartially in the algorithm so that all of them can contribute to fulfilling the grid planning principles.

The results of the planning algorithm are discussed in chapter 5. The application of the proposed planning method on a real HV grid showed that the combined use of OHLs and DPC represents the most economical planning variant. This variant, in consideration of the 3 % curtailment limit, enables a higher utilization of the existing grid and reduces the length of the required CGE measures to about 63 % compared with the application of OHLs alone. This combined variant also leads to a reduction of the total costs to about 70 %.

When the DPC is not applied, the use of UGCs for the planning of the HV grid is, according to the planning algorithm, about 4.25 times more expensive than the application of OHLs. In addition, the length of the required UGCs is 2.2 times greater than the length of the required OHLs. Due to the application of the DPC, subject to the 3 % curtailment limit, the length of the required UGCs was reduced to 51 % compared to the UGC variant. The total costs of the grid planning were also reduced to 57 % compared to the use of UGCs alone.

The results of the planning algorithm also showed that the use of only BSS for the expansion of HV grids is technically feasible and could replace the CGE, but this variant is still currently not economical due to the necessary high storage capacities in this case. This variant also leads to the highest losses in the grid. However, when combined with the DPC, the total costs and incurred losses can be decreased to 15 and 76.5 %, respectively, compared with the application of BSS alone.

The combined application of UGCs, BSS and DPC could lead to a more economical expansion solution than the use of BSS or UGCs individually. As illustrated by the results of the planning algorithm, the total costs of this planning variant represent 14.6 % of the BSS variant costs, and 53.8 % of the UGC variant costs. Due to the combined application of UGCs, BSS and DPC, subject to the 3 % curtailment limit, the UGC length required was reduced to about 40.5 % compared to the application of UGCs alone. This variant could be applied especially in the case of low public acceptance toward CGE with OHLs.

For the planning of the MV grid, the grid restrictions considered in the planning algorithm in this work are the compliance of the node voltages with the allowed voltage band and the compliance of the power flow with the power-carrying capacity of the lines in the (n-0) state. The planning instruments implemented in the planning algorithm to fulfil these grid restrictions are UGCs, BSS and DPC.

The application of the planning algorithm to a real MV grid showed that the DPC, in consideration of the 3 % curtailment limit, is sufficient to prevent the prognosticated congestion without further CGE measures. In this case, the application of DPC represents the most economical variant for the grid planning.

However, depending on the grid and the adopted RES scenario, the application of only DPC subject to the 3 % curtailment limit could be insufficient to prevent all prognosticated congestion in other MV grids. In that case, CGE measures or BSS can be further applied.

The results of the planning algorithm also showed that the combined application of UGCs and BSS in the considered MV grid is more economical than the application of only UGC or BSS by 11 and 44.7 %, respectively. Furthermore, the total length of the required UGCs based on this combined application was reduced to about 4.2 % compared with the planning variant based only on UGC.

The use of BSS as the only planning instrument for both HV and MV distribution grids did not prove to be economically viable compared to DPC and CGE. The BSS require high storage capacities to prevent the overloads, especially when they are high, which leads to high investment costs. However, a combined use of BSS with DPC or UGC or both could be more economically viable and competitive compared to CGE based on UGC. Since the (n-1) criterion is not a prerequisite for the planning of MV grids in the generation case, the requirements concerning grid expansion for MV grids are less strict than for HV grids. Therefore, the use of BSS and DPC could be more cost-efficient in MV and LV grids than in HV grids.

Furthermore, the sensitivity analysis of the total costs, described in chapter 7, revealed that the use of BSS in HV grids could be cost-efficient when combined with OHL and DPC only when BSS prices decrease by about half or more compared to the current prices. A participation of the BSS in the European Day-Ahead electricity market in parallel with the grid-supporting application investigated in chapter 6, could generate profits from the electricity trade. Nevertheless, the accruing profits remain small compared with the total costs of the grid-supporting application. Additionally, such a utilization of BSS for both grid-supporting and market-based purposes is still currently not clearly defined from the regulatory point of view.

The DPC is usually insufficient to prevent all congestion in HV grids due to the 3 % curtailment restriction. Even without considering the 3 % curtailment limit, the application of DPC in HV grids can be, to a certain extent, more expensive than the application of OHLs, according to the current costs of curtailment and OHLs. This applies in the case of high integration of RES and high prognosticated overloads. Furthermore, using DPC means that the curtailed RES energy is definitely wasted. This could be justifiable to a certain extent when limited to the 3 % annual feed-in energy of the plant to prevent grid congestion and avoid high investment costs in CGE measures. However, the long-term energy transition goals in Germany target 80 % coverage of the electricity consumption through

RES by 2050 [87]. As illustrated through the sensitivity analysis, a high integration of RES and especially of wind plants into the grid requires significantly more CGE in the HV grid. Therefore, according to the current prices, a need-oriented CGE using OHLs combined with DPC remains, in the long-term and at high voltage levels, the most cost-efficient solution to cope with the targeted integration of RES into the grid.

The planning algorithm proposed in this work delivers the optimal cost-effective planning solution of distribution grids automatically and spares the grid planner the trial of several planning variants. Regarding the increasing challenges encountered by the grid operators today and in the future, the proposed planning algorithm could give assistance by determining need-oriented and cost optimized planning solutions that help to achieve the energy transition goals in Germany and, at the same time, reduce new required CGE measures.

At the beginning of this dissertation, the following scientific thesis was introduced:

It is possible to reduce the required CGE due to the increasing integration of RES through the inclusion of the innovative planning instruments BSS and DPC in the grid planning, and still decrease the total expansion costs.

This thesis can be validated based on the planning results achieved for the considered HV and MV grid. Due to the optimization of the total costs within the grid planning process in the developed planning algorithm, the following results have been delivered:

- The combined application of OHLs and DPC in the considered HV grid is more economical than the use of OHLs alone and enables, at the same time, a reduction of the required CGE based on OHLs (see chapters 5.1.1 and 5.1.2).
- The combined application of UGCs and DPC in the considered HV grid is more economical than the use of UGCs alone, and enables, at the same time, a reduction of the required CGE based on UGCs (see chapters 5.1.3 and 5.1.4).
- The combined application of UGCs, BSS and DPC in the considered HV grid is more economical than the use of UGCs alone or the combined use of UGCs and DPC, and enables, at the same time, a reduction of the required CGE based on UGCs (see chapters 5.1.3, 5.1.4 and 5.1.8).
- The combined application of UGCs and BSS in the considered MV grid is more economical than the use of UGCs alone and enables, at the same time, a reduction of the required CGE based on UGCs (see chapters 5.2.1 and 5.2.4)

All results presented in this work are based on the simplifications described in chapter 3, and assume a perfect prognosis of the load consumption and the generation feed-in power. They are also based on the assumptions, technical parameters and specific costs outlined in chapter 4 for OHLs, UGCs, BSS and DPC. The resulting profits from the electricity market, as considered in this work, also assume a perfect prognosis of the electricity prices. In reality, prognoses are not perfect, and the technical parameters and specific costs can also vary from the selected values. Furthermore, an exact LFC could also deliver different values compared to the linearized LF methods. Therefore, the planning results presented in this work are not to be considered as absolute exact values. These results could diverge depending on the adopted input data and assumptions. In order to validate the proposed planning method, further comparison with the results of the classic planning of distribution grids should be realized [88]. In addition to that, the planning method could be improved further, for instance, by considering the reactive power flow in the optimization constraints in the case of HV grid planning. Moreover, other planning instruments, such as tap-changer transformers [89, 90], weather-dependent current rating of OHLs [91, 92] or the possibility of adding completely new routes for additional power lines [7, 8], could be included in the planning algorithm.

9 List of Literature

[1] German Energy Agency (dena). Ergebnispapier des dena-Stakeholder-Prozesses - Höhere Auslastung des Höhere Auslastung des Stromnetzes. Berlin, 2017. https://www.dena.de/fileadmin/dena/Dokumente/Pdf/9209_Ergebnispapier_dena-Stakeholder-Prozess-Hoehere_Auslastung_Stromnetze.pdf (accessed August 31, 2022).

[2] German Federal Ministry for Enconomic Affairs and Energy (BMWi). Zweiter Fortschrittsbericht zur Energiewende, die Energie der Zukunft, Berichtsjahr 2017 – Kurzfassung. Berlin, 2019.

[3] German Federal Ministry for Enconomic Affairs and Energy (BMWi). The Energy Industry Act (Energiewirtschaftsgesetz – EnWG). Berlin, 2005.

[4] Drees, T., Medert, H., Meinecke, M., Halici, C. Netzentwicklungsplan Strom 2035 (2021), erster Entwurf, 2021. https://www.netzentwicklungsplan.de/de/netzentwicklungsplaene/netzentwicklungsplan-2035-2021 (accessed August 31, 2022).

[5] The Bundesnetzagentur for Electricity, Gas, Telecommunications, Post and Railway (Bundesnetzagentur). Bericht zum Zustand und Ausbau der Verteilnetze 2020. Bonn, 2021.

[6] Moser, A. Netzbetriebsmittel und Systemdienstleistungen im Hoch- und Höchstspannungsnetz. Institut für Elektrische Anlagen und Netze, Digitalisierung und Energiewirtschaft: Aachen, 2021.

[7] ef.Ruhr GmbH (ed.). Verteilnetzstudie für das Land Baden-Württemberg, Technische Universität Dortmund: Dortmund, 2017.

[8] German Energy Agency (dena). Ausbau- und Innovationsbedarf der Stromverteilnetze in Deutschland bis 2030 (dena-Verteilnetzstudie). Dena: Berlin, 2012.

[9] Braun, M., Krybus, M., Becker, H., Bolgaryn, R., Dasenbrock, J., Gauglitz, P., Horst, D., Pape, C., Scheidler, A., Ulffers, J. Verteilnetzstudie Hessen 2024 – 2034. BeringPoint and Fraunhofer IEE: Kassel, 2018. https://www.house-of-energy.org/mm/2018_Verteilnetzstudie_Hessen_2024_bis_2034.pdf (accessed August 31, 2022).

[10] Bergische Universität Wuppertal, Lehrstuhl für Elektrische Energieversorgungstechnik; Siemens AG Energy Management Division, Digital Grid, Power Technologies International. Planungs- und Betriebsgrundsätze für ländliche Verteilungsnetze. Wuppertal, Erlangen, 2016.

[11] DKE Deutsche Kommission Elektrotechnik Elektronik Informationstechnik in DIN und VDE; DIN Deutsches Institut für Normung e. V. DIN EN 50160 – Merkmale der Spannung in öffentlichen Elektrizitätsversorgungsnetzen, Deutsche Fassung EN 50160, 2010.

[12] Netze BW GmbH. 2019.

[13] SimBench-Konsortium, Diskussion zu Planungs- und Betriebsgrundsätzen. 2017. https://simbench.de/wp-content/uploads/2019/02/20171027_Telko_PuB_ausgefuellt.pdf (accessed August 31, 2022).

[14] Steffens, P. Innovative Planungsgrundsätze für ländliche Mittelspannugsnetze. Dissertation Bergische Universität Wuppertal, Schwelm, 2018.

[15] ef.Ruhr, IAEW der RWTH Aachen, Bergische Universität Wuppertal. Gutachten zur Weiterentwicklung der Strom-Verteilnetze in Nordrhein-Westfalen auf Grund einer fortschreitenden Sektorenkopplung und neuer Verbraucher. Dortmund, 2021.

[16] Resch, M., Bühler, J., Klausen, M., Sumper, A. Impact of operation strategies of large scale battery systems on distribution grid planning in Germany, Reviews, Renewable and Sustainable Energy, 2017; 74: 1042-1063, http://dx.doi.org/10.1016/j.rser.2017.02.075.

[17] Liebenau, V., Schwippe, J., Kuch, S., Rehtanz, C. Network extension planning considering the uncertainty of feed-in from renewable energies. Proceedings of the 2013 IEEE Grenoble Conference, Grenoble, France, June 16-20, 2013; pp. 1-6.

[18] Wiest, P. Probabilistische Verteilnetzplanung zur optimierten Integration flexibler dezentraler Erzeuger und Verbraucher. Dissertation, University of Stuttgart. sierke Verlag: Weingarten, 2018.

[19] Pilo, F., Jupe, S., Silvestro, F., C. Abbey and co. Planning and Optimization Methods for Active Distribution Systems. CIGRE Brochure number 591, CIGRE, Paris, France, August 2014.

[20] Alhaider, M., Fan, L. Mixed integer programming based battery sizing. Energy Systems, 2014; 5: 787-805.

[21] Emmanuel, M., Jain, A., Bryce, R., Latif, A., Ghosh, S., Nagarajan, A. Impacts of control set-points on battery energy storage performance for peak shaving application. 2020 47th IEEE Photovoltaic Specialists Conference (PVSC), 2020.

[22] Mahmud, K., Morsalin, S., Kafle, Y.R., Town, G.E. Improved peak shaving in grid-connected domestic power systems combining photovoltaic generation, battery storage, and V2G-capable electric vehicle. 2016 IEEE International Conference on Power System Technology (POWERCON), 2016.

[23] Karanki, S.B., Xu, D. Optimal capacity and placement of battery energy storage systems for integrating renewable energy sources in distribution system. 2016 National Power Systems Conference (NPSC), 2016.

[24] Lazzeroni, P., Repetto, M. Optimal planning of battery systems for power losses reduction in distribution grids, Electric Power Systems Research, 2019; 167: 94-112.

[25] Alzahrani, A., Alharthi, H., Khalid, M. Minimization of Power Losses through Optimal Battery Placement in a Distributed Network with High Penetration of Photovoltaics. Energies, 2020; 13: 140. doi:10.3390/en13010140.

[26] Tachibana, M., Palmer, M.D., Matayoshi, H., Senjyu, T., Funabashi, T. Improvement of power system voltage stability using battery energy storage systems. 2015 International Conference on Industrial Instrumentation and Control (ICIC), 2015.

[27] Kawabe, K., Yokoyama, A. Study on short-term voltage stability improvement using batteries on extra-high voltage network. 2013 IEEE Grenoble Conference, 2013.

[28] Sagara, M., Sediqi, M.M., Senjyu, T., Danish, M.S.S., Funabashi, T. Voltage stability improvement by optimal active power and reactive power output control of storage battery system. 2016 IEEE Region 10 Conference (TENCON), 2016.

[29] Laribi, O., Wiest, P., Rudion, K. Optimal Dimensioning and Operation of a Grid-Supporting Energy Storage System. IEEE ISGT Europe 2017, September 26-29, 2017, Turin, Italy. doi: 10.1109/ISGTEurope.2017.8260325.

[30] Buchner, M., Laribi, O., Rudion, K. Bestimmung der Betriebsweise eines Speichers zur Netzentlastung auf Basis Linearer Optimierung. Tagung Zukünftige stromnetze für Erneuerbare Energien 2018, January 30-31, 2018, Berlin, p. 235.

[31] Laribi, O., Miller, M., Wiest, P., Rudion, K., Fischer, F., Lübbe, T. Netzausbauoptimierung in den Verteilnetzen durch Einsatz moderner Planungsmethoden. Ingenieur Spiegel, 2018; 4: 29.

[32] Laribi, O., Wiest, P., Rudion, K. Dimensioning and Positioning of Storage Systems under the consideration of the (n-1) Security Criterion in High Voltage distribution Grids. IEEE ISGT Europe 2018, October 21-25, 2018, Sarajevo, Bosnia-Herzegovina. doi: 10.1109/ISGTEurope.2018.8571633.

[33] Laribi, O., Rudion, K., Schnaars, J. Planung des Hochspannungsnetzes unter Berücksichtigung von Speichern und dynamischer Spitzenkappung. Internationaler ETG-Kongress 2019, May 8-9, 2019, Esslingen am Neckar, Deutschland, p. 411.

[34] Laribi, O., Rudion, K., Lübbe, T. Optimal Planning of High-Voltage Distribution Grids under the Combined Use of Energy Storage Systems and Dynamic Feed-In Management. 25th International Conference on Electricity Distribution, June 3-6, 2019, Madrid, Spain.

[35] Laribi, O., Rudion, K., Nägele, H. Combined Grid-supporting and Market-based Operation Strategy for Battery Storage System. 6th IEEE International Energy Conference, September 28 – October 1, 2020, Tunis, Tunisia. doi: 10.1109/ENERGYCon48941.2020.9236468.

[36] Bundesnetzagentur for Electricity, Gas, Telecommunications, Post and Railway (Bundesnetzagentur). Bedarfsermittlung 2019-2030, Bestätigung Netzentwicklungsplan Strom, 2019.

[37] Forum Network Technology/Network Operation in the VDE. Power peak curtailment as new degree of freedom by network planning. Berlin, 2017.

[38] Miller, M., Rudion, K., Fischer, F., Nägele, H. Optimal Distribution Grid Expansion Planning under Consideration of Dynamic DG Curtailment. CIRED 2020 Berlin Workshop, Paper 0386, September, 2020.

[39] Miller, M., Rudion, K., Fischer, F., Nägele, H. Probabilistic Approach for Distribution Grid Planning under Consideration of Line Loading Indicators. 9th International Conference on Renewable Power Generation – RPG 2021, Dublin, Ireland, March, 2021.

[40] Koopmann, S., Scheufen, M., Schnettler, A. Integration of Stationary and Transportable Storage Systems into Multi-Stage Expansion Planning of Active Distribution Grids. IEEE PES ISGT Europe 2013, 2013.

[41] Shen, X., Shahidehpour, M., Han, Y., Zhu, S., Zheng, J. Expansion Planning of Active Distribution Networks With Centralized and Distributed Energy Storage Systems. IEEE Transactions on Sustainable Energy, 2017; 8(1): 126-134. doi: 10.1109/TSTE.2016.2586027.

[42] Wiest, P., Rudion, K., Probst, A. Efficient integration of (n - 1)-security into probabilistic network expansion planning, International Journal of Electrical Power and Energy Systems, 2018; 94: 151-159. doi: 10.1016/j.ijepes.2017.07.002.

[43] Wiest, P., Gross, D., Rudion, K., Probst, A. Rapid identification of worst-case conditions: improved planning of active distribution grids. IET Generation, Transmission & Distribution, 2017; June. 2412-2417.

[44] Netzgesellschaft Ostwürttemberg DonauRies GmbH. 2017).

[45] Schärli, U., Tenbohlen, S. Lecture notes. Elektrische Energienetze II, University of Stuttgart, 2019.

[46] Glover, J.D., Sarma, M.S., Overbye, T.J. Power System Analysis and Design. 5th Edition. Cengage Learning.

[47] Brunner, M. Auswirkungen von Power-to-Heat in elektrischen Verteilnetzen. Dissertation, University of Stuttgart, Klagenfurt, 2017.

[48] Bolognani, S., Dörfler, F. Fast power system analysis via implicit linearization of the power flow manifold. Fifty-third Annual Allerton Conference Allerton House, UIUC, Illinois, USA, September 29 – October 2, 2015.

[49] Bolognani, S., Zampieri, S. On the Existence and Linear Approximation of the Power Flow Solution in Power Distribution Networks. IEEE Transactions on Power Systems, 2016; 31(1): 163-172. doi: 10.1109/TPWRS.2015.2395452.

[50] Chachuat, B. Mixed-Integer Linear Programming (MILP): Model Formulation. McMaster University, http://macc.mcmaster.ca/maccfiles/chachuatnotes/07-MILP-I_handout.pdf (accessed March 25, 2021).

[51] Gurobi Optimizer. Mixed-Integer Programming (MIP) – A Primer on the Basics. https://www.gurobi.com/resource/mip-basics/ (accessed March 29, 2021).

[52] Rockstäschel, S. A Branch-and-Bound Algorithm for Multiobjective Mixed-integer Convex Optimization. Springer Spektrum: Wiesbaden, 2020.

[53] Gurobi Optimizer. Choosing the right algorithm. https://www.gurobi.com/documentation/9.1/refman/choosing_the_right_algorit.html (accessed March 29, 2021).

[54] Gurobi GmbH. Gurobi Optimization Working With Multiple Objective. https://www.gurobi.com/documentation/9.0/refman/working_with_multiple_obje.html (accessed March 31, 2021).

[55] Consentec GmbH. Grundlagen für eine Berechnungsmethode zum Kostenvergleich zwischen Kabeln und Freileitungen sowie zur Festlegung eines Mehrkostenfaktors. Aachen, 2013. http://www.news.admin.ch/NSBSubscriber/message/attachments/31007.pdf (accessed November 10, 2021).

[56] Mitteldeutsche Netzgesellschaft Strom mbH. Neubau 110-kV Hochspannungsfreileitung Abzweig Oberelsdorf Bl. 1013, Vergleichsrechnung zur Bewertung einer alternativen Verkabelung. Freiberg, 2017. https://www.uvp-verbund.de/documents/ingrid-group_ige-iplug-sn/F543A667-0376-41C4-84D7-70DE6F66C0CE/Erl%C3%A4uterungsbericht-Anlage%203.pdf (accessed November 10, 2021).

[57] Brakelmann, H. Netzverstärkungs-Trassen zur Übertragung von Windenergie: Freileitung oder Kabel? Rheinberg, 2004. https://www.wind-energie.de/fileadmin/redaktion/dokumente/pressemitteilungen/2018/20180103-brak-studie-2004.pdf (accessed November 10, 2021).

[58] Hofmann, L., Oswald, B.R. Vergleich Erdkabel – Freileitung im 110-kV-Hochspannungsbereich. Leibniz Universität Hannover, December 16, 2010. https://docplayer.org/10801305-Gutachten-zum-vergleich-erdkabel-freileitung-im-110-kv-hochspannungsbereich.html (accessed November 10, 2021).

[59] Hofmann, L., Oswald, B.R. Wirtschaftlichen Vergleich von Kabeln, Freileitungen und Freileitungen mit Zwischenverkabelung im 110-kV-Hochspannungsbereich. Hannover, May 2011. https://docplayer.org/20978513-Gutachten-zum-wirtschaftlichen-vergleich-

von-kabeln-freileitungen-und-freileitungen-mit-zwischenverkabelung-im-110-kv-hochspannungsbereich.html (accessed November 10, 2021).

[60] nkt cables GmbH. Hoch- und Höchstspannungskabelanlagen. https://opendata.uni-halle.de/bitstream/1981185920/13222/8/D01_HS-Kabel.pdf (accessed November 10, 2021).

[61] Sillaber, A. Leitfaden zur Verteilnetzplanung und Systemgestaltung, Springer Vieweg: Wiesbaden, Innsbruck, 2016.

[62] Newspaper Maeil Business. Hyundai Electric to build 150-MW ESS for Korea Zinc. July 27, 2017. https://pulsenews.co.kr/view.php?year=2017&no=505105 (accessed August 15, 2021).

[63] Der Spiegel. Tesla Battery storage power plant. Spiegel Wirtschaft, December 1, 2017. https://www.spiegel.de/wirtschaft/unternehmen/tesla-nimmt-in-australien-weltgroesste-batterie-in-betrieb-a-1181326.html (accessed September 24, 2020).

[64] WEMAG. Battery storage power plant, Schwerin, Germany. https://www.wemag.com/sites/default/files/20170714%20Faktenblatt%20WEMAG%20Batteriespeicher.pdf (accessed August 19. 2021).

[65] Shz. Battery storage power plant Flensburg. April 6, 2017. https://www.shz.de/lokales/flensburger-tageblatt/grosse-lithium-ionen-batterie-entsteht-bei-flensburg-id16529056.html (accessed August 19, 2021).

[66] Battery storage power plant Wendelstein. 2018. https://www.zfk.de/energie/strom/artikel/batteriespeicher-wendelstein-ist-in-betrieb-2018-07-17/ (accessed July 1, 2020).

[67] eins energie in sachsen GmbH & Co. KG, Batteriespeicher, https://www.eins.de/%C3%BCber-eins/infrastruktur/energiewende/batteriespeicher (accessed September 24, 2020).

[68] Fraunhofer Institute for Systems and Innovation Research ISI. High-energy batteries 2030+ and prospects for future battery technologies – Fraunhofer ISI presents an updated energy storage roadmap. 2017.

[69] Zapf, M. Stromspeicher und Power-to-Gas im deutschen Energiesystem; Rahmenbedingungen, Bedarf und Einsatzmöglichkeiten. Springer Vieweg: Wiesbaden, 2017.

[70] Tesla. Datasheet Powerpack 2.5 system. https://www.intermepro.com/wp-content/uploads/2020/07/Datasheet_Powerpack2-5_All.pdf (accessed September 24, 2020).

[71] Tesla, Overall System Specs Powerpack. https://www.tesla.com/powerpack?redirect=no (accessed September 24, 2020).

[72] Weaver, J.F. USA's largest cluster of batteries, including Tesla Megapack, inching forward. CommercialSolarGuy, March 3, 2020. https://commercialsolarguy.com/2020/03/03/tesla-megapack-inching-forward/ (accessed August 31, 2022).

[73] Zeitung für kommunale Wirtschaft. Batterispeicher Wendelstein. 2018. https://www.zfk.de/energie/strom/artikel/batteriespeicher-wendelstein-ist-in-betrieb-2018-07-17/ (accessed July 1, 2020).

[74] Öko-Institut e.V. Photovoltaik Wechselrichter, Entwicklung der Vergabekriterien für ein klimaschutzbezogenes Umweltzeichen. Yumpu. December 6, 2012. https://www.yumpu.com/de/document/view/5317507/studie-aeurzprosa-photovoltaik-wechselrichteraeuroe-a-ko-institut-ev (accessed August 31, 2022).

[75] The German Wind Energy Association (Bundesverband WindEnergie e.V). Netzverstärkungs-Trassen zur Übertragung von Windenergie: Freileitung oder Kabel?. 2004.

[76] The Bundesnetzagentur for Electricity, Gas, Telecommunications, Post and Railway (Bundesnetzagentur). Quarter report about grid and system security measures for the year and fourth quarter of 2018. 2019.

[77] Mitteldeutsche Netzgesellschaft Strom mbH. Neubau 110-kV-Hochspannungsleitung Großräschen – Altdöbern, Bl. 6805 – Vergleichsrechnung zur Bewertung einer alternativen Verkabelung. Kolkwitz, 2017. https://docplayer.org/140210368-Neubau-110-kv-hochspannungsleitung-grossraeschen-altdoebern-bl-6805.html (accessed August 31, 2022).

[78] NEW-Grid Management Consult GmbH. Neubau der 110-kV-Hochspannungsfreileitung – Abzweig Oberelsdorf – Wirtschaftlichkeitsbetrachtung Freileitung vs. Kabel. Erfurt, 2019.

[79] Leprich, U., Guss, H., Weiler, K., Ritzau, M., Macharey, U., Igel, M., Diegler, J. Ausbau elektrischer Netze mit Kabel oder Freileitung unter

besonderer Berücksichtigung der Einspeisung Erneuerbarer Energien. June 20, 2011, Saarbrücken. https://www.erneuerbare-energien.de/EE/Redaktion/DE/Downloads/Studien/bmu-studie-ausbau-elektrischer-netze.pdf?__blob=publicationFile&v=2 (accessed August 31, 2022).

[80] Sauer, D., Haberschusz, D., Kairies, K-P., Kleinsteinberg, B., Knips, M., Kwiecien, M., Lewerenz, M., Mareev, I., Münderlein, J., Rücker, F., Sabet, P.S., Thien, T., Warneke, A., Winter, M., Yurdagel, Y., Zappen, H. Einführung in die Energieeffizienz von Batteriespeichersystemen. Conference Batterieforum Deutschland 2017, Berlin, 2017. doi: 10.13140/RG.2.2.26518.55365.

[81] Tschöke, H., Gutzmer, P., Pfund, T. Elektrifizierung des Antriebsstrangs. Springer Vieweg: Magdeburg, 2019.

[82] Bricklebrit Lastgangbepreisung. Electricity exchange in Leipzig, www.bricklebrit.de (accessed July 2, 2019).

[83] HAASE Gesellschaft m.b.H. Overhead line conductors (AL1/ST1A) according to EN 50182:2001 (1), www.haase.at (accessed November 10, 2021).

[84] Informationsplattform der deutschen Übertragungsnetzbetreiber. https://www.netztransparenz.de/ (accessed July 2, 2019).

[85] EEX AG. List of Services and Prices of EEX AG. Leipzig, https://www.eex.com/de/ (accessed September 11, 2020).

[86] Shahan, Z. Tesla Powerwall & Powerpacks per-kWh Lifetime Prices vs Aquion Energy, Eos Energy, & Imergy. CleanTechnica. 2015. https://cleantechnica.com/2015/05/09/tesla-powerwall-powerblocks-per-kwh-lifetime-prices-vs-aquion-energy-eos-energy-imergy/ (accessed April 6, 2021).

[87] German Federal Ministry for Economic Affairs and Energy. Erneuerbare Energien in Zahlen. Octorber 2020.

[88] Laribi, O., Rudion, K. Optimized Planning of Distribution Grids Considering Grid Expansion, Battery Systems and Dynamic Curtailment. Energies, 2021; 14: 5242. https://doi.org/10.3390/en14175242.

[89] Früh, H., Wiest, P., Rudion, K. Evaluation of Voltage Control methods in Low Voltage Grids based on Probabilistic Methods. ETG Kongress 2017, Bonn, Germany, November 2017.

[90] Małkowski, R., Izdebski, M., Miller, P. Adaptive Algorithm of a Tap-Changer Controller of the Power Transformer Supplying the Radial Network Reducing the Risk of Voltage Collapse. Energies, 2020; 13: 5403. https://doi.org/10.3390/en13205403.

[91] Miller, M., Rudion, K., Nägele, H., Schnaars, J. Weather-Dependent Current Ratings of Overhead Lines in the Probabilistic High Voltage Distribution Grid Planning. CIRED 2021 Conference, Geneva, Switzerland, 2021.

[92] Miller, M., Wiest, P., Rudion, K., Fischer, F. Determination of Constant Seasonal Values for the Current Rating of Overhead Lines in the Network Planning. 25th International Conference on Electricity Distribution, Paper 1972, June 2019.